ANALYSIS OF METAL IONS IN WATER USING SAM-MODIFIED EQCM ELECTRODES

Thesis submitted for the degree of

Doctor of Philosophy

At the University of Leicester

By

Agab Mohamed Hewas

Department of Chemistry

University of Leicester

December 2013

Dedicated to the souls of my parents

Title: Analysis of metal ions in water using SAM-modified EQCM electrodes.

Author: Agab M. Hewas

Abstract:

The toxic nature of some metal ions makes it necessary to monitor their concentrations in the environment. In this thesis there are two fundamental objectives. The first is to develop a portable electrochemical sensor, which is capable for detecting and monitoring Pb^{2+}, Ni^{2+} and Co^{2+} rapidly, selectively and accurately. The second is to develop an extraction procedure for these metal ions by using some ionic liquids (ILs), with the QCM and colorimetric indicators being used to investigate this process. Mercaptosuccinic acid (MSA), 2, 2'-Thiodisuccinic acid (2.2'-TDS), 4-Mercaptobenzoic acid (4-MBA) and 4-Mercaptophenylacetic acid (4-MPAA) thiols were used to prepare self-assembled monolayers on the gold electrodes of 10MHz AT-cut piezoelectric quartz crystal resonators. The extent of immobilisation of each ligand was determined by measuring the resonant frequency change of the crystal and the quality of the SAM was investigated voltammetrically, with $[Fe(CN)_6]^{3-/4-}$ as a probe redox couple. The focus was on Au-MSA as the most effective ligand for Pb^{2+}, Ni^{2+} and Co^{2+}. Adsorption of these metal ions, individually and competitively, by Au-MSA from aqueous solution was measured as a function of solution concentration and the data fitted to a range of isotherms. Structural and compositional information on the SAMs was acquired using Raman spectroscopy and XPS.

Acknowledgements

I would like to express my true gratitude to my supervisor Prof. Karl S. Ryder for giving me the opportunity to pursue my doctoral studies, and also for his continuous guidance, encouragement and invaluable suggestions and pointers during our periodic discussions.

I also need to acknowledge the help and suggestions provided by Prof. A. Robert Hillman, my second supervisor, for his valuable comments during the course of my research work. I would like to thank Prof. Andrew P. Abbott, the Head of the Department of Chemistry, for his efforts to facilitate all administrative transactions and for his valuable scientific advice.

I am very thankful to Dr Jose Portoles, from the University of Newcastle, who assisted me with the analysis of the XPS samples which enabled me to complete this work. My sincere thanks also goes to Dr. Graham Clark of the Department of Engineering at the University of Leicester for enabling me to clarify my thoughts during training sessions on the Raman Spectroscopy provided by himself, and to Dr. Andrew D. Ballantyne from the Department of Chemistry for his invaluable advices and general observations whilst I was finalizing my doctoral thesis. My thanks will also go to both of Dr. Andrew Hudson and Dr. Alex Goddard for their beneficial discussion.

I wish to convey my thanks to my group and to my colleagues at the Department of Chemistry, being very friendly throughout my years of research at the Department.

I am very grateful to all the members of my family for their support to complete my research. Finally, and above all I would like to thank the Government of Libya for the financial support I received. I need to convey my sincerest thanks to all the staff at the Libyan Embassy in London and particularly the Cultural Attaché and his team.

Agab / December 2013

List of contents

Contents

List of tables

List of figures

List of abbreviations

Acronyms of chemicals	
DI	De-ionized water
MSA	Mercaptosuccinic acid
2,2'-TDS	2, 2'-Thiodisuccinic acid
4-MBA	4-Mercaptobenzoic acid
4-MPAA	4-Mercaptophenylacetic acid
3-MPTS	3-Mercaptopropyltrimethoxysilane
IPA	Isopropanol
DMG	Dimethylglyoxime
[BMIM][PF_6]	1-Butyl-3-methylimadazolium hexafluorophosphate
[Hbet][Tf_2N]	Betaine [bis(trifluoromethylsulfonyl)imide]
Acronyms of techniques	
CV	Cyclic Voltammogram
QCM	Quartz Crystal Microbalance
EQCM	Electrochemical Quartz Crystal Microbalance
XPS	X-ray Photoelectron Spectroscopy
AAS	Atomic Absorption Spectroscopy
ICP-OES	Inductively Coupled Plasma Optical Emission Spectroscopy
GFAAS	Graphite Furnace Atomic Absorption Spectroscopy
SERS	Surface Enhanced Raman Spectroscopy
Acronyms of terms	
SAM	Self-Assembled Monolayer
IL	Ionic Liquid
IUPAC	International Union of Pure and Applied Chemistry
IARC	International Agency for Research on Cancer
TC	Transfer Coefficient
MCL	Maximum Contaminant Level
WHO	World Health Organization
MW	Molecular Weight
CE	Chemical Enhancement
EME	Electro-Magnetic Effect

Contents

1 General introduction

Overview

For a long time the accuracy of measuring very low concentration of toxic metal ions was a matter of concern for researchers. However, different techniques and procedures were developed for monitoring the concentration of these metal ions in the surrounding environment such as: atomic absorption spectroscopy (AAS), inductively coupled plasma optical emission spectroscopy (ICP-OES), and Graphite Furnace Atomic Absorption Spectroscopy (GFAAS). But these analytical devices are very expensive. Moreover, they are bulky and often different gases and high energy sources are required. Furthermore, they usually take a long time to prepare and longer to analyse the sample.[1]

In recent years electroanalytical methods including anodic stripping voltammetry, potentiometric stripping analysis, and quartz crystal microbalance (QCM) have been commonly used for this purpose. The QCM is an extremely sensitive mass sensor with detection limit in the sub-nanogram range.[2] But there are some of challenges should be considered like detection limit of loaded mass, and the interference with trap liquid molecules, which can vibrate at the same amplitude and acceleration of the quartz producing an additional frequency change, also the interference between all possible existing species.

1.1 Heavy metals

Heavy metals are chemical elements that have a specific gravity (a measure of density) at least five times that of water. Naturally, they are components of the Earth's crust and cannot be degraded or destroyed. No less than 20 of these metals are classified as toxic and half of them have been emitted into the environment in quantities that pose grave

risks to human health.[3, 4] At least five of these metallic elements in one form or another are accepted as human carcinogens by the International Agency for Research on Cancer (IARC), including arsenic, cadmium, hexavalent chromium, and inorganic lead compounds. There are also some other metallic elements less harmful, like copper, nickel and cobalt.

1.1.1 Sources of pollution and natural levels

Heavy metals (e.g. As, Cd and Pb) are environmental pollutants mainly of anthropogenic origin.[5, 6] The increasing thrust for industrialisation and urbanisation has been identified as the cause of heavy metal pollution. Both industry and agriculture have contributed considerably to the elevated concentrations of heavy metals through waste disposal, thermal power plants, chlor-alkali industry, mine wastes, sewage treatment plants, atmospheric deposition, fertilisers, pesticides and the application of sewage sludge in arable land[7, 8]; other sources of heavy metals are battery factories and erupted volcanoes as a nature source.[9, 10]

In suburban areas the use of industrial or municipal wastewater in irrigation is common practice in many parts of the world.[11, 12, 13] Wastewater irrigation is known to contribute significantly to the heavy metal content of soils and plants.[14, 15] However, the presence of these contaminants in plants raises the possibility of poisoning humans via the food chain, and for that reason, the uptake for each toxic metal, or transfer coefficient (TC) has to be calculated. Mathematically TC is equal to metal concentration in plant tissue above the ground, divided by the total metal concentration in the soil.[16]

Chromium: According to World Health Organization (WHO) the maximum Contaminant Level (MCL) of total chromium in drinking water should be less than 0.05 mg/l[17, 18] and for hexavalent chromium is 0.0032 mg/l.[19] However, Cr comes number

sixteen in the priority list of most hazardous substances depending on the Agency for Toxic Substances and Disease Registry. The two largest sources of chromium emission in the atmosphere are from volcanic activity, windblown sand, chemical manufacturing industry and combustion of natural gas, oil, and coal[20, 21]; other sources are: cement producing, wood preservatives, ceramics manufacturing, and glassmaking.[22] Fortunately, TC factor for chromium is comparatively low in range 0.01-0.1.[16]

Lead: The most significant contributors of lead emissions into the atmosphere are lead gasoline additives, smelters, battery plants[23], paint, having lead pipes in water supply systems, radiator repair shops and some other industrial sources such as lead mining, soldering, welding, and coal combustion. According to WHO the upper limit recommended for lead in drinking water should be less than 0.01 mg/l[24], a reduction from the previous limit 0.05-0.1 mg/l.[17, 25] However, same as chromium, lead also has TC factor within 0.01-0.1.[16]

Cadmium: The two largest sources of cadmium to the environment are fossil fuel emissions and incineration of municipal wastes.[26, 27] Other sources are metal plating industries, sites using pigments in plastic, ceramics and glass manufacturing, welding, and smelting. First edition of the guidelines for drinking water quality, published in 1984 indicated that a guideline value recommended for cadmium in drinking water was 0.005 mg/l[17, 28] and now considered to be 0.003 mg/l.[24] TC factor for cadmium is very high 1-10.[16]

Arsenic: Arsenic has both natural and anthropogenic sources, about 60% from two major sources, copper smelting and coal combustion; the other primary sources are wood preservatives, insecticides, leaded gasoline, glass production, and electronic manufacturing, such as microwave devices, lasers, and semiconductors. In 1993 WHO

reduced the presence of arsenic in drinking water to 0.01 mg/l instead of 0.05 mg/l[29] in its guidelines. The TC factor for arsenic is reasonably low compared to some other metals 0.01-0.1.[16]

Nickel: This element often comes from chemical or catalytic processes, combustion sources, or incineration of waste and sewage sludge. However, the greatest contribution of nickel in ambient air was produced by the combustion of fossil fuels. The average concentrations of total nickel in drinking water set up from 3–7 mg/l with concentrations occasionally above 35 mg/l.[30] TC for nickel is in the medium range 0.1-1.[16]

Copper: Fertilizers like $CuSO_4.5H_2O$, $CuSO_4.3Cu(OH)_2$ and copper oxides used in agriculture are the main sources for copper.[31, 32] The medium concentration of copper in natural water (rivers, lakes, and oceans) is between 0.004–0.01 mg/l. However, WHO has set up the maximum value of copper in the drinking water to be 2.0 mg/l[33], as copper also has high and wide range of TC 0.1-10.[16]

Cobalt: cobalt sources can either be anthropogenic produced by human activities like manufacturing, or natural such as corrosion, weathering, sea water spray, and volcanoes.[31] However, its concentration in drinking water is rarely to be detected because its concentration is very low 0.0001-0.005 mg/l.[34] Cobalt has similar TC value to chromium, lead, arsenic, where TC is 0.01-0.1for each one of them.[16]

1.1.2 Environmental and health hazards

Heavy metals have long been a matter of serious concern due to their effects on environment and human beings. Their potential accumulation in human tissue and bio magnifications through the food chain creates both human health and environmental problems[35].

Exposure and accumulation of heavy metals from multiple sources has been linked with developmental retardation, various cancers, kidney damage, autoimmunity, cramps, nausea, vomiting, diarrhea, stomach pain, headache, sweating, and a metallic taste in the mouth (some more symptoms are show in the table 1:1); In some cases the exposure may even lead to death if it takes place over a long time or the concentration was a very high, more information about the symptoms for some toxic metal ions can be found in a book titled Environmental chemistry, written by Dr. B. K. Sharma.[36]

The monitoring of these metal ions has become essential in the surrounding environment for health risk assessment.[37] There are several classical analytical techniques used for the investigation of their concentrations as mentioned before, but recently, electro-analytical methods such as anodic stripping voltammetry potentiometric stripping analysis and electrochemical quartz crystal microbalance became commonly used for such investigations.[38,39] For example, the EQCM is often used for the in-situ monitoring of the electrode mass. It is also possible to estimate the change in the viscosity (η) and density (ρ) of the electrolyte near the electrode by means of EQCM.[40,41] TC values for some toxic metals together with common clinical symptoms (when they reach the human) are calculated in table 1:1.

Table 1:1 show transfer coefficient for some metal ions from soil to plant and the symptoms caused at the human being, by each one.

Metal	TC Transfer coefficient (from soil to plant)	Symptoms of some common toxic metals (when they reach human body)
Cr^{6+}	0.01-0.1	Disorders skin and respiratory, ulceration of skin, inhaled it causes cancer.
Pb^{2+}	0.01-0.1	Anaemia, disruption of haemoglobin synthesis, damage to nervous, brain and kidneys.
Cd^{2+}	1-10	Cramps, nausea, vomiting, diarrhoea and disorders of respiratory system and kidneys
As^{3+}	0.01-0.1	Skin cancer, hyper-pigmentation, keratosis, black foot disease.
Ni^{2+}	0.1-1	Dermatitis; myocarditis, encephalopathy.
Cu^{2+}	0.1-10	Vomitus, irritation, hemorrhage, hemolysis.
Co^{2+}	0.01-0.1	Metallic taste in the mouth, cardiomyopathy and goiter.

1.2 Thiols

Since gold surface is inert, it has to be modified by using some ligands in order to make it more effective and selective for the selected metal ions, and for this purpose thiols (which tend to be interactive spontaneously with gold surface) were used.

Thiols (RSH) are class of sulphur-containing organic compounds (R) that have the ability to remove the mercury from its solutions as crystalline precipitates. Hence they are usually called mercaptans, which is an old term meaning (mercury capturing).[42, 43] This term has been generalized by the international union of pure and applied chemistry (IUPAC) to include any organic compound that has a sulfhydryl group or thiol group (functional group composed of a sulphur and a hydrogen atom -SH).[44]

In general, the deprotonated form (RS^-) called a thiolate which more chemically reactive than the protonated thiol form (RSH).

1.2.1 Physical and chemical properties of thiols

Thiol compounds can be easily distinguished from the other chemical compounds due to their following physical properties:[45, 46, 47]

- Highly flammable
- Low molecular weight thiols have an associated stench
- They have lower boiling points and less soluble in water than analogous alcohols.
- Their bond has relatively low polarity than analogous alcohols.
- Show little association by hydrogen bonding

Table 1:2 shows a comparison between some thiols and analogues alcohols regarding boiling point.

Thiol	bP c^{o}	Alcohol	bP c^{o}
Methane thiol	6	Methanol	65
Ethane thiol	35	Ethanol	78
1-Butane thiol	98	1-Butanol	117

Regarding chemical properties all thiols are strong irritants and can be toxic at high concentration, they also have good ability to capture mercury atoms from their solutions. Thiols are stronger in their acidity than analogous alcohols, and easier oxidized as in the following reaction:

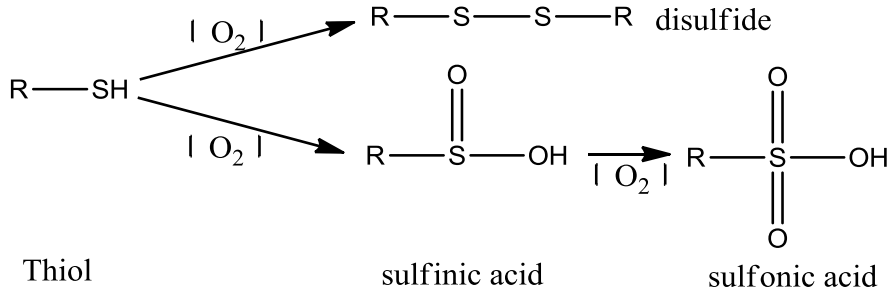

Reaction 1-1 represents the oxidation reaction process of thiol compounds.

1.2.2 Self - assembled monolayer of thiols

Self-assembly as a term refers to the spontaneous formation of alkyl thiols molecules , which forms as a special structure in few nanometers thickness on the surface[48]. These molecules are connected with substrate in such a way to form very complex structures with lower degrees of freedom (immobilised). Some SAMs can be easily formed by spontaneous adsorption (self-organise) from aqueous phase on clean metal[49] and others can be more difficult. The kinetics of the SAM adsorption goes through a two-step process[50]. In the initial step a fast growth of the SAMs (80-90 % of the final value of surface coverage or thickness) occurs within the first 2-3 minutes. This is followed by a slower step in which film thickness approach an equilibrium value in an approximate timescale of 10 – 20 h[51-52]. Many factors can influence the properties of SAMs such as the chain length, the functionality of the end group, nature of the solvent, immersion time and the surface morphology of the underlying substrate (electrode).

Alkanethiols are the most common example as a SAMs on metals (Au & Ag) or even on semiconductor surfaces (GaAs & Si oxide). Each molecule of alkanethiol can be divided in three different parts: the head (linking group), the backbone (main chain), and the terminal specific group (molecules attend to be deposited must have an active functional groups) as in this simple structure.[53, 54]

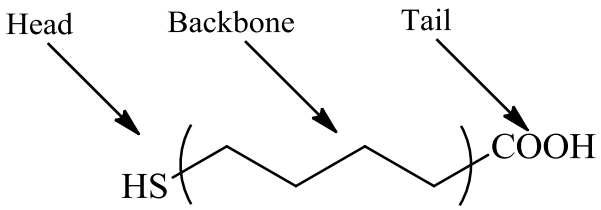

Figure 1:1 represents the main components of any alkanethiol.

In case of aliphatic thiol, sulphur atom links the main chain to the metal surface through a strong covalent bond (40-45 kCal / mol) by losing of a hydrogen atom, in order to form gold thiolate[55], see Figure 1:*2*, in certain orientation and angle, where α is the angle between the molecular backbone and the surface normal direction.[56, 57] After the formation of SAM, all physical and chemical properties are controlled by the end group (hydroxyl and carboxyl groups give hydrophilic layer, while a functional group such methyl can turns the layer hydrophobic)[58].

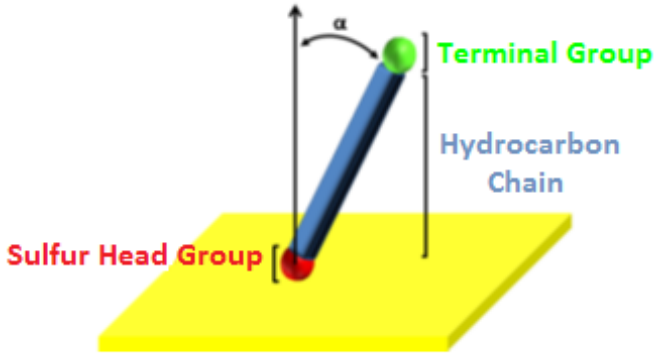

Figure 1:2 cartoon representation of a thiol adsorbed on an Au (111) surface.

1.2.3 Chemisorpion and Physisorption processes on substrates

The process of the interaction between the adsorbate and the substrate, that takes place via Van der Waals forces, called physisorption. Almost all gases undergo a physisorption when they contact with surfaces. Any molecule attached with substrate in such a way has the ability to leave the surface spontaneously after a certain time. The energy that is lost in this process is at the same magnitude of the condensation enthalpy (about 20kJ mol^{-1}); typically, physisorption is considered the first step to chemisorption.

Chemisorption represents chemical bond between the physisorbed molecule and the substrate with a high value for the enthalpy compared with physisorption (about 200kJ

mol^{-1}) which makes this process highly exothermic. Accordingly these processes can be identified by measuring the related energies.[59-61]

1.3 Ionic liquids

The fact that the many of heavy metal ions are toxic, this requires developing the alternative methods to extract them from the environment. Strong inorganic acids were used for this purpose but they are toxic, expensive and difficult to deal with. However, ionic liquids have desirable properties since the majority of them are inexpensive, safe and handy.

In general ionic liquids can be separated into first and second generation liquids, where the first generation liquids are those based on eutectics and second generation have discrete anions[62], and the first paper related to synthesis of ionic liquid (IL) was published in 1914 by Walden[63], but at that time, this report gained a little attention. The first generation of ILs was unstable in air and water.[64-66]

In 1992 another IL based on imidazolium has been reported by Wilkes and Zaworotko, which was very stable in both air and water environments, and therefore researchers used this IL in different applications and experiments.[67] After few years, Suarez and his colleagues managed to prepare IL as organic phase which become easier to separate from aqueous phase. Lately, the development of ILs for specific tasks began increasing rapidly, and researchers demonstrated that the structure of ionic liquids can fabricate many desirable properties. Consequently, they are often referred to as designer solvents.[68] Table 1-3 shows the most common groups of cations, and the anions[69], which are often used for preparing ionic liquids.

Table1:3 shows the most common cations and anions used to prepare ionic liquids.

	Some discrete anions used in preparing IL		Some discrete cations used in preparing IL	
	Name	structure	Name	structure
Water-miscible	Halides water-miscible	Cl^-, Br^-, ….etc	Imidazolium	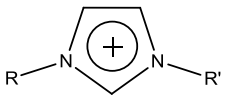
	Nitrates & Acetate	CH_3COO^-, NO_3^-	Pyrazolium	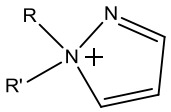
	chloroaluminates	$[Al_2Cl_4]^-$, $[Al_2Cl_7]^-$	Thiozolium	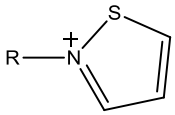
	Tetra fluoroborate	BF_4^-	Pyrrolidinium	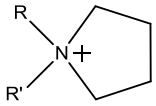
	dicyanamide	$N(CN)_2^-$	Pyridinium	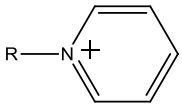
	alkyl sulphates water-immiscible	RSO_4	Tetra alkyl ammonium	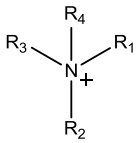
	hexafluoroborate	BF_6^-	Tetra alkyl phosphonium	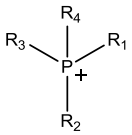
Water-immiscible	hexafluorophosphates	PF_6^-	Tri alkyl sulfonium	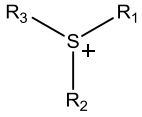

Typically, ionic liquids are composed of one ion with a delocalized charge and another organic component, which prevents the formation of a stable crystal lattice, thus they are used in large-scale chemical applications as reagents and solvents and the most important applications are extraction, electro-analytical chemistry, sensing and

chromatography.[70] The following bullet points highlight some of the key features of ionic liquids.[62, 71-73]

1. Negligible vapour pressure
2. Non-flammable
3. Its melting point normally below 100C^{o}
4. Higher density than water (1-1.6 g cm^{-3})
5. Often, high viscosity
6. Bulky organic cations and poorly coordinating inorganic anions
7. Most of them, easy to prepare
8. Ionic liquids represent an excellent solvent for organic, inorganic and polymeric materials
9. Most ionic liquids have good thermal stability
10. Surface tensions of ILs are lower than that for water (72.7 Nm^{-1} at 20 C^{o}) but higher than the values for dodecane (25.6 Nm^{-1} at 20 C^{o}). As the alkyl chain length on the ILs increases the surface tension value decreases towards the values for the alkanes.

1.4 Deep eutectic solvent

Since we talked about ionic liquid, it may be worthy to give a brief definition of eutectic solvent based on ionic liquid. The term eutectic comes from Greek language, where word Eutektos means easily melted[62].

Eutectic system is a mixture of two chemical compounds (A & B) in certain chemical composition at which the minimum freezing point occurs, It should be noted, that there is only one unique mixture of A and B, that has a lower melting point than any other mixture of these compounds. This particular mixture is called the eutectic mixture.

The melting point of the eutectic mixture is called the eutectic point as in figure 1:3. As an example for this type of green solvents; in 2007 Abbott and his group managed to prepare a new class of IL based on zinc chloride and donor molecules (acetamide or urea).[74]

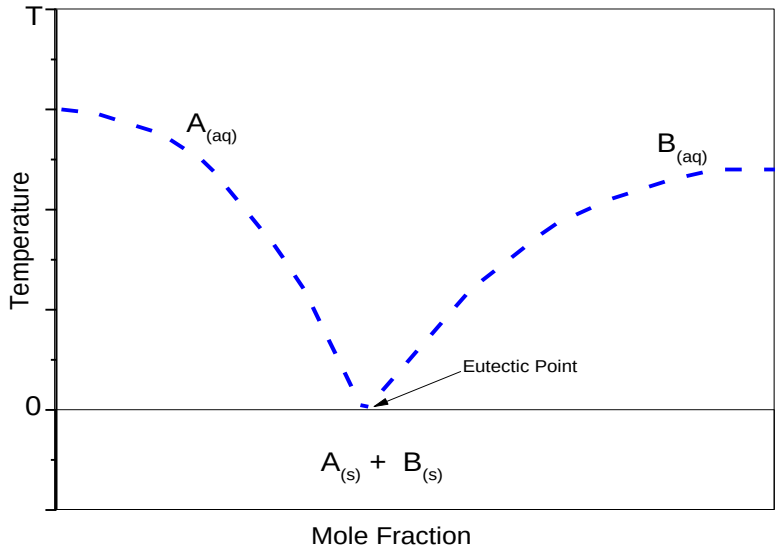

Figure 1:3 schematic representation of a eutectic point on a two component phase diagram.

1.5 Aims and objectives

There are two fundamental aims of the research; the first one is to develop a sensitive electrochemical sensor in order to determine the concentration of heavy metal environmental pollutants such as Ni^{2+}, Co^{2+} and Pb^{2+} using a technique that is rapid, accurate and mobile for felid measurements. The techniques that will be used in the experiments are cyclic voltammetry (CV) and quartz crystal microbalance (QCM), by using one side of the gold surfaces in QCM as modified working electrode (electrochemical sensor). These two techniques are very helpful tools to study and investigate the amount of the element ions at very low concentrations; and they are also easy to use and cheap, moreover they do not require well-equipped labs. The other techniques that will be utilised are Raman Spectroscopy and X-ray Photoelectron

Spectroscopy (XPS), in order to monitor the surface compositions, and to find out the real surface structure. In this study, quartz crystal microbalance will be modified with self-assembled monolayer (SAM), which provided with certain ligands. The purposes of using this technique is to investigate trace metal ions such as lead, cobalt and nickel in aqueous media (Simulated samples). The performance of the most effective ligand towards individual species in the solution will also be detected. For more accuracy the value of interested metal ions should be evaluated many times by using QCM, also Raman and XPS techniques should be used, with the aim of confirming any definite outcome.

The second aim in this work is to develop an extraction technique for monitoring the heavy metal pollutants using ionic liquid electrolytes as an alternative method for aqueous extraction procedure which typically require strong inorganic acids. So in short, this investigation needs to go through the following stages:

1. Selected thiols will be bound to the surface of gold electrodes to form self – assembled monolayer with carboxyl groups as chelating agents. At this point I would take about the chemistry, and how this would be achieved, then discuss how the QCM sensor would work.
2. The quality of the created self – assembled monolayer will be studied and investigated by using different kinds of techniques in order to find out the best thiol to form an effective ligand.
3. Modified electrodes mounted on quartz crystal resonators will be exposed to metal ion solutions (single and mixed ions) and their capabilities for electrochemical and acoustic wave detection will be determined.

4. Selectivity of the SAM modified electrodes towards targeted metal ions will be studied by estimating the binding constants in single and mixed ion solutions after fitting the data to different isotherms.
5. The immiscible ionic liquid will be used to extract the intended metal ions from their aqueous solutions and for the first time QCM will be used in a special way to follow this process closely.
6. Confirming the extraction processes for each metal ion, by using some coloured indicators.

1.6 References

1. C. Braungardt, E. P. Achterberg and M. Nimmo, *Analytica Chimica Acta*, 1998, **377**, 205-215.
2. S. C. Ng, X. C. Zhou, Z. K. Chen, P. Miao, H. S. O. Chan, S. F. Y. Li and P. Fu, *Langmuir*, 1998, **14**, 1748-1752.
3. S. P. Dubey and K. Gopal, *Journal of Hazardous Materials*, 2007, **145**, 465-470.
4. M. Kazemipour, M. Ansari, S. Tajrobehkar, M. Majdzadeh and H. R. Kermani, *Journal of Hazardous Materials*, 2008, **150**, 322-327.
5. J. M. Pacyna and E. G. Pacyna, *Environmental Reviews*, 2001, **9**, 269-298.
6. J. Nriagu, in *Control and Fate of Atmospheric Trace Metals*, eds. J. Pacyna and B. Ottar, Springer Netherlands1989, vol. 268, ch. 1, pp. 3-13.
7. P. K. Rai and B. D. Tripathi, *Toxicological & Environmental Chemistry*, 2008, **90**, 247-257.
8. Y. Cui, Y.-G. Zhu, R. Zhai, Y. Huang, Y. Qiu and J. Liang, *Environment International*, 2005, **31**, 784-790.
9. A. Bielicka, I. Bojanowska and A. Wisniewski, *Polish journal of environmental studies*, 2005, **14**, 5-10.
10. *Understanding Environmental Pollution*, Cambridge University Press.
11. A. Qishlaqi, F. Moore and G. Forghani, *Environmental monitoring and assessment*, 2008, **141**, 257-273.
12. S. Barbagallo, G. Cirelli and S. Indelicato, *Wastewater Reclamation, Recycling and Reuse*, 2001, **43**, 43-50.
13. S. S. Amiri, H. Maralian and A. Aghabarati, *African Journal of Biotechnology*, 2008, **7**.

14. N. Sridhara Chary, C. T. Kamala and D. Samuel Suman Raj, *Ecotoxicology and Environmental Safety*, 2008, **69**, 513-524.

15. K. P. Singh, D. Mohan, S. Sinha and R. Dalwani, *Chemosphere*, 2004, **55**, 227-255.

16. B. J. Alloway, *Heavy metals in soils*, Blackie Academic & Professional1995.

17. M. Athar and S. B. Vohora, *Heavy Metals And Environment*, New Age International Publishers Limited1995.

18. C. A. Brebbia and J. S. A. do Carmo, *Water Pollution VIII: Modelling, Monitoring And Management*, WIT Press2006.

19. J. DeZuane, *Handbook of Drinking Water Quality*, Wiley1997.

20. J. Guertin, J. A. Jacobs and C. P. Avakian, *Chromium(VI) Handbook*, Taylor & Francis2004.

21. T. Bajda, *Science of The Total Environment*, 2005, **336**, 269-274.

22. N. A. Greene and V. R. Morris, Examination of Heavy Metals and Particulate Matter Exposures and Effects in Susceptible Wards in the Washington, DC Region, 2004.

23. L. Järup, *British medical bulletin*, 2003, **68**, 167-182.

24. Ú. O. Spring, *Water resources in Mexico*, Springer Berlin Heidelberg2011.

25. R. C. Gupta, *Veterinary Toxicology: Basic and Clinical Principles*, Elsevier Science2011.

26. M. A. Adams, *Shellfish and Public Health: Lead, Cadmium, Chromium, Arsenic, and Nickel in Shellfish*, DIANE Publishing Company1994.

27. S. Berglund, R. D. Davis, P. L'Hermite and C. o. t. E. Communities, *Utilization of Sewage Sludge on Land: Rates of Application and Long-Term Effects of Metals*, Springer1984.

28. W. H. Organization, *Guidelines for drinking-water quality: Vol. 1: Recommendations*, WORLD HEALTH ORGN2004.
29. P. Ravenscroft, H. Brammer and K. Richards, *Arsenic Pollution: A Global Synthesis*, Wiley2011.
30. D. G. Barceloux and D. Barceloux, *Clinical Toxicology*, 1999, **37**, 239-258.
31. D. C. Adriano, *Trace Elements in Terrestrial Environments: Biogeochemistry, Bioavailability, and Risks of Metals*, Springer2001.
32. A. C. Twort, D. D. Ratnayaka and M. J. Brandt, *Water supply*, Arnold/IWA Publishing2000.
33. N. F. Gray, *Drinking water quality*, Cambridge University Press2008.
34. D. G. Barceloux and D. Barceloux, *Clinical Toxicology*, 1999, **37**, 201-216.
35. S. Dudka and W. P. Miller, *Journal of environmental science and health. Part. B, Pesticides, food contaminants, and agricultural wastes*, 1999, **34**, 681-708.
36. B. K. Sharma, *Environmental Chemistry*, Krishna Prakashan.
37. B. A. Fowler, G. F. Nordberg, M. Nordberg and L. Friberg, *Handbook on the Toxicology of Metals*, Elsevier Science2011.
38. E. P. Achterberg and C. Braungardt, *Analytica Chimica Acta*, 1999, **400**, 381-397.
39. E. P. Achterberg and C. M. G. van den Berg, *Marine Pollution Bulletin*, 1996, **32**, 471-479.
40. D. A. Buttry and M. D. Ward, *Chemical Reviews*, 1992, **92**, 1355-1379.
41. H. Miyashiro, Y. Katayama, M. Watanabe and T. Miura, 2013.
42. T. N. Sorrell, *Organic chemistry*, University Science Books2006.
43. B. MEHTA and M. MEHTA, *ORGANIC CHEMISTRY*, PHI Learning2005.
44. H. S. Stoker, *Organic and Biological Chemistry, 6th ed*, Brooks/Cole2011.

45. C. S. Foote, W. H. Brown, B. L. Iverson and E. V. Anslyn, *Organic Chemistry*, BROOKS COLE Publishing Company2011.

46. H. S. Stoker, *General, Organic, and Biological Chemistry*, BROOKS COLE Publishing Company2012.

47. F. A. Bettelheim, W. H. Brown, M. K. Campbell and S. O. Farrell, *Introduction to General, Organic, and Biochemistry*, Brooks/Cole, Cengage Learning2010.

48. J. C. Love, L. A. Estroff, J. K. Kriebel, R. G. Nuzzo and G. M. Whitesides, *Chemical Reviews-Columbus*, 2005, **105**, 1103-1170.

49. J. I. E. Xu and H.-L. Li, *Journal of Colloid and Interface Science*, 1995, **176**, 138-149.

50. W. Pan, C. Durning and N. Turro, *Langmuir*, 1996, **12**, 4469-4473.

51. D. K. Schwartz, *Annu Rev Phys Chem*, 2001, **52**, 107-137.

52. G. Haehner, C. Woell, M. Buck and M. Grunze, *Langmuir*, 1993, **9**, 1955-1958.

53. R. Yamada and K. Uosaki, *Langmuir*, 1997, **13**, 5218-5221.

54. H. Wano and K. Uosaki, *Langmuir*, 2001, **17**, 8224-8228.

55. S. D. Evans and A. Ulman, *Chemical Physics Letters*, 1990, **170**, 462-466.

56. L. H. Dubois and R. G. Nuzzo, *Annual review of physical chemistry*, 1992, **43**, 437-463.

57. A. R. Bishop and R. G. Nuzzo, *Current Opinion in Colloid & Interface Science*, 1996, **1**, 127-136.

58. D. L. Allara, *Biosensors and Bioelectronics*, 1995, **10**, 771-783.

59. D. J. Lavrich, S. M. Wetterer, S. L. Bernasek and G. Scoles, *The Journal of Physical Chemistry B*, 1998, **102**, 3456-3465.

60. S. M. Wetterer, D. J. Lavrich, T. Cummings, S. L. Bernasek and G. Scoles, *The Journal of Physical Chemistry B*, 1998, **102**, 9266-9275.

61. B. Mutaftschiev and N. A. T. O. S. A. Division, *Interfacial Aspects of Phase Transformations*, Springer1982.

62. F. Endres, D. MacFarlane and A. Abbott, *Electrodeposition from Ionic Liquids*, Wiley2008.

63. M. D. Joshi and J. L. Anderson, *RSC Advances*, 2012, **2**, 5470.

64. R. J. Soukup-Hein, M. M. Warnke and D. W. Armstrong, *Annual review of analytical chemistry*, 2009, **2**, 145-168.

65. X. Han and D. W. Armstrong, *Accounts of chemical research*, 2007, **40**, 1079-1086.

66. M. Lopez-Pastor, B. M. Simonet, B. Lendl and M. Valcarcel, *Electrophoresis*, 2008, **29**, 94-107.

67. F. Endres and S. Z. El Abedin, *Physical Chemistry Chemical Physics*, 2006, **8**, 2101-2116.

68. S. Keskin, D. Kayrak-Talay, U. Akman and Ö. Hortaçsu, *The Journal of Supercritical Fluids*, 2007, **43**, 150-180.

69. N. V. Plechkova and K. R. Seddon, *Chem Soc Rev*, 2008, **37**, 123-150.

70. S. Pandey, *Analytica Chimica Acta*, 2006, **556**, 38-45.

71. K. N. Marsh, J. A. Boxall and R. Lichtenthaler, *Fluid Phase Equilibria*, 2004, **219**, 93-98.

72. J. Huddleston and R. Rogers, *Chemical Communications*, 1998, 1765-1766.

73. A. Shariati and C. J. Peters, *The Journal of Supercritical Fluids*, 2003, **25**, 109-117.

74. A. P. Abbott, J. C. Barron, K. S. Ryder and D. Wilson, *Chemistry*, 2007, **13**, 6495-6501.

Contents

2 Methodology

2.1 Electrochemical techniques

Cyclic voltammetry (CV) and quartz crystal microbalance (QCM) are the main techniques used in this study. The basic principles of these two techniques will be presented in this chapter, as well as the Raman and x-ray photoelectron spectroscopy (XPS) techniques.

2.1.1 Cyclic voltammetry

Cyclic voltammetry was first reported in 1938 and described theoretically by Randles.[1] This technique is still considered to be the most appropriate electrochemical approach in order to elucidate the nature of electrochemical processes. It provides good insight into the electron-transfer reactions and also helps the study of chemical kinetics that often follows this process. Furthermore, this technique is often used in different kinds of adsorption taking place at electrode surface.

CV is based on the relationship between current and voltage, where useful information about the analyte can be drawn from the measurement of current density (current normalised to the electrode surface area) and the applied potential producing a cyclic voltammogram.

The equipment required to perform cyclic voltammetry consists of potentiostat connected to three electrodes (working, reference, and auxiliary) immersed in sample solution. The potentiostat applies and maintains the potential between the working and reference electrode while at the same time measuring the current at the working electrode. (During the experiment, charge flows between the working electrode and the

auxiliary electrode) The resulting cyclic voltammogram is recorded by the computer as a graph of current versus potential.

An example of cyclic voltammogram for an electrochemically solution-phase reversible electron transfer process is shown in figure 2:1.

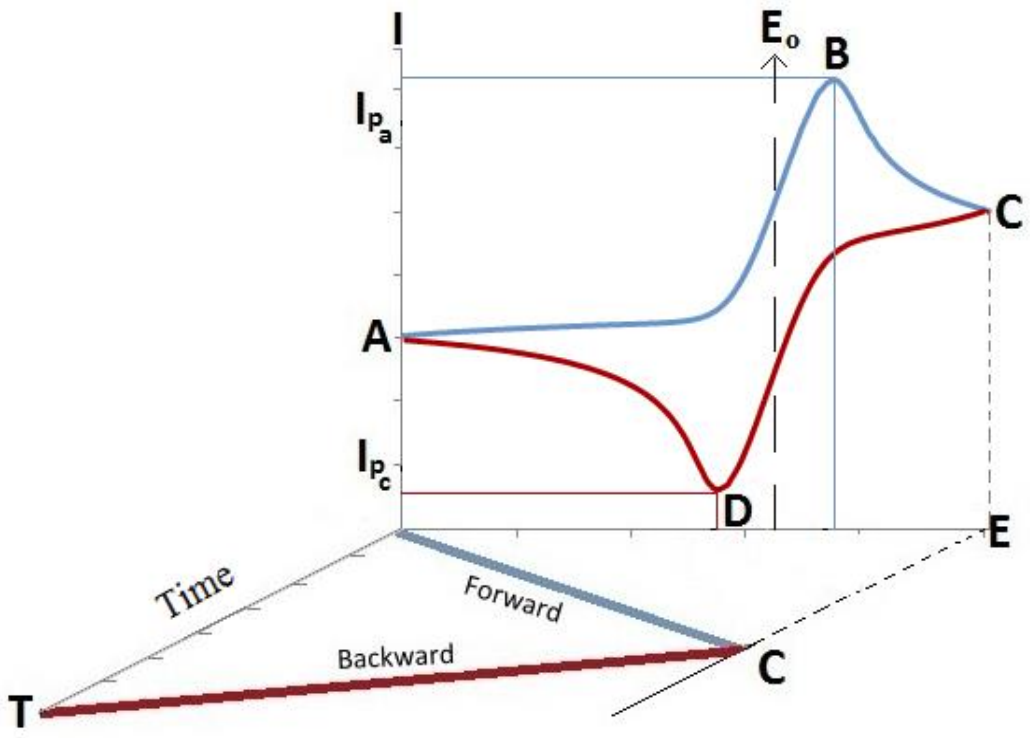

Figure 2:1 is typical cyclic voltammogram for a reversible redox process, representing the change in the current with changing voltage, combined with the changes in voltage with time.

Figure 2:1 shows the oxidation process starts from (A) the initial potential to (C) the switching potential, where the scan is running in positive direction an oxidation reaction will take place (blue part of the voltammogram). The resulting current is called anodic current (I_a) and the highest point in the curve named anodic peak current (I_{pa}). With a corresponding value of E occurs at (B) called the anodic peak potential (E_{pa}), and it is

reached when all of the species at the electrode surface has been oxidized; in this stage, the current is limited by diffusion of the reactant species to the electrode surface.

At point C, potential switching to scan back negatively from C to A again, where a reduction process is taking place (red part of the voltammogram) at a constant potential sweep rate (scan rate applied can vary from a few millivolts per second to a hundred volts per second). Likewise current termed cathodic current (I_c) with cathodic peak current (I_{pc}) at lowest point (D), and also the potential at D would be cathodic peak potential (E_{pc}). In this case the majority of the species at the electrode surface should be reduced now.

There are some major factors that govern the reaction rate and current at the electrode, such as mass transfer to the electrode surface, electrode surface area, and the rate of the reaction. Regarding the peak characterisations (width and height), they can also be affected by sweep rate, electrolyte concentration and electrode material.[2, 3]

2.1.1.1 Electrode solution system

In a typical three electrode cell, the potential is applied to the working electrode (Au or Pt) with respect to a reference electrode (SCE or Ag/AgCl), while the role of an auxiliary electrode (Pt net) completes the electrical circuit.

The transfer of charge to the electrode surface can be described either as a homogeneous phase, when it is carried out through an agent, or heterogeneous, when it is carried out through an electrode, so the electrode reaction is always a heterogeneous process.

In the electrode solution system, there are four regions; electrode surface, double layer (1-10 nm), diffusion layer (10^3-10^6 nm) and the bulk of the solution[4], as depicted in the next figure 2:2.

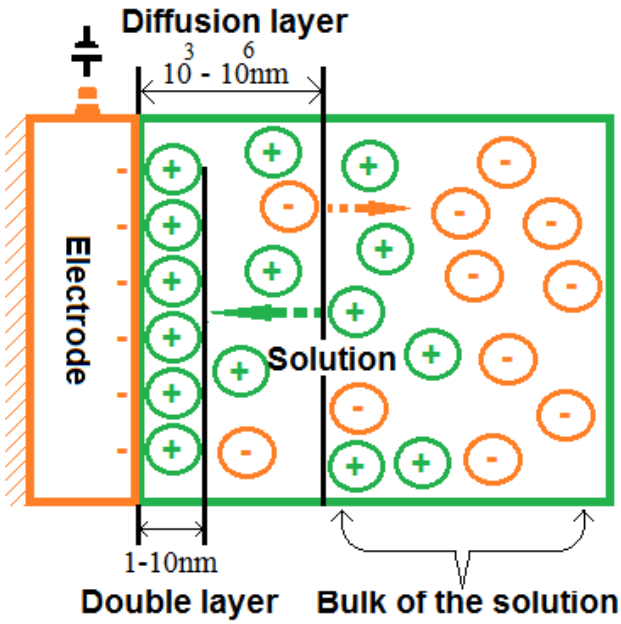

Figure 2:2 shows the characterize zones for electrode / solution system at negatively charged electrode.

In general the reaction between redox species and electrode surface has to be one of two different processes: Faradaic or non-Faradaic.[5]

Faradaic process takes place when redox reaction of the species is controlled by Faraday's law[6], this shows that the amount of charge is proportional to the amount of reactant converted in moles. In this case the electrode surface is classified as a charge transfer electrode because the extent of the reaction depends on the charge passing through the electrode surface. However, in non-Faradaic process, adsorption and desorption of the species at electrode surface are most likely to produce an electric current.

$R \rightleftharpoons O + ne^-$ 2-1

In the above reaction, if the electron transfer rate in forward and reverse direction is the same (high), the reaction is described as a reversible reaction, as in figure 2:3.

Additionally the difference between anodic and cathodic peak potentials at room temperature can be tested and measured:

$$\Delta E_p = E_{p_a} - E_{p_c} = \frac{59}{n} \text{ mV}, \quad 2\text{-}2$$

Where n is the number of electrons involved. This value should be independent of the scan rate, but in real practical experiments ΔE_p slightly increases with scan rate due to the resistance of the solution (R_s) between the working and the reference electrodes.[7]

In a reversible process the current is controlled by mass transport, and peak current can be calculated by using Randles-Sevcik equation[8]:

$$i_p = (2.69\times10^5)\, n^{3/2} A D^{1/2} C v^{1/2} \quad 2\text{-}3$$

This equation is valid at room temperature (25^{o}C), where i_p is peak current in amps, n is the number of electrons transferred in the redox event, A is the electrode area in cm^2, D is the diffusion coefficient in cm^2/s, C is the concentration in mole/cm^3 and ν is the scan rate in V/s.

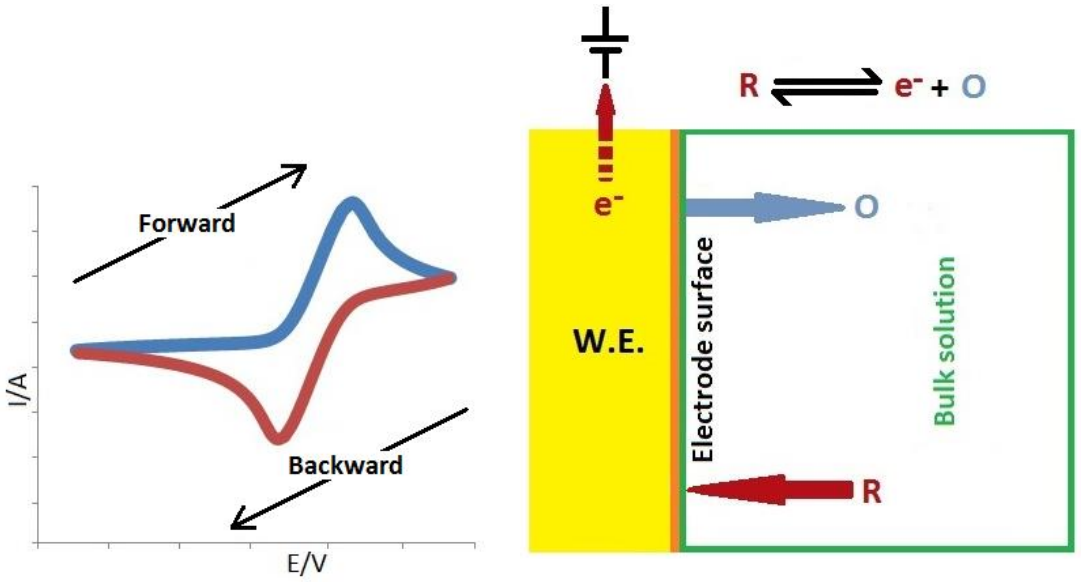

a **b**

Figure 2:3 (a) typical cyclic voltammogram for reversible reaction, (b) schematic diagram represent electron transfer process at planar electrode.

On the other hand at irreversible process, backward reaction will be negligible and the reaction can be expressed as follows:

$$O + ne^- \longrightarrow R \qquad 2\text{-}4$$

In this case ΔE_p is dependent on the scan rate because the system is no longer at equilibrium.[9] Figure 2:4 is representing this process, and the difference between anodic and cathodic peak potentials is as follows:

$$E_p = E^o - \frac{RT}{\propto nF}\left[0.78 - \ln\frac{K^o}{D^{\frac{1}{2}}} + \ln\left(\frac{\propto nF\nu}{RT}\right)^{\frac{1}{2}}\right] \qquad 2\text{-}5$$

Where $\propto$ the electron transfer rate, n is the number of electrons involved, K^o is the heterogeneous electron transfer coefficient in cm/s, and the rest of symbols are as

mentioned before. Randles-Sevcik equation will also undergo some little changes to be suitable for calculating peak current.

$$i_p = 2.99\times10^5 n\,[(1-\alpha)n]^{\frac{1}{2}}\,AC(Dv)^{1/2} \qquad 2\text{-}6$$

Where α is the rate of electron transfer, and the rest of the symbols are the same as mentioned before with equation 2-7.

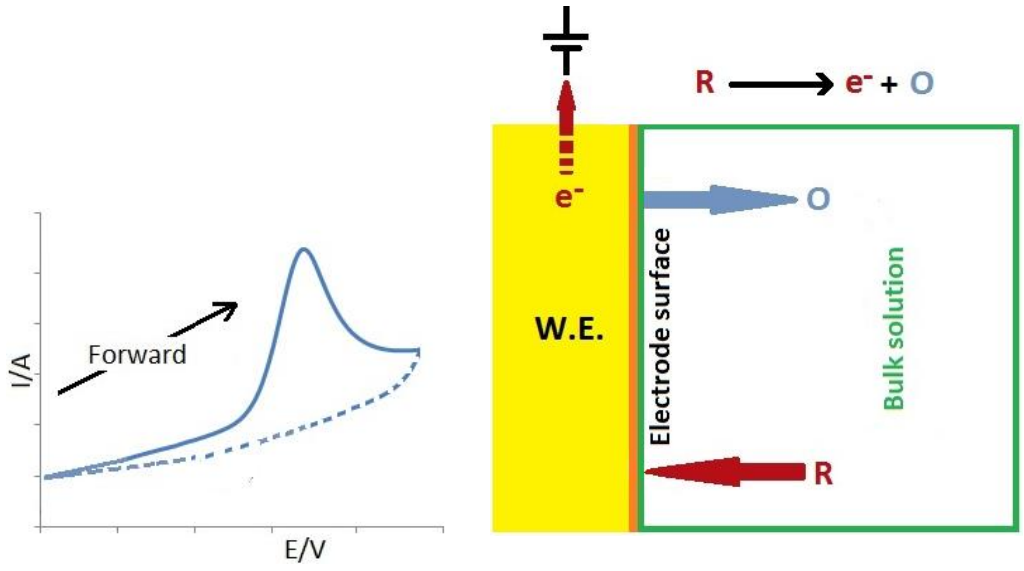

a **b**

Figure 2:4 (a) typical cyclic voltammogram for irreversible reaction, (b) schematic diagram represent electron transfer process at planar electrode.

Between reversible and irreversible reactions there is another process which is termed quasi-reversible, where peak current is increasing with $\nu^{1/2}$ but not linear, also ΔE_p is bigger than $\frac{0.0059}{n}$ V. In quasi-reversible reaction current is controlled by both of charge transfer kinetic and mass transport[9, 10].

2.1.2 Quartz crystal microbalance

Quartz crystal microbalance is an extremely sensitive device, capable of detecting mass changes; the core of quartz crystal microbalance is a quartz oscillator, which can be excited by applying an alternating voltage, and that's known as piezoelectric phenomena. Piezoelectric term, mainly comes from the Greek language, where (piezein) means (press).[11, 12]

This small powerful tool consists of a very thin quartz crystal wafer in certain cut, since it can either be a wafer crystal in AT-cut mode by cutting the quartz in 35.15^{o} (It is the angle at which a resonator plate is cut from the quartz crystal in relation to the original crystallographic axes), or BT-cut, where cutting angle is 49^{o}. At these two different orientations the temperature coefficient is always close to zero (0-50^{o}C).[13, 14, 15] A clear idea can be found in figure 2:5.

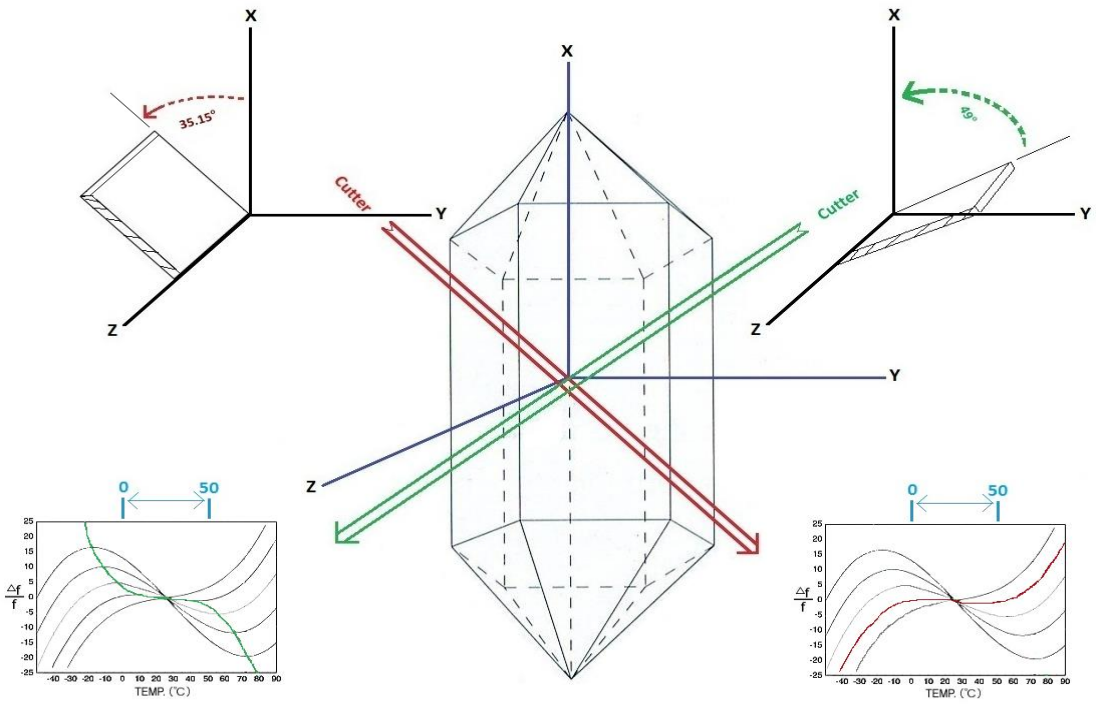

Figure 2:5 shows Schematic diagram of AT & BT-cut quartz crystal plates from a nature quartz stone.

The crystal wafer is sandwiched between two noble metal electrodes (often gold or Platinum) as in figure 2:6. These electrodes have two purposes; (1) to allow the alternating electric current to pass across the crystal while detecting the quartz oscillation; (2) one of them can play a working electrode role in an electrochemical quartz crystal cell.[16]

QCM is mainly used as a mass sensor for a small mass change, down to 10^{-4} ng (gravimetric analysis)[17], or to probe material properties so this technique has a wide variety of applications.[18, 19]

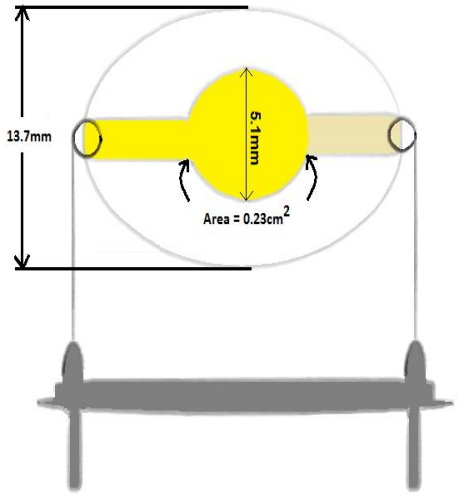

Figure 2:6 represents some characteristics of a typical piezoelectric crystal coated with gold.

2.1.2.1 Piezoelectricity

In 1880 Curie discovered that compression, torsion or electrical changes on the surface of a quartz crystal, any of them can causes a kind of deformation; this phenomenon is called the piezoelectric effect as previously mentioned. The linear deformation of the crystal as a result of an applied electric field is referred to as reciprocal piezoelectric effect[20], figure 2:7.

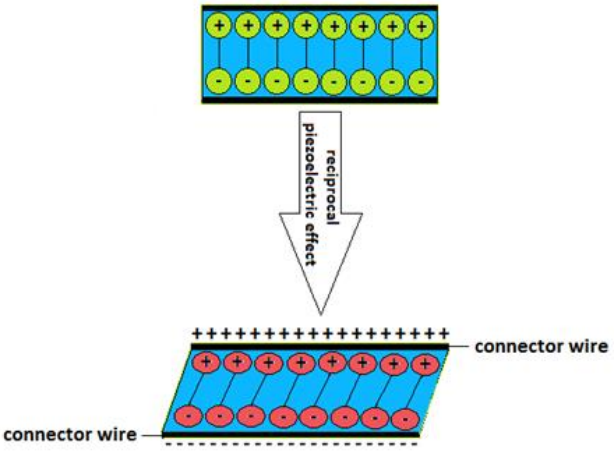

Figure 2:7 phenomenon of reciprocal piezoelectric effect

Piezoelectricity is fundamental characteristic in quartz crystal microbalance technique, which can be depicted mathematically as follows:

$\vec{p} = e^{\vec{x}}$ 2-8

Where $\vec{p}$ is an induced polarization, $\vec{x}$ is a sufficiently small stretch. However this exponential relationship is appropriate only for a small strain.

2.1.2.2 Sauerbrey equation

A linear relationship between frequency change Δf and mass loading Δm was derived by Sauerbrey in 1959, since he embodied Δf for the resonator with Δm in equation considered to be a very important equation in this field.[21, 22, 17]

$$\Delta f = -\frac{2f_o^2}{A\sqrt{\rho_q \mu_q}} \Delta m \qquad 2\text{-}9$$

Where: ρ_q is the density of quartz (2.64 g cm^{-3}), μ_q is the shear modulus At-cut (2.94 gcm^{-1} s^{-2}), f_o is the resonant frequency (Hz), A is the active crystal area (Area between electrodes in cm^2).

This equation is based on a model with the following assumptions:

- The deposited mass must be rigid.
- The added mass has to be evenly distributed.
- The added mass should be less than 2% of the crystal mass.

Under these conditions, inserting the fundamental properties of quartz, and for resonators with a base frequency of 10 MHz, equation 2-8 becomes:

$$\Delta m = -1.1\ \Delta f \qquad 2\text{-}10$$

In general, when quartz crystal electrode operates in aqueous solution, unlike in air, the resonator will be viscously coupled to the contacting liquid. This results in damping due to viscous energy dissipation and effective mass coupling of a viscously entrained layer. The frequency shift associated with this layer is given by[23]:

$$\Delta f = -f_o^{3/2}(\eta_L\ \rho_L/\pi\ \eta_q\ \rho_q)^{1/2} \qquad 2\text{-}10$$

where η_L is the conventional viscosity of the liquid and ρ_L is the density of the liquid.

2.1.2.3 Electrochemical quartz crystal microbalance (EQCM):

EQCM offers the possibility to measure and study very small mass and density changes at the surface of an electrified interface, which allows the in- situ detection and monitoring of species at a microscopic level, (as small as a few nanograms).[24, 25] In this case various electrochemical parameters, such as potential, current, and charge at the working electrode, are conducted simultaneously with the acquisition of the corresponding frequency and resistance changes

To use a quartz crystal for the electrolysis; the electrodes must be connected and controlled electronically, in addition the measurement has to be carried out in liquid. The examined response takes place on only one face of the crystal, which is in contact with aqueous solution.[26] In figure 2:8 schematic representations depicts the main components of EQCM technique.

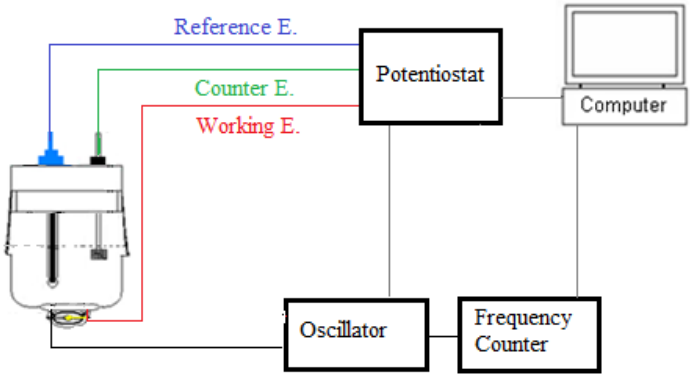

Figure 2:8 schematic representation of the structure of EQCM apparatus

2.2 Spectroscopic techniques

In addition to cyclic voltammetry and quartz crystal microbalance, Raman and x-ray spectroscopy (XPS) techniques were also used to study surface bound metal ions and compounds of material. In the following paragraphs some of the main characteristics and basic principles for these are discussed.

2.2.1 Raman spectroscopy

Raman spectroscopy is based on the phenomenon called Raman scattering, which was discovered by the Indian scientist named Raman in 1928. This technique is not destructive so that it has been successfully used in a wide range of possible applications.[27] A single mode laser source is used to illuminate the sample. This source should give appropriate energy to excite the molecules from the ground state to an excited electronic state (partial excitation for the electron) and then measuring the

scattered light caused by the following relaxation process, which is either stokes scattering when the emitted energy is weaker than the incident energy, or anti-stokes scattering when the emitted energy is stronger than the incident energy, while the process is called Rayleigh scattering if the energies for the incident and scattering light were the same as it can be seen in figure 2:9.

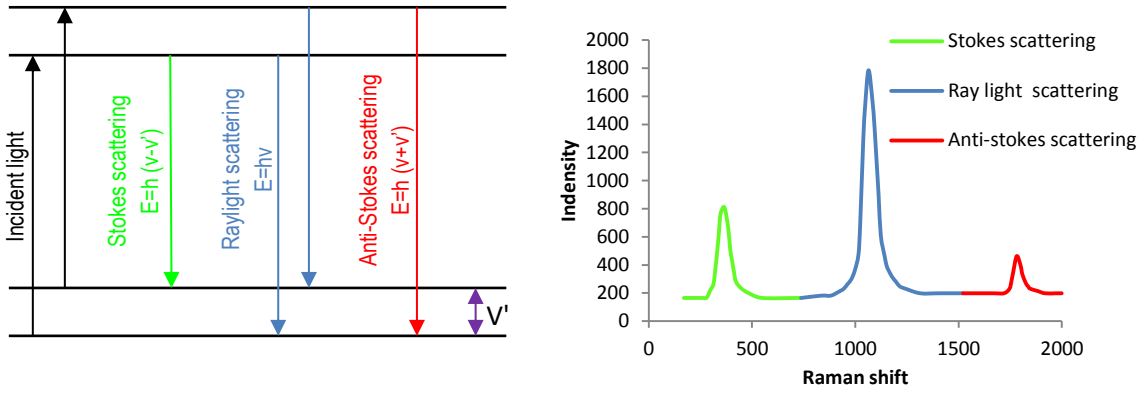

a b

Figure 2:9 (a) shows three different types of emitted radiations,where v' is the energy difference between the incident and scattered photons, (b) shows the peak intensity for each type.

Anti-Stokes lines are appreciably less intense than Stokes lines, and for that reason Stokes lines are the most commonly used part of the spectrum. Under restricted rules Raman shift equals to the vibrational energy of sample molecules ($cm^{-1} = \frac{1}{\lambda}$), which makes it highly specific, and can be used as a fingerprint of the immobilized molecules. Important information can be obtained about binding molecules and the orientation with any shifts of vibrational mode.[28, 29]

Raman spectrum represents the relation between the intensity of Raman scattered light and Raman shift. This technique is suitable for symmetric molecules, where vibration process of the molecules causes a change in the polarizability (α) which is in line with

centre preservation so that symmetric molecules are Raman active.[30] While IR is more convenient for asymmetric molecules since the vibration of the molecule causes dipole moment change and thus there is no centre of symmetry any more. Some differences between these two techniques can be found in the next table.

Table 2-1 comparison between Raman and infrared techniques

	IR	Raman
1	Absorption spectroscopy	Scattering spectroscopy
2	Required sample preparation	Does not required sample preparation
3	Vibrational mode of molecules	Momentary distortion of electrons
4	H_2 and N_2 Molecules can be detected	Such molecules can't be detected
5	Measurement background has a value	Zero-background measurement
6	Detection limit less sensitivity	Detection limit more sensitivity

2.2.2 Surface enhanced Raman spectroscopy

Surface enhanced Raman spectroscopy (SERS) is used to get a good enhancement of Raman signal from Raman-active analyte molecules on certain prepared metal surfaces often coinage metals (Au, Ag, Cu), where Raman intensity signal could increase by (10^4-10^6) times, and in some cases it reaches (10^{14})[31, 32], and the advantages here is both surface selectivity and high sensitivity, which allows it to be used in different systems (catalytic, biological, and organic systems) , whereas Raman is neither.[33, 34]

As previously mentioned, SERS is used in order to give a great enhanced for weak Raman signal. The enhancement was discovered by Fleischmann, Hendra and Mcquillain in 1974 at the University of Southampton, UK.[35] At that time, the prevailing idea was that the main factor behind the improvement was to increase the surface area[36], e.g. coated roughened silver with pyridine gave it enhancement of Raman spectrum. However, Jennmaire and Van Duyne demonstrated that surface area is not the main factor, which confirmed at the same time by Albrecht and Creighton.[37]

So far the real mechanisms of SERS are still not clear, and suffice it to say there are two possibilities which cannot be separated easily; the first one based on electromagnetic effect for the enhancement (EME) or the excitation of localized surface plasmon's, while the second mechanism relies on the charge transfer effect of the adsorbed molecule or chemical enhancement (CE).[38]

2.2.3 X-ray photoelectron spectroscopy

X-ray is a well-established tool to investigate the structure of organic films; it can also be used for studying desired elements in the film at nm level.

The basic principle in this technique is to use the emitted electrons at ultra-high vacuum (UHV) for gathering some quantitative and qualitative information[39, 40], according to the following ionization process steps:

- Absorption an adequate energy photon (hv) by sample atom
- Electron is emitted from core-level of the atom leaving a hole
- Another electron from outer shell relaxes to fill that space in the process emitting energy as photons.

The atomic processes of photoelectron emission are schematically illustrated in the diagram of the energy levels, figure 2:10.

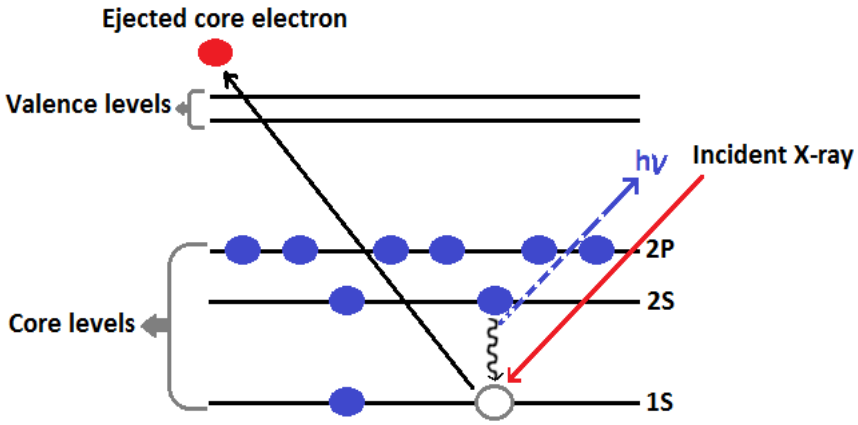

Figure 2:10 Schematic diagram of XPS process, indicating the way of the emitted photons of atom core level.

Depending on preservation energy principle, the overall energy for the incident beam of X-ray (hv) + initial state (E_I), should be equal to the overall total energy of kinetic energy (K_E) + the energy at the final state (E_F). Therefore, one can calculate the binding energy (BE) of the released electron by using the following equation.[41, 42]

$$(hv + E_I) = (K_E + E_F) \quad \Rightarrow \quad BE = hv - K_E = E_F - E_I \qquad 2\text{-}11$$

2.2.4 Elemental and chemical state information

XPS technique has often been used to detect the interaction between surface chemical groups on an adsorbent and adsorbate species, because the creation of a chemical bond between a metal ion and atom or a group of atoms on the surface leads to change the distribution of the electrons around the corresponding atoms, where electron-withdrawing ligands can raise their BE, while electron donating ligand can lower the binding energy BE of the core level electrons.[43, 44, 45]

Each element produces a set of XPS peaks at characteristic binding energy values. However, these values directly indicate the presence of that element. The characteristic peaks are corresponding to the electron configuration of the electrons within the atoms,

e.g., 1s, 2s, 2p, 3s, etc. Furthermore, the number of detected electrons (area under the peak) is directly related to the amount of the element.[46]

XPS is distinct from the rest of the surface techniques being it is more selective, where in XPS the probe depth of SAM is 0.5 to 5 nm[47, 48], while in EDAX for example it reaches 50 nm to 1 µm through the thickness of the example[49]. This property enables XPS to investigate the upper thin layer of the specimen.

2.3 References

1. A. Eswari and L. Rajendran, *Russian Journal of Electrochemistry*, 2011, **47**, 181-190.
2. C. G. Zoski, *Handbook of electrochemistry*, ELSEVIER SCIENCE & TECHNOLOGY2007.
3. E. Gileadi, E. Kirowa-Eisner and J. Penciner, *Interfacial electrochemistry: an experimental approach*, Addison-Wesley Pub. Co., Advanced Book Program1975.
4. P. Zanello and R. S. o. Chemistry, *Inorganic Electrochemistry: Theory, Practice and Applications*, Royal Society of Chemistry2003.
5. D. D. Zhou, E. Greenbaum and E. S. Greenbaum, *Implantable Neural Prostheses 2: Techniques and Engineering Approaches*, Springer London, Limited2010.
6. M. Faraday, *Philosophical Transactions of the Royal Society of London*, 1834, **124**, 55-76.
7. P. A. Christensen and A. Hamnet, *Techniques and Mechanisms in Electrochemistry*, Springer1994.
8. P. Trulove, *Physical and Analytical Electrochemistry (General) - 213th ECS Meeting*, The Electrochemical Society2008.
9. J. Wang, *Analytical Electrochemistry*, Wiley2006.
10. C. M. A. Brett and A. M. O. Brett, *Electrochemistry: Principles, Methods, and Applications*, Oxford University Press, Incorporated1993.
11. C. Lu and A. W. Czanderna, *Applications of Piezoelectric Quartz Crystal Microbalances*, Elsevier Science1984.

12. F. G. Banica, *Chemical Sensors and Biosensors: Fundamentals and Applications*, Wiley2012.
13. J. C. Whitaker, *The Electronics Handbook, Second Edition*, Taylor & Francis2005.
14. R. F. Schmitt, J. W. Allen, J. F. Vetelino, J. Parks and C. Zhang, *Sensors and Actuators B: Chemical*, 2001, **76**, 95-102.
15. G. Y. Yu and G. I. o. Technology, *Magnetic Quartz Crystal Microbalance*, Georgia Institute of Technology2008.
16. M. R. Deakin and D. A. Buttry, *Analytical Chemistry*, 1989, **61**, 1147A-1154A.
17. V. M. Mecea, *Analytical Letters*, 2005, **38**, 753-767.
18. A. R. Hillman, *Solid State Ionics*, 1997, **94**, 151-160.
19. N. Gulati and M. S. University, *Use of QCM Technology for Measuring Barrier Properties of Biodegradable Packaging Material*, Michigan State University2008.
20. J. D. S. Ballantine, R. M. White, S. J. Martin, A. J. Ricco, E. T. Zellers, G. C. Frye, H. Wohltjen, M. Levy and R. Stern, *Acoustic Wave Sensors: Theory, Design, & Physico-Chemical Applications*, Elsevier Science1996.
21. V. M. Mecea, *Sensors and Actuators A: Physical*, 2006, **128**, 270-277.
22. J. Janata, *Principles of Chemical Sensors*, Springer2009.
23. K. Keiji Kanazawa and J. G. Gordon, *Analytica Chimica Acta*, 1985, **175**, 99-105.
24. S. Bruckenstein and S. Swathirajan, *Electrochimica Acta*, 1985, **30**, 851-855.
25. A. Mirmohseni, M. Shojaei, M. A. Feizi, F. F. Azhar and M. Rastgouye-Houjaghan, *Journal of environmental science and health. Part A,*

Toxic/hazardous substances & environmental engineering, 2010, **45**, 1119-1125.

26. M. R. Deakin, T. T. Li and O. R. Melroy, *Journal of Electroanalytical Chemistry and Interfacial Electrochemistry*, 1988, **243**, 343-351.
27. R. S. Krishnan and R. K. Shankar, *Journal of Raman Spectroscopy*, 1981, **10**, 1-8.
28. D. W. Hatchett, R. H. Uibel, K. J. Stevenson, J. M. Harris and H. S. White, *Journal of the American Chemical Society*, 1998, **120**, 1062-1069.
29. A. Kudelski, *Journal of Raman Spectroscopy*, 2003, **34**, 853-862.
30. N. Colthup, *Introduction to Infrared and Raman Spectroscopy*, Elsevier Science2012.
31. K. Kneipp, H. Kneipp, I. Itzkan, R. R. Dasari and M. S. Feld, *Chemical Reviews*, 1999, **99**, 2957-2976.
32. M. Moskovits, *Reviews of Modern Physics*, 1985, **57**, 783-826.
33. A. Campion and P. Kambhampati, *Chemical Society Reviews*, 1998, **27**, 241.
34. M. J. Weaver, S. Zou and H. Y. H. Chan, *Analytical Chemistry*, 2000, **72**, 38 A-47 A.
35. M. Fleischmann, Hendra, P.J. and McQuillan, A.J., *J. Chem. Soc. Chem. Commn.*, 1973, **1**, 80-81.
36. T. R. Jensen, M. D. Malinsky, C. L. Haynes and R. P. Van Duyne, *The Journal of Physical Chemistry B*, 2000, **104**, 10549-10556.
37. M. G. Albrecht and J. A. Creighton, *J. Am. Chem. Soc.*, 1977, **99**, 5215-5217.
38. P. Kambhampati, C. M. Child, M. C. Foster and A. Campion, *The Journal of Chemical Physics*, 1998, **108**, 5013.

39. J. Yarwood, R. Douthwaite, S. Duckett, G. E. Ball and T. Keyes, *Techniques, Materials and Applications*, Royal Society of Chemistry2010.

40. Y. Leng, *Materials Characterization: Introduction to Microscopic and Spectroscopic Methods*, Wiley2009.

41. J. Huang and J. C. Hemminger, *Journal of the American Chemical Society*, 1993, **115**, 3342-3343.

42. J. C. Vickerman and I. Gilmore, *Surface Analysis: The Principal Techniques*, Wiley2011.

43. X. Zhang and R. Bai, *Langmuir*, 2002, **18**, 3459-3465.

44. X. Zhang and R. Bai, *Journal of Materials Chemistry*, 2002, **12**, 2733-2739.

45. R. Bai and X. Zhang, *Journal of Colloid and Interface Science*, 2001, **243**, 52-60.

46. K. J. Rao, *Structural Chemistry of Glasses*, Elsevier Science2002.

47. D. Jiang, Y. Zeng, M. Singh and J. Heinrich, *Ceramic Materials and Components for Energy and Environmental Applications: Ceramic Transactions*, Wiley2010.

48. L. J. Brillson, *Surfaces and Interfaces of Electronic Materials*, Wiley2012.

49. A. Khursheed, *Scanning Electron Microscope Optics and Spectrometers*, World Scientific2011.

3 Experimental

3.1 Chemicals and solutions

All reagents and solvents were of standard analytical grade and used without further purification, as they are listed in the following table. Solutions were prepared by using De-ionized (DI) water, which were obtained from cation and anion exchange resin columns.

Table 3-1 shows a list of the most important chemicals and solvents used in this study, with their sources and the purities.

No.	Chemical name	Formula	Molecular weight (MW)	Purity	Supplier company
1	Mercaptosuccinic acid	$C_4H_6O_4S$	150.15 g/mol	98%	Alfa Aesar
2	2, 2'-thiodisuccinic acid	$C_8H_{10}O_8S$	266.22 g/mol	98%	Alfa Aesar
3	4-Mercaptobenzoic acid	$C_7H_6O_2S$	154.19 g/mol	99%	Sigma Aldrich
4	4-Mercaptophenylacetic acid	$C_8H_8O_2S$	168.21 g/mol	97%	Sigma Aldrich
5	Ethanol	C_2H_6O	46.07 g/mol	99.5%	Sigma Aldrich
6	Lead nitrate	$Pb(NO_3)_2$	331.23 g/mol	96%	Sigma Aldrich
7	Nickel nitrate hexahydrate	$Ni(NO_3)_2.6H_2O$	290.81 g/mol	85 %	Sigma Aldrich
8	Cobalt nitrate hexahydrate	$Co(NO_3)_2.6H_2O$	291.03 g/mol	98%	Sigma Aldrich
9	Hydrogen peroxide	H_2O_2	34.01 g/mol	30%	BDH
10	Sulphuric acid	H_2SO_4	98.08 g/mol	98%	Fisher Scientific
11	Betainum hydrochloride	$C_5H_{12}ClNO_2$	153.61 g/mol	99%	Sigma Aldrich
12	Bis (trifluoromethane) sulfonimide lithium salt	$C_2F_6LiNO_4S_2$	287.09 g/mol	99%	Sigma Aldrich
13	1-butyl-3-methylimidazolium chloride	$C_8H_{15}ClN_2$	174.67 g/mol	98%	Sigma Aldrich
14	Potassium hexafluorophosphate	KPF_6	184.06 g/mol	98%	Sigma Aldrich
15	Dichloromethane	CH_2Cl_2	84.93 g/mol	99%	Fisher Scientific
16	Dimethylglyoxime	$C_4H_8N_2O_2$	116.12 g/mol	99%	Sigma Aldrich
17	Anhydrous magnesium sulphate	$MgSO_4$	120.37 g/mol	99.5%	Sigma Aldrich
18	Pyridine	C_5H_5N	79.10 g/mol	99%	Fisher Scientific
19	Sodium rhodizonate dibasic	$C_6Na_2O_6$	214.04 g/mol	97%	Sigma Aldrich

3.1.1 Preparation of thiol solutions

Thiol solutions were prepared in 10mM concentration by dissolving pure thiol compounds of analytical grade in absolute ethanol at room temperature. The ethanol used was deoxygenated by passing nitrogen gas through it for about half an hour to remove all dissolved oxygen. The following were the required weights of thiols for the prepared solutions.

In order to prepare 10 mM ethanolic solution of mercaptosuccinic acid, 0.300 g of mercaptosuccinic acid was dissolved in 200 ml of deoxygenated absolute ethanol. Whereas, 200 ml ethanolic solution 0.01 M of Thiodisuccinic acid was prepared by dissolving 0.532 g of 2, 2'-thiodisuccinic acid in deoxygenated absolute ethanol. However, preparation of 4-Mercaptobenzoic acid 0.01 M required 0.308 g, of this thiol in pure deoxygenated ethanol. And similarly 4-Mercaptophenylacetic acid was prepared in 200 ml by dissolving 0.336 g of it in pure deoxygenated ethanol to get 0.01 M solution of it.

3.1.2 Preparation of metal ion Solutions

Standard solution (1000 ppm) of each metal ion being studied was prepared in 1000 ml as stock solution. In case of lead standard solution, lead ions was prepared by dissolving 1.598 g of lead nitrate in De-ionized water and diluted to 1000 ml.

A solution of nickel ions was also prepared by dissolving 4.955 g of nickel nitrate hexahydrate in De-ionized water and diluted to 1000 ml. Standard solution of cobalt ions was prepped by dissolving 4.938 g of cobalt nitrate hexahydrate in De-ionized water then diluted up to 1000 ml. From these standard solutions a series of different concentrations were prepared in 1 to 100 ppm range for each of them.

All measurements were made for single metal ion solution individually for each of the lead, nickel and cobalt (non-competitive binding) at the natural pH values of stock solutions (6.3, 5.8 and 5.9 respectively), and for the mixtures as well.

3.1.3 Preparation of Piranha solution

A fresh Piranha solution was required to clean the gold surface. This solution was prepared by mixing hydrogen peroxide 30% and sulphuric acid 98% (1:3 by volume)[1,]

3.1.4 Preparation of ionic liquid solutions

Two kinds of ionic liquid were prepared as a miscible ionic liquid, the first one is betaine [bis(trifluoromethylsulfonyl)imide] symbolizes [Hbet][Tf_2N], which prepared according to this procedure[2, 3]:

In step one 1M betainum hydrochloride solution was prepared by adding 153.61 g of $(CH_3)_3N^+CH_2COOH \cdot Cl^-$, to 250 ml of De-ionized water, and separately 287.08 g of lithium bis(trifluoromethylsulfonyl) imide was dissolved in 500 mL De-ionized water to get 1M aqueous solution.

At step two the first solution was added gradually under stirring to the second for 1 h at room temperature. The aqueous phase separated from the ionic liquid phase. After separation of the phases, the ionic liquid phase was washed three times with small amounts of water until no chloride impurities could be detected in the washings by the silver nitrate test.

In step three produced ionic liquid was evaporated to dryness (70-120 °C) in vacuum on a rotary evaporator for 24h. The produced ionic liquid was kept in dry and warm place.

The second ionic liquid is 1-butyl-3-methylimadazolium hexafluorophosphate ([BMIM][PF_6])[4, 5], which is also a miscible with water. The next procedure was followed to prepare this type of ionic liquid:

65.6 g of 1-butyl-3-methylimidazolium chloride was charged in one-necked round bottomed flask; and 69.3 g (0.37 mol, 1 equiv) of potassium hexafluorophosphate was dissolved in 70 mL of distilled water. These two reactants were mixed and the reaction mixture was stirred at room temperature for 2 hour; then allowed to settle down to give two-phase system. The organic phase was washed three times with 50 mL of water and dried under reduced pressure, further drying was carried out by adding 100 mL of dichloromethane and 35 g of anhydrous magnesium sulphate to separate ionic liquid phase free of water.

The suspension particulars were filtered one hour later, and the volatile material was removed under reduced pressure at 30°C for two hours. This afforded 86.4 g of 1-butyl-3-methylimidazolium hexafluorophosphate as a light yellow viscous liquid.

3.2 Procedures:

3.2.1 Cyclic voltammetry

The characterization of the quality of prepared SAMs was investigated by using different techniques, and the first one was the cyclic voltammetry, where an Auto lab PGSTAT20 potentiostat controlled by GPES software (Ecochemie, Holland) was used for this purpose and three electrode cell (gold quartz crystal as a working electrode silver / silver chloride as a reference electrode and platinum gauze is the counter electrode). The results and discussions will be presented later in the in chapter four.

3.2.2 Quartz crystal impedance measurements

The technique used in this part of study is an electrochemical quartz crystal microbalance model (Agilent / HP E5061A) network analyser with 10 MHz At-cut gold quartz crystal produced by international crystal manufacturing company, Oklahoma City, USA. However, the purpose of measuring the change in frequency of QCM is to find out the quality of formed SAMs, rigidity and the thickness of these SAMs. All experimental data were fitted by means of fitting software, which developed by prof. Karl S. Ryder, in Microsoft Excel.

3.2.3 Quartz crystal microbalance cell

Unpolished AT-cut quartz crystal (10MHz) was installed at the base of standard microbalance cell by using silicone rubber adhesive (3145 RTV-CLEAR MIL-A-45146), which is a stable glue at room temperature and takes about 24 hours to dry. In this process all diligence has been taken to avoid any contact between the adhesive and the centre circular part of the electrode, since any tiny spot of glue on this area will cause highly damp for crystal oscillation and thus reduces the sensitivity of QCM towards mass changing. Figure 3:1shows the ordinary cell used.

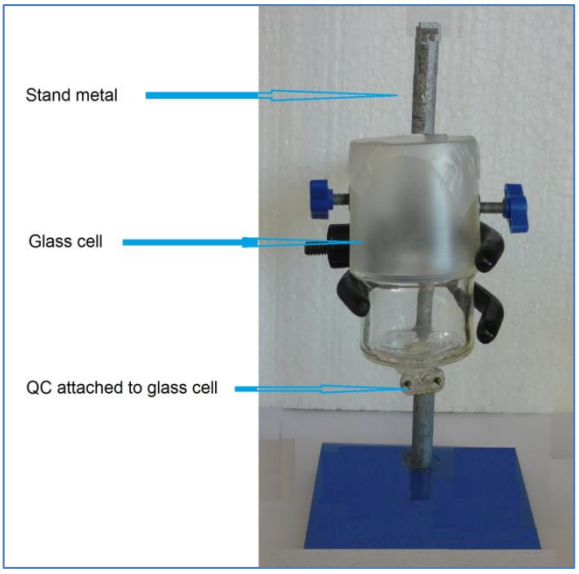

Figure 3:1 shows a picture of an ordinary glass cell attached with quartz crystal, which has plug jacks of lead to connect the crystal with the outer circle.

3.2.4 Electrochemical cell

The only one different between the Quartz crystal microbalance cell previously mentioned and electrochemical cell is the electrodes required, again no sealant was allowed to contact the mass sensitive centre of the electrode. The solution of analysis in this cell was purged with nitrogen to remove dissolved oxygen and then blanketed with the nitrogen gas in order to keep it deoxygenated. All experiments were performed at room temperature, using silver / silver chloride as a reference electrode and Platinum gauze as a counter electrode.

3.2.5 Raman technique

The Raman measurements were conducting by introduces dried samples (powder or Au coated glass slide) to LabRAM HR Raman spectrograph instrument, imported from HORIBA Company, France. All results and discussions are in chapter five.

3.2.6 XPS technique

XPS measurements were performed in NEXUS at the University of Newcastle, using monochromated K-Alpha Thermo Scientific Spectrometer (Cat. No. IQLAADGAAFFACVMAHV), made in Britain. Sample preparation and results will discuss in chapter five.

3.2.7 Coating a glass microscope slide with gold

In order to coat glass microscope slide with a very thin gold film, a silanisation process has to be followed, which is the best way for cleaning out the slide of any contaminants and getting a good thin film of gold on the substrate[6, 7, 8].

Firstly sonicate substrate in Decon (commercial detergent), rinse with DI and then sonicate with DI, before drying with compressed air, secondly reflux the substrate in isopropanol (IPA) 400ml, containing fresh 3-mercaptopropyltrimethoxysilane (3-MPTS) 12 ml and DI 12ml for 15min (left it until it reaches room temperature), and thirdly rinse and sonicate in clean IPA blow dry with compressed air. Repeat the reflux rinsing a further two times before starting coating process at 80 μA for 200 seconds by evaporated god metal in a large chamber, rotary-pumped coating system ideally of gold coater, model Q300R (Serial No 11008) manufacturing by the Company of Electron Microscopy Sciences in 2011 at Hatfield in USA, and then keep slides under vacuum in a clean desiccator, for a day (Metallization process). The coated slide produced, should have about 30 nm film thickness.

3.2.8 Cleaning gold substrates

Gold, whether on quartz crystal as a working electrode or coated on glass microscope slide, needs to be cleaned of any molecules or contaminants that could prevent the

interested ligand to interact with this substrate. Cleaning procedure initially started by immersion the substrate in Piranha solution preparing as mentioned in section (3.1) for a minimum of 30 min, followed by rinsing with absolute ethanol and then washing by DI-water, finally dried tightly with nitrogen gas.

3.2.9 Modified gold substrates with SAMs

After cleaning gold substrates they were modified by immersing them in modification solutions overnight (24 hours). Then washed in DI-water very well before being dried under stream of nitrogen, hence they will be ready for taking the measurements.

Modifying gold electrodes on quartz crystal was done by adding 20 ml of 0.01M ethanolic thiol solution to the QCM cell, (see figure 3:1) for 24 hours, which is enough to form a full monolayer on the gold surface. The treatment was carried out at room temperature. A similar procedure was followed for modifying gold substrates coated on a glass slide. However in this case, gold-coated wafers were cut into small slices (1.3cm × 2.6cm) size, before being immersed in the thiol solution overnight at room temperature. Coated glass slide was rinsed with ethanol and De-ionized water, after that blown dry with nitrogen gas[9,10,11, 12]. Preparation of SAM on gold-coated glass slice is explained in figure 3:2.

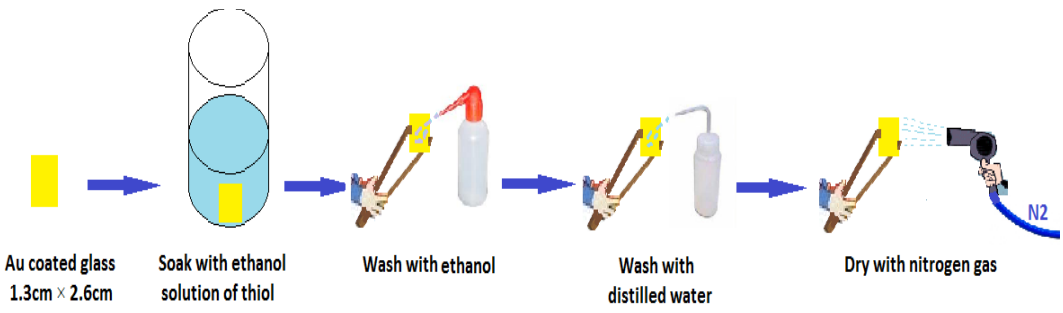

Figure 3:2 Preparation method of MSA on a glass microscopy slice

3.3 References

1. S. M. Rosendahl and I. J. Burgess, *Electrochimica Acta*, 2008, **53**, 6759-6767.
2. C. Jagadeeswara Rao, R. Venkata Krishnan, K. A. Venkatesan, K. Nagarajan and T. G. Srinivasan, *Journal of Thermal Analysis and Calorimetry*, 2009, **97**, 937-943.
3. P. Nockemann, B. Thijs, S. Pittois, J. Thoen, C. Glorieux, K. Van Hecke, L. Van Meervelt, B. Kirchner and K. Binnemans, *The journal of physical chemistry. B*, 2006, **110**, 20978-20992.
4. K. M. Booker, C. I. Holdsworth, M. C. Bowyer and A. McCluskey.
5. S. Carda-Broch, A. Berthod and D. W. Armstrong, *Anal Bioanal Chem*, 2003, **375**, 191-199.
6. A. R. Hillman, P. M. Saville, A. Glidle, R. M. Richardson, S. J. Roser, M. J. Swann and J. R. P. Webster, *Journal of the American Chemical Society*, 1998, **120**, 12882-12890.
7. M. E. McGovern, K. M. R. Kallury and M. Thompson, *Langmuir*, 1994, **10**, 3607-3614.
8. C. M. Halliwell and A. E. G. Cass, *Analytical Chemistry*, 2001, **73**, 2476-2483.
9. C. D. Bain, H. A. Biebuyck and G. M. Whitesides, *Langmuir*, 1989, **5**, 723-727.
10. H. A. Biebuyck, C. D. Bain and G. M. Whitesides, *Langmuir*, 1994, **10**, 1825-1831.
11. E. B. Troughton, C. D. Bain, G. M. Whitesides, R. G. Nuzzo, D. L. Allara and M. D. Porter, *Langmuir*, 1988, **4**, 365-385.
12. R. A. Drawhorn and N. L. Abbott, *The Journal of Physical Chemistry*, 1995, **99**, 16511-16515.

4 Gravimetric analysis of SAMs

Introduction

Both the cyclic voltammetry and Quartz crystal microbalance techniques have been used to study the formation of all SAMs. This can provide information about the quality of the blocking monolayer and to seek out important information of more related factors such as thickness, stability and rigidity.

4.1 Cyclic voltammograms for all SAMs

Cyclic voltammetry is the easiest technique for monitoring self-assembled monolayer on gold electrode, so initial studies focused on this, in order to identify the defects in the SAMs, this indicates the extent of the electrode coverage. Thus the best thiol for metal ion binding can be chosen as a ligand on the gold surface electrode throughout the rest of this study.

In these experiments, the redox behaviour of $[K_3Fe(CN)_6]$ solution as a reversible couple was utilized to probe the packing structure of the formed monolayers. In general, the experimental results clearly demonstrated that, I-E curves corresponding to the oxidation and reduction reactions of $[K_3Fe(CN)_6]$ solution were decreased by the surface modification with all SAMs.

4.1.1 Results and discussion

Each of the next figures 4:1, 4:2, 4:3 and 4:4 consists of a double cyclic voltammograms; one belongs to the bare gold electrode and the other to the modified one, which is covered with a certain kind of self-assembled monolayer prepared by immersion gold electrode in 10 mM solution of thiol for 24 hours. Both experiments

were conducted under the same conditions, in aqueous solution of 0.025 M $K_3Fe(CN)_6$ + 0.5M KCl at 100mVs^{-1} scan rate.

The following cyclic voltammograms show that the packing structure of some formed monolayers has a clear influence on them. In figure 4:1 a typical cyclic voltammetric response is noted in that for $[Fe(CN)_6]^{3-/4-}$ at bare gold electrode (black curve) and a gold electrode modified with MSA (red curve). It can also be seen that the peak current is significantly suppressed by the MSA modification. The monolayer formation tends to limit the closest approach of the redox molecules towards the electrode surface, decreasing the rate of electron transfer.

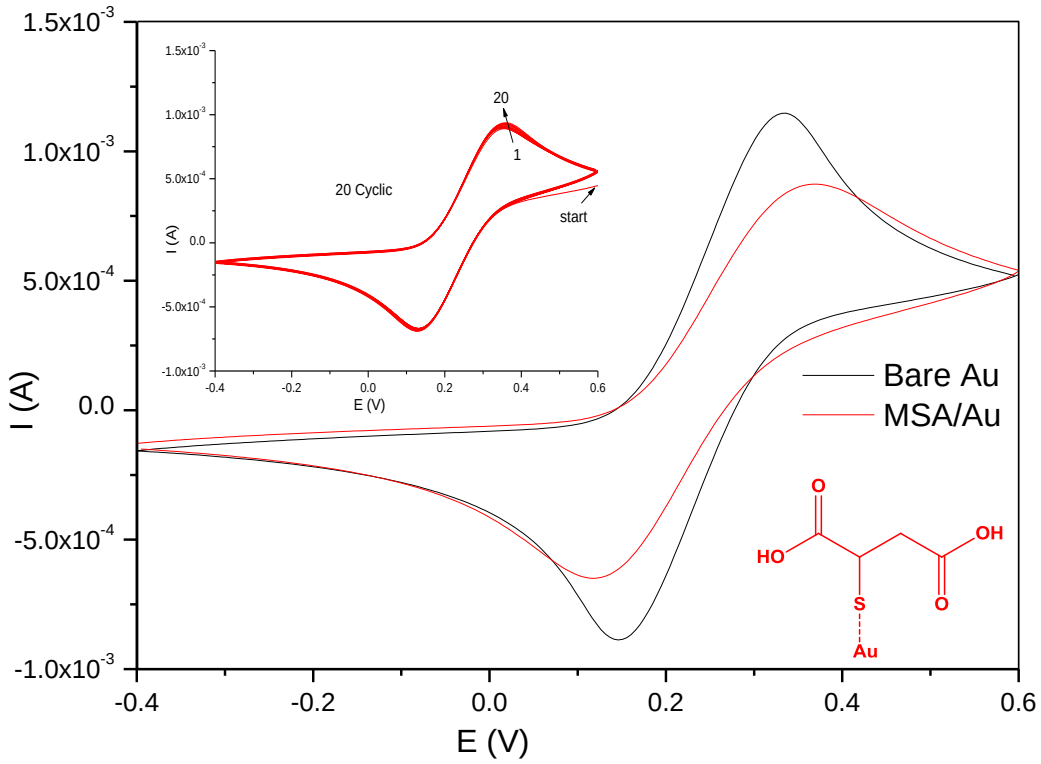

Figure 4-1 cyclic voltammograms of bare and modified gold electrode with mercaptosuccinic acid in 0.025M $K_3Fe(CN)_6$ + 0.5M KCl at 100mVs^{-1} scan rate, 48h immersion. Inset: the effect of repetitive cycling on the stability of MSA ligand on gold surface after 20 cyclic.

In order to confirm the stability of Au-MSA, the cyclic was repeated up to 20 times at the same conditions. However, a slight increase in peak current started from cyclic number one up to cyclic number seven had been noticed, after that all the rest of voltammograms became identical on each other, and peak currents were at similar volumes, which means that after cycle number seven there is no loss of the ligand from gold surface.

In the case of 2, 2'-thiodisuccinic acid the result was different as can be seen in figure 4:2 where the redox behaviour of $[Fe(CN)_6]^{3-/4-}$ system on Au and Au/ 2,2'-TDS, were almost the same, they are matched with each other, since both have the same shape and nearly same values of peak current. This means there was limited SAM formation produced on the surface.

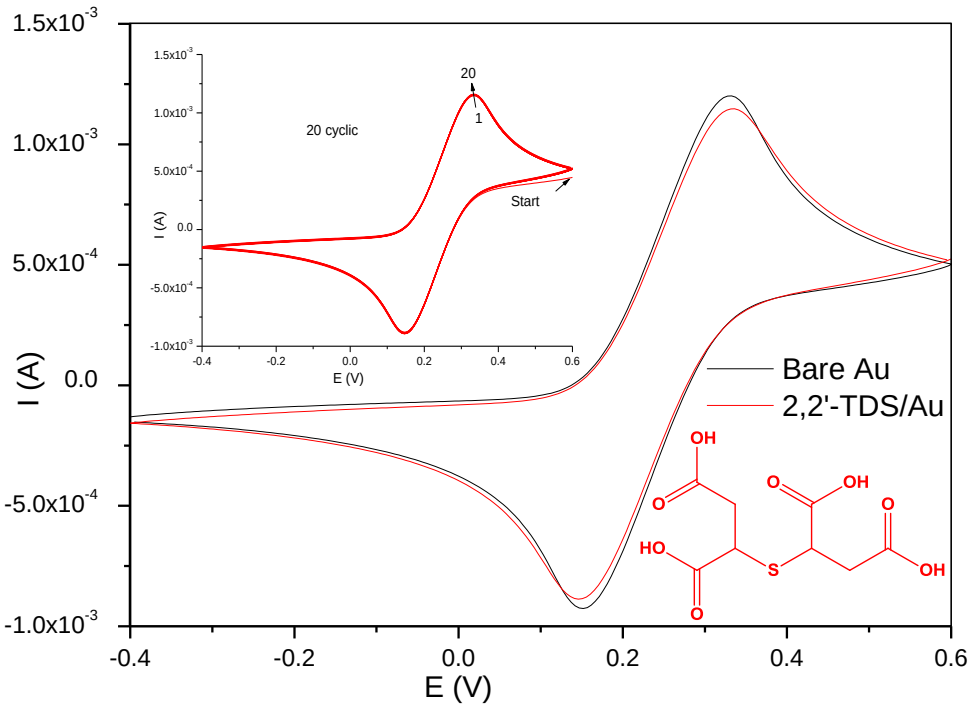

Figure 4-2 cyclic voltammograms of bare and modified gold electrode with 2,2'-thiodisuccinic acid in 0.025M $K_3Fe(CN)_6$ + 0.5M KCl at 100mVs^{-1} scan rate, 48h immersion. Inset: the effect of repetitive cycling on the stability of 2,2'-TDS ligand on gold surface after 20 cyclic.

Regarding the aromatic thiols 4-MBA and 4-MPAA as shown in figures 4:3 and 4:4, there is not much difference between them as can be seen in the following figures, where both show the same reversible redox behaviour. However, peak current and peak potential for bare and modified electrodes are slightly different for some extent. Similarly, black curve belongs to bare gold electrode, and red one for the modified once.

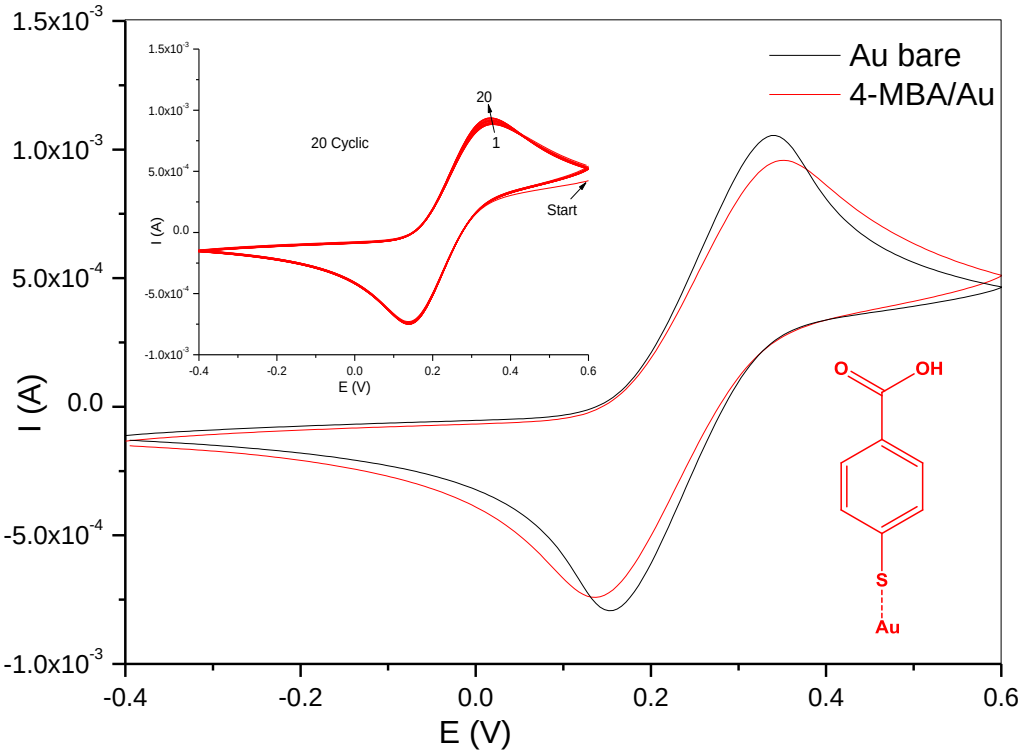

Figure 4-3 cyclic voltammograms of bare and modified gold electrode with 4-mercaptobenzoic acid in 0.025M $K_3Fe(CN)_6$ + 0.5M KCl at 100mVs^{-1} scan rate, 48h immersion. Inset: the effect of repetitive cycling on the stability of 4-MBA ligand on gold surface after 20 cyclic.

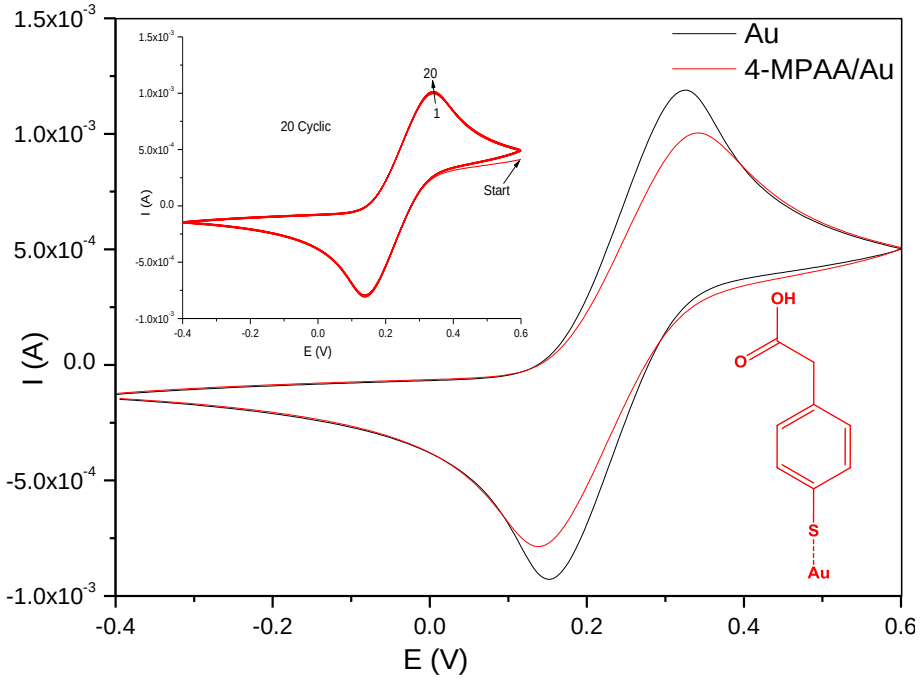

Figure 4-4 cyclic voltammograms of bare and modified gold electrode with 4-mercaptophenylacetic acid in 0.025M $K_3Fe(CN)_6$ + 0.5M KCl at 100mVs^{-1} scan rate, 48h immersion. Inset: the effect of repetitive cycling on the stability of 4-MPAA ligand on gold surface after 20 cyclic.

4.1.2 Calculation of electron transfer rate constant through SAMs

Again cyclic voltammetry is the best option among all available techniques to determine the electron transfer kinetics (K') through the attached SAM on gold surface, and for this purpose, peak potential separation ($\Delta E_P = E_{pa(Ox)}-E_{Pc(red)}$) should be calculated from cyclic voltammograms corresponding to each SAM used, and then the number of electrons involved in the reaction at 25^{o}C can also be calculated by using the following relationship:

$$\Delta E_P = \frac{0.0591}{n} \qquad 4\text{-}1$$

Exponential function curve in figure 4:5, is adapted from standard theoretical results (Table *4-1*)[1], and used to find out the value of the kinetic parameter (ψ).

Table 4-1: the relation between peak potential differentiation and kinetic parameter.

ψ	20	7	6	5	4	3	2	1	0.75	0.5	0.35	0.25	0.1
ΔE_p (mV)	61	63	64	65	66	68	72	84	92	105	121	141	212

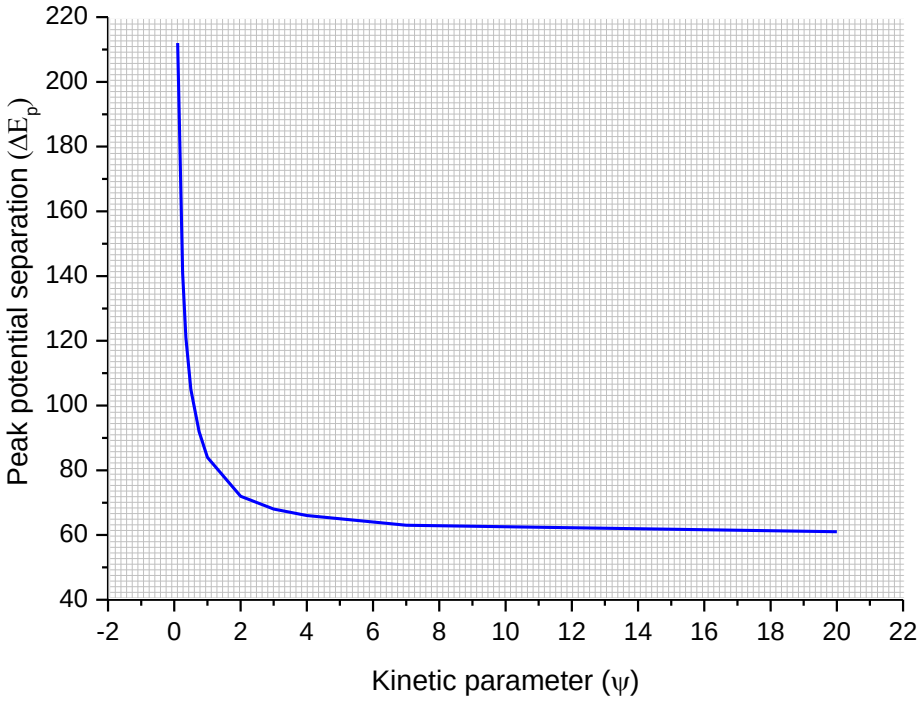

Figure 4-5 the relation between peak potential differentiation and kinetic parameter quoted from reference.[1]

These reliable data (n and Ψ) utilises to determine the electron transfer rate constant (k') by using the following equation[2]:

$$\Psi = \left(\frac{D_O}{D_R}\right)^{\frac{\alpha}{2}} K^{'} / \left(D_o \pi \nu \left(\frac{nF}{RT}\right)\right)^{\frac{1}{2}} \qquad 4\text{-}2$$

Where D_o, D_R are the diffusion coefficients (cm^2 s^{-1}), of the oxidised and reduced species in solution, ν is the scan rate (Vs^{-1}), n is the electron stoichiometry, F is Faraday constant, T is the temperature in Kelvin, R is the gas constant and $K^{'}$ is the electron transfer rate constant. However, ΔEp value depends only on Ψ if α = 0.5, (Ψ values often start from 0.1 to 7)[2] and taking into consideration that when $\frac{i_{p,a}}{i_{p,c}} = 1$; then $\frac{D_O}{D_R} = 1$.

Thus equation (2) can be abbreviated as follows:

$$K'=\psi\left[\frac{\pi DnvF}{RT}\right]^{1/2} \qquad 4\text{-}3$$

Under the experimental conditions $\left[\frac{\pi DnvF}{RT}\right]^{1/2} = 8.188\times10^{-5}$, depending on this one can simplify equation 3 to be as following:

$$K'= \Psi\ 8.188\times10^{-5} \qquad 4\text{-}4$$

This equation is used to estimate the electron transfer rate constant, which can be used to indicate the rate of the process at all SAMs.

Cyclic voltammograms of an aqueous solution 0.05 M $K_3Fe(CN)_6$ + 0.5M KCl for gold electrode, before and after modified with each thiol, were taken at scan rate 100 mVs^{-1}, then peak potential differentiation estimated for each case (Au & Au/SAM), as presented in next figures. However, by using ΔEp values and the above curve in figure 4:5, one can find out the kinetic parameter Ψ corresponding to each case. Since the value of the diffusion coefficient for $K_3Fe(CN)_6$ under experimental conditions is 7.64×10^{-6} cm^2 s^{-1} at room temperature ($25C^o$), and by using equation 4, one can estimate the value of the electron transfer rate, before and after the modification process at gold surface for all thiols used. However, all these factors were calculated as summarised below in table 4:2.

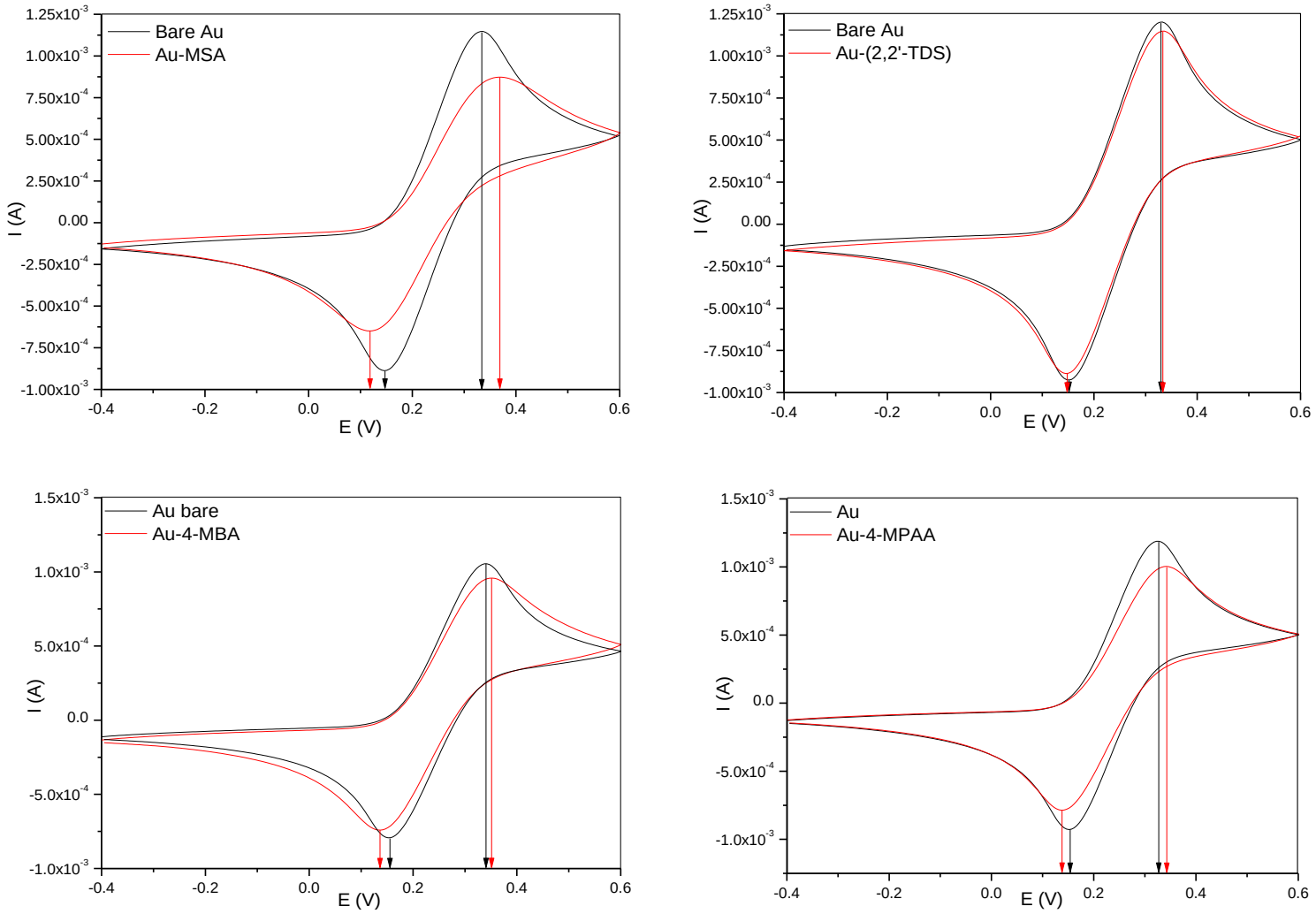

Figure 4-6 shows the peak potential differentiation taken for typical redox species at 100mV/s scan rate at modified and bare gold electrode with different SAMs.

Table 4-2 shows the electron transfer rate constant K' for 0.05 M $[Fe(CN)_6]^{3-/4-}$ + 0.5M KCl at all bare and SAMs modified gold electrodes, calculated by comparison of experimental data with the exponential curve above, where scan rate is 100mV/s, and diffusion coefficients is 7.64×10^{-6} cm^2 s^{-1} at room temperature (25C^o).

Scan rate	Active area	$E_{pa(ox)}$	$E_{PC(red)}$	ΔE_P	ψ	K' (cms^{-1})
$100mVs^{-1}$	Au	0.3363	0.1459	0.1904	0.1226	1.138×10^{-5}
	MSA/ Au	0.3666	0.1177	0.2489	<0.1	$<8.188\times10^{-6}$
	Au	0.3310	0.1508	0.1802	0.1795	1.667×10^{-5}
	2,2'-TDS/ Au	0.3334	0.1482	0.1852	0.1226	1.138×10^{-5}
	Au	0.3388	0.1543	0.1845	0.1226	1.138×10^{-5}
	4-MBA/ Au	0.3513	0.1363	0.2150	<0.1	$<8.188\times10^{-6}$
	Au	0.3271	0.1516	0.1755	0.1485	1.37910^{-5}
	4-MPAA/ Au	0.3429	0.1383	0.2046	<0.1	$<8.188\times10^{-6}$

4.1.3 Conclusion

The monolayer delays the electron transfer rate by increasing the distance between gold surface and the reactants in the solution.

From table 4-2, electron transfer rate constant for this system was decreased by forming SAMs on gold electrode for all thiols used; except 2,2'-TDS, where the values of K' were almost the same for both cases (Au & 2,2'-TDS/Au). Again this result presented the poor quality of this SAM. So it can be concluded that:

- Cyclic voltammograms give an easy way to judge the quality of the SAM, particularly regarding pinhole defects.
- The overall rate of the redox reaction is controlled by mass transfer effects for the bare electrode as indicated by the significantly decreased of the current (figure 4:6).

- The decrease in the number of the defects can be confirmed by investigating the K' values for $[Fe(CN)_6]^{3-/4-}$ couple, which gives lower value at low defects, for different structure of SAMs.

4.2 Applied QCM for monitoring SAM on gold electrode

The frequency of clean dry QCM was measured (f_{Au}, to find out any shift in frequency after the formation of the SAM) then thiol solution (10 mM) is added to the cell. In this study, 24h immersion time was long enough to form full monolayer on the gold surface, but in general the concentration of thiol solution has a big influence on this process as reported in the literature[3, 4]. Next day, cell was emptied, dried with nitrogen gas and again re-measured the new frequency for modified crystal now ($f_{SAM/Au}$).

The difference in frequency between the two above cases was calculated as follows:

$$\Delta f_{SAM} = f_{SAM/Au} - f_{Au} \qquad 4\text{-}5$$

This method was repeated three times for more accuracy. Frequency shifts were measured twice for wet and dry crystal for each SAM.

4.2.1 Span window

Studying the rigidity for the established SAMs, requires the plotting of the admittance versus the responses of the frequency, where there is no change in the shape of the signal, simply a change in the position of the signal on the frequency axis. However, before starting to use this technique, it's important to have a rough estimate to the span window in order to get good impedance spectra for each added thiol on the crystal. So for any thiol with one sulphur group (single bond with gold surface), and by using a simple assumption, and that is the single bond (Au···ligand) allows this molecule to be in rotation motion around itself, e.g. mercaptosuccinic acid.

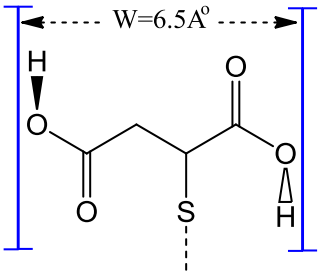

The bond between gold surface and MSA is a single bond, and that makes it easy to rotate around X axis covering a very small area with diameter = the width of this molecular (6.5 A^o) as in next schematic diagram.

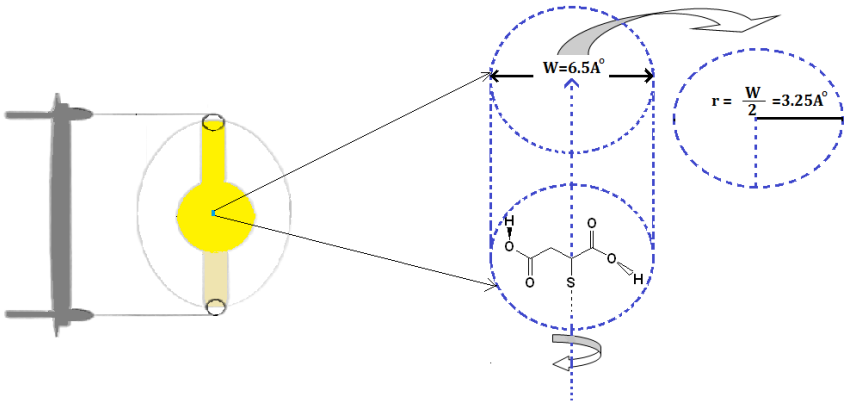

Figure 4-7 imaginary schematic diagram represent the spin motion of MSA on gold substrate

So the covered area A= πr^2

Where r = 3.25A^o = 3.25×10^{-8} cm

A = 3.14 × $(3.25\times10^{-8}$ cm$)^2$ =3.318×10^{-15} cm^2

The molecular numbers of MSA = $\frac{crystal's\ area}{molecular's\ area} = \frac{0.23\ cm^2}{3.318\times10^{-15} cm^2 molecular^{-1}}$

= 6.93×10^{13} molecules

Then numbers of mole = $\frac{6.93\times10^{13} molecular}{6.023\times10^{23}\frac{molecular}{mol}}$ = 1.15 $\times10^{-10}$ mole

Therefore the added mass of (MSA) = $(1.15 \times 10^{-10} mol) \times 150.15 \frac{g}{mol}$ = $1.7\times 10^{-8} g$

= 17.27 ng.

From Sauerbrey equation, frequency change $\Delta f = -1.1\times \Delta m = -1.1\times 17.27 ng$

=19Hz

However, ∂f (distance between two points on the curve) must to be less than this value at least ten times, therefore ∂f=1.9Hz

The number of points driving the frequency response caption is = 800

$\partial f = \frac{span}{No\ of\ points}$

Based on this; $1.9 = \frac{span}{800}$ so the span =1520 Hz = 1.52 KHz.

This simple method could be generalized to calculate the required span for any experiment as long as the added thiol has one sulphur atom to bind with a gold surface via a single bond.

Quartz crystal impedance spectra in figures 4:8, 4:9, 4:10 and 4:11 show the results for all SAMs formed by; MSA, 2, 2'-TDS, 4-MBA and 4-MPAA respectively and they are as follows:

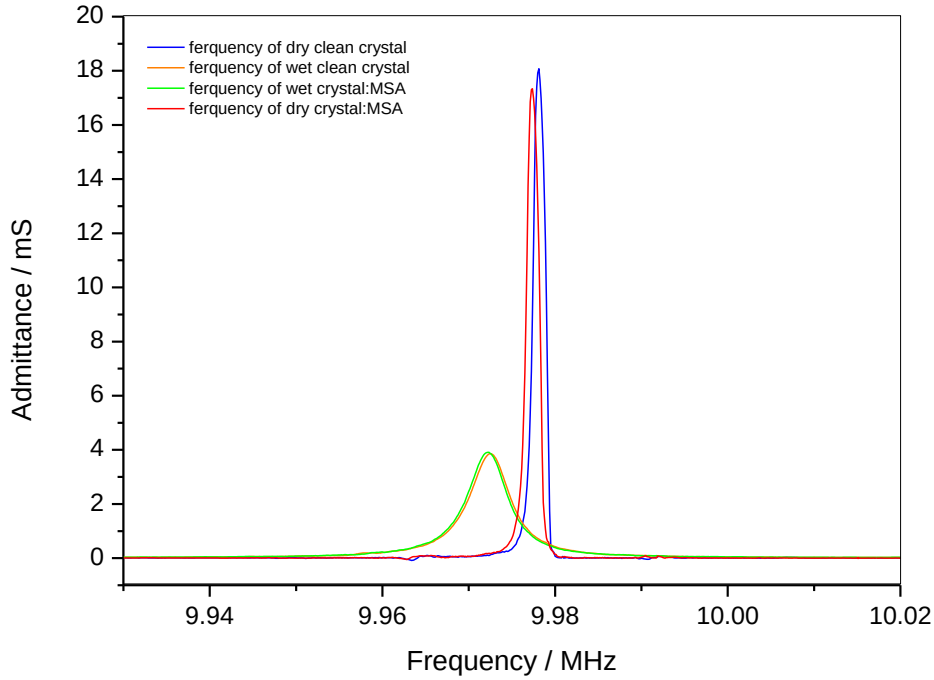

Figure 4-8 crystal impedance spectra for a bare gold electrode and gold electrode modified with mercaptosuccinic acid after 48h on wet and dry crystals.

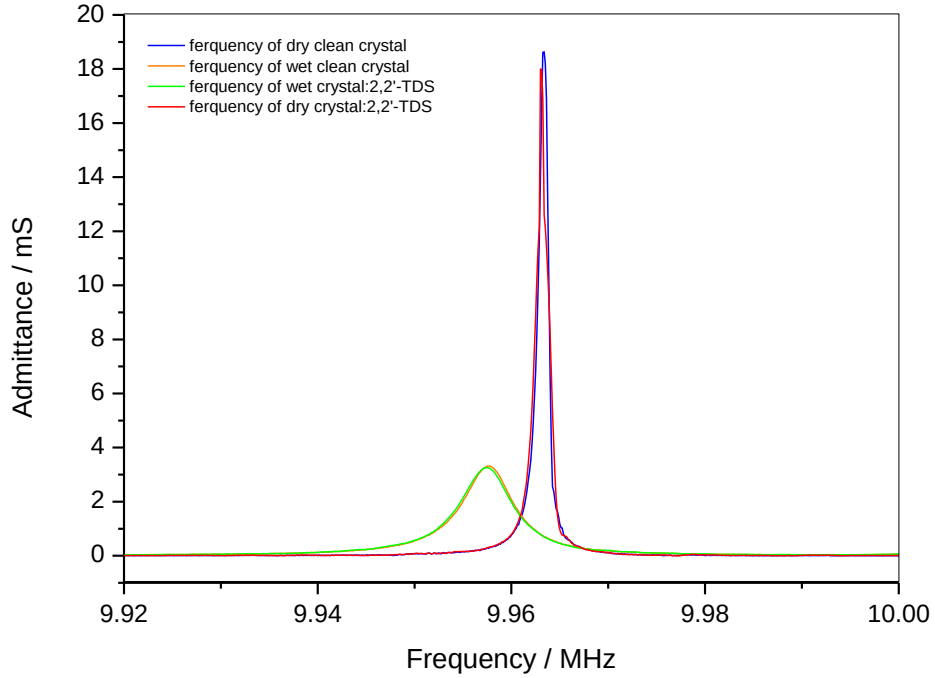

Figure 4-9 crystal impedance spectra for a bare gold electrode and gold electrode modified with 2, 2'-thiodisuccinic acid after 48h on wet and dry crystals.

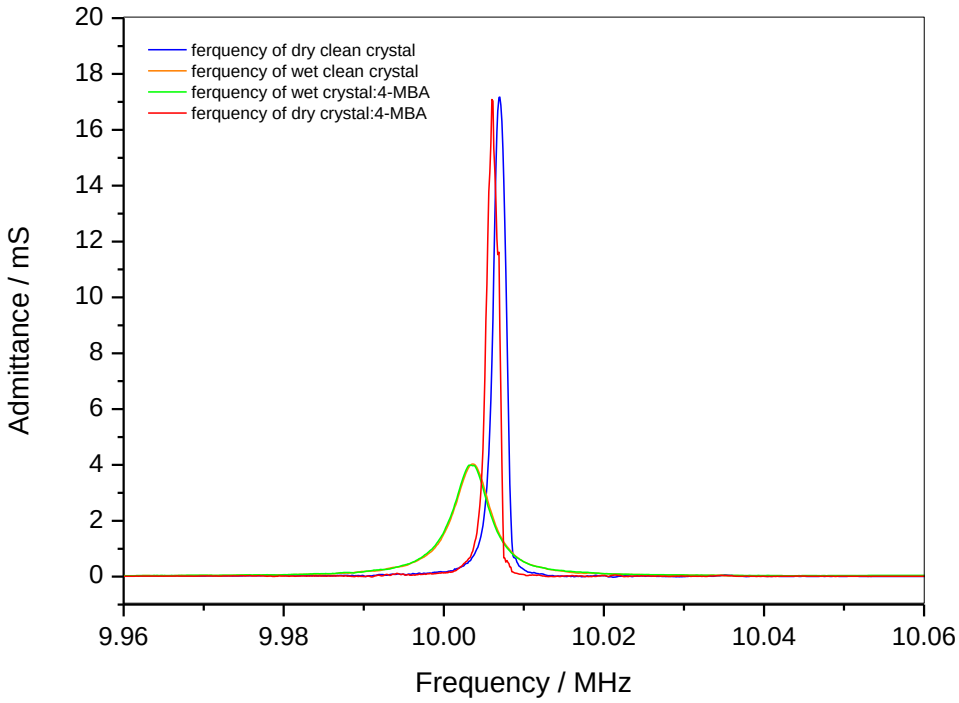

Figure 4-10 crystal impedance spectra for a bare gold electrode and gold electrode modified with 4-mercaptobenzoic acid after 48h on wet and dry crystals.

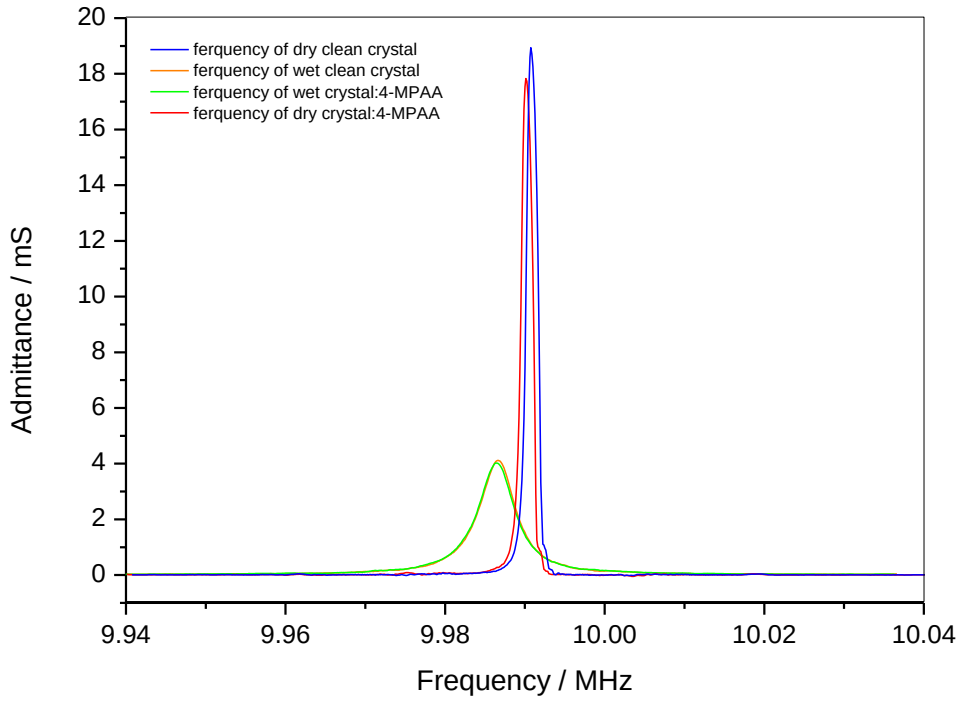

Figure 4-11 crystal impedance spectra for a bare gold electrode and gold electrode modified with 4-mercaptophenylacetic acid after 48h on wet and dry crystals.

The above results of measuring frequency change for dry crystals, clean and modified with SAMs are presented in the next table. The results show that –Δf for MSA was very small (23Hz), in comparison with 4-MBA and 4-MPAA, (39Hz and 41Hz respectively), while the frequency shifts for 2, 2'-TDS was even smaller (negligible).

Table 4-3 the shift of frequency for dry crystals modified with SAMs, after 48h.

SAM	Dry cell			
	$f_{(clean\ cell)}$	$f_{(modified\ cell)}$	-Δf (MHz)	-Δf (Hz)
MSA	9.978125	9.978102	0.000023	23
2,2'-TDS	9.980710	9.980694	0.000016	16
4-MBA	9.977750	9.977711	0.000039	39
4-MPAA	9.991250	9.991209	0.000041	41

The results for wet crystals were different, because of the ability for rough surfaces (unpolished crystal) to entrap liquids within their cavities, effecting on the frequency measured, there is also a kind of hydrophilicity, which normally undergoes to an alteration during the adsorption of the mass on the crystal.

Table 4-4 shows the shift of frequency for wet crystals modified with SAMs, after 48h.

SAM	Wet cell			
	$f_{(clean\ cell)}$	$f_{(modified\ cell)}$	-Δf (MHz)	-Δf (Hz)
MSA	9.972375	9.972354	0.000021	21
2,2'-TDS	9.975750	9.975735	0.000015	15
4-MBA	9.972125	9.972091	0.000034	34
4-MPAA	9.986625	9.986587	0.000038	38

In general, frequency change of dry crystals modified with SAMs is higher than for wet modified crystals. The structure of aromatic thiol SAMs could be responsible for higher change in frequency noticed compared with aliphatic thiols.

4.2.2 The thickness for self-assemble monolayer

In order to calculate the thickness for each monolayer of these SAMs depending on the shift of frequency, the same above procedure was repeated with lower concentrations of thiol solutions and for longer immersed time by taking an advantages of Sauerbrey equation (previously mentioned in section 2.1.2.2), density and the initial area for piezoelectric device ($0.23cm^2$) . The outcome calculations are in table 4-5.

Table 4-5 calculate the thickness for each monolayer formed on gold surface

SMA	MSA	2,2′-TDS	4-MBA	4-MPAA
-Δf (Hz)	22	negligible	24	26
Mass = -1.1× -Δf (ng)	24.2	-	26.4	28.6
m (g)	2.42×10^{-8}	-	2.64×10^{-8}	2.86×10^{-8}
d (g/cm^3)	1.52	-	1.34	1.29
Volume, V= $\frac{m}{d}$ (cm^3)	1.5×10^{-8}	-	1.9×10^{-8}	2.2×10^{-8}
A (cm^2)	0.23	-	0.23	0.23
Thickness, T= $\frac{V}{A}$ (cm)	6.9×10^{-8}	-	8.5×10^{-8}	9.6×10^{-8}
Thickness (A^O)	6.9	-	8.5	9.6

The result of comparing the thickness for each SAM with the thickness calculated by Chem. 3D and PC Spartan is in the next table, where reasonable matches of the thickness values are presented. The structures of all studied SAMs in three dimensional are in the appendix (see figures I & II).

Table 4-6 shows the calculated thickness for some SAMs from impedance spectra, and comparing with the thickness values gained from Chem. 3D & PC Spartan.

SMA	MSA	2,2′-TDS	4-MBA	4-MPAA
Thickness calculated by Chem. 3D (A^o)	5.83	5.98	7.93	8.95
Thickness calculated by PC Spartan (A^o)	5.637	5.892	7.149	8.518
Thickness calculated from data (A^o)	6.9	-	8.5	9.6

Impedance spectroscopy for 4-MBA and 4-MPAA, both of them have significant change in frequency, shows more mass is added to the bare gold surface compared with aliphatic thiols, thereby the electrode surface should have a higher coverage or possibly even blocked, so density of defect is low. However, CV result shows that the surface is not blocked; because cyclic voltammograms undergoes small change compared with MSA, as can be seen in section (4.1.1). This means some electrons still have the ability to reach gold electrode surface through these moleculars. The reason behind this behaviour is that the aromatic thiols have double bonds in flux motion (resonance) as in figure 4:12 (a & b).

Such molecules are electrical conductors. Electrons can pass through them from solution bulk to gold electrode surface. It can also be concluded that 4-MBA is more effective for transfer electrons than 4-MPAA, since in the first one the charge is distributed through the ring and outside of it to reach the carboxylic group, while in 4-MPAA the resonance motion for double bands are restricted or contracted inside the benzene ring (less spreading for the charge).

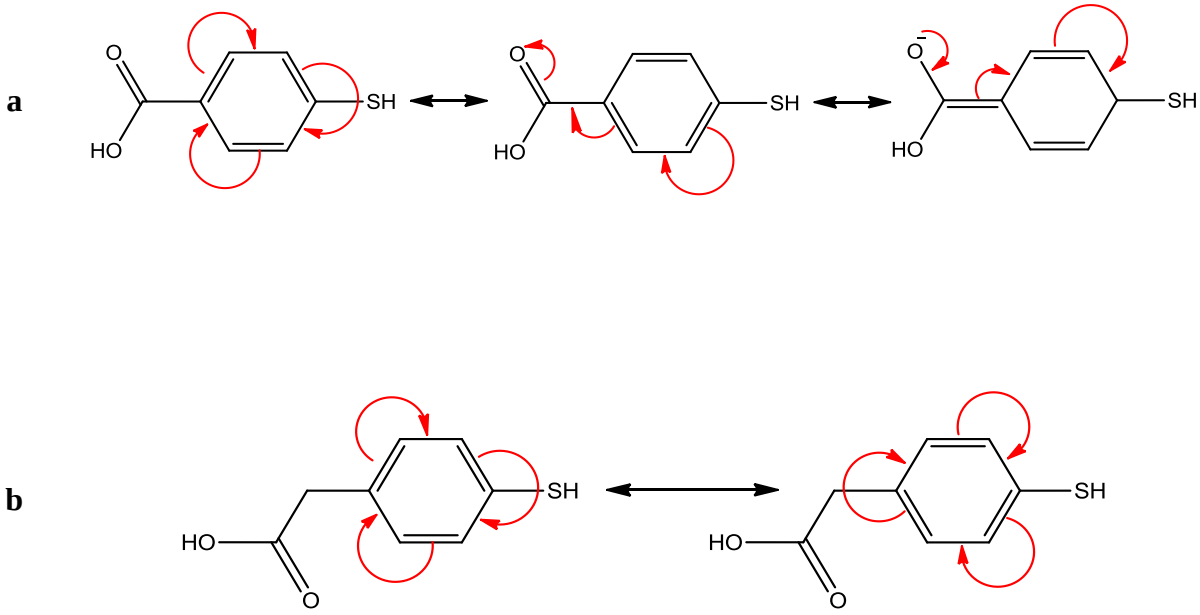

Figure 4-12: a) the phenomenon of resonance in the benzene ring of 4-mercaptobenzoic acid and spread of the shipment through it, b) the phenomenon of resonance in the benzene ring of 4-mercaptophenyalacetic acid and spread of the shipment through it.

4.2.3 Trace metal ion analysis using QCM

Introduction

It has been confirmed that, when the surface of the quartz crystal electrode is coated by an active layer, which has the ability to interact with the environment of interest, a very sensitive sensor can be created.[5]

Here the study of modified quartz crystal will be used as an extremely sensitive mass sensor to investigate lead, nickel and cobalt concentration. There are three different kinds of the processes to analyse the trace metal ions in aqueous solution by using QCM, and these procedures are: electro-depositing, electro-stripping and sorption with active ligands. Electro- deposition is probably the most common procedure used in this field, but electro-stripping can also be used[6]. Figure 4:13 represents clear schematic diagram for these three possible processes. However, in this work the focus will be on the third type, despite it is more complicated, where the sorption of trace metal ions will take place by an effective ligands immobilised on gold crystal.

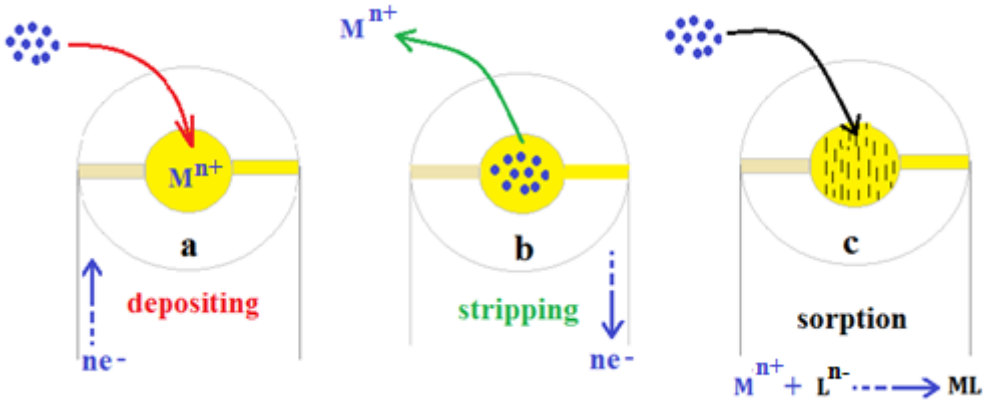

Figure 4-13 schematic shape shows all possible mechanisms for sensing metal ions by taking advantages of a) electro-deposition, b) electro-stripping and c) attracted with immobilised ligands.

In the past, the dominant idea among scientists was that quartz crystal cannot resonate in solution and for that reason the analysis of metal ions was conducted on the following lines:

- Deposit metal ions on gold crystal
- Rinse it with De-ionized water
- Dry gold crystal with nitrogen gas
- measure the differential in frequency

This method has high sensitivity as compared with the electro-gravimetric analysis but it takes a long time, and also it cannot be reproduced[6].

Since Nomura and his colleague Bastians indicated that there is a possibility of being the crystal oscillates in aqueous media, the experimental design was conducted where in situ analysis became possible, and later on he also shows that some metal ions are adsorbed spontaneously on the crystal in the absence of any ligand, which is an interference problem.[7, 8]

QCM has been used as a sensor for trace metal ion analysis by immobilised ligands on one side of gold surface, which is in contact with the solution. The next descriptions are for using gold-mercaptosuccinic (Au-MSA) as a sensor, which should work effectively in capturing trace metal ions in aqueous solutions. The first step is to prepare a very stable ligand on the gold electrode surface from this thiol, and at the second step the SAM should be bonded with each of interested metal ions, which was characterised by using different techniques, such as cyclic voltammetry, QCM and Raman spectrometer. The last step was also divided into the next two stages.

Here different concentrations of each metal ion were reacted with Au-MSA to identify which metal ion interacts more with this ligand. Then fitting the obtained data of changing in frequency to the most common kinds of isotherms (Langmuir, Frumkin, Temkin and Freundlich), which can give us some insight for guessing the process type and then one can put these isotherms in order (more linearity best fitting).

Secondly, the Sauerbery equation was used to calculate any change in mass at electrode surface (gravimetric analysis). However, a wide range of the concentrations of interested metal ions (10 ppm to 100 ppm), should be studied in order to estimate the binding constant value for each metal ion with the most effective ligand.

Using QCM to study the complexation process of trace metal ions with SAM

In order to study trace metal ions at ppm level in aqueous solutions; all steps mentioned in section (4.2) were repeated, followed by adding an aqueous solution of metal ion being studied (100 ppm) to the cell provided with modified gold, for a certain contact time before being emptied and dried with nitrogen gas, and then measuring the change in frequency ($f_{SAM\text{-}M,\ d}$) again. However, the shift in frequency corresponding to added metal ions can be calculated as follows:

$$\Delta f_M = f_{SAM,\ d} - f_{SAM\text{-}M,\ d} \qquad 4\text{-}6$$

The next step was the use of the Sauerbrey equation in order to convert Δf to Δm as mentioned before in section (2.1.2.2).

4.2.4 Complexation metal ions with Au-MSA & the molar ratio M:MS-Au

Since MSA was the best choice among the four different thiols for modifying gold surfaces, this thiol has been used as SAM on a gold electrode to study of very low concentration of lead, cobalt and nickel ions in aqueous media.

A gold mercaptosuccinate modified quartz electrode was exposed to 100 ppm of metal ions at room temperature in the glass cell described in section (3.2.3). The molar ratio for mercaptosuccinate ligand and all the possible structures for each metal ion complex (M:MS-Au, $M(NO_3)_2$:MS-Au, $M(NO_3)_2.H_2O$:MS-Au and $M(NO_3)_2.6H_2O$:MS-Au) were taken into the account. Table 4-7 shows the result.

Table 4-7 Results of frequency shifts of binding Au-MSA with some metal ions and the change in mass, the concentration of metal ions were 100ppm. í is the mole ratio between the metal ions and Au-MSA on dry crystal.

	Pb	MSA	Ni	MSA	Co	MSA
-Δf (Hz)	46	20	12.3	24	13	23
Δm (ng)	50.6	22	13.5	26.4	14.3	25.3
No of mole M:MS-Au	$\frac{50.6}{207.2}$ = 0.24	$\frac{22}{150.15}$ = 0.14	$\frac{13.5}{58.69}$ = 0.23	$\frac{26.4}{150.15}$ = 0.18	$\frac{14.3}{58.93}$ = 0.24	$\frac{25.3}{150.15}$ = 0.17
Mole ratio (í)	$\frac{0.24}{0.14}$ = 1.7		$\frac{0.23}{0.18}$ = 1.2		$\frac{0.24}{0.17}$ = 1.4	
No of mole $M(NO_3)_2$:MS-Au	$\frac{50.6}{331.23}$ = 0.15	$\frac{22}{150.15}$ = 0.14	$\frac{13.5}{182.7}$ = 0.074	$\frac{26.4}{150.15}$ = 0.18	$\frac{14.3}{182.9}$ = 0.078	$\frac{25.3}{150.15}$ = 0.17
Mole ratio (í)	$\frac{0.15}{0.14}$ = 1.07		$\frac{0.07}{0.18}$ = 0.41		$\frac{0.078}{0.17}$ = 0.45	
No of mole $M(NO_3)_2.H_2O$:MS-Au	$\frac{50.6}{349.23}$ = 0.14	$\frac{22}{150.15}$ = 0.14	$\frac{13.5}{200.7}$ = 0.067	$\frac{26.4}{150.15}$ = 0.18	$\frac{14.3}{200.9}$ = 0.07	$\frac{25.3}{150.15}$ = 0.17
Mole ratio (í)	$\frac{0.14}{0.13}$ = 1		$\frac{0.067}{0.18}$ = 0.37		$\frac{0.07}{0.17}$ = 0.4	
No of mole $M(NO_3)_2.6H_2O$:MS-Au	$\frac{50.6}{439.23}$ = 0.11	$\frac{22}{150.15}$ = 0.14	$\frac{13.5}{290.8}$ = 0.046	$\frac{26.4}{150.15}$ = 0.18	$\frac{14.3}{291.03}$ = 0.049	$\frac{25.3}{150.15}$ = 0.17
Mole ratio (í)	$\frac{0.11}{0.14}$ = 0.8		$\frac{0.07}{0.18}$ = 0.25		$\frac{0.049}{0.17}$ = 0.28	

The result in the above table, indicates the molar ratio (**í)** between lead ions and mercaptosuccinate ligand Pb:MS-Au was 1.7, and for nickel Ni:MS-Au **í** equal 1.2, while for cobalt Co:MS-Au **í** appeared to be 1.4.

4.2.5 Binding constant for individual metal ion

In this part of study modified quartz crystal microbalance with mercaptosuccnic acid was used to study all of which lead, cobalt and nickel, under the same conditions separately, in concentration range 1 ppm - 100 ppm, with particular attention described for studying the adsorption isotherms.

The experimental data was fitted into four isotherms, as follows.

The first model was the Langmuir isotherm, which was originally developed to describe the adsorption of any species in gas phase onto activated carbon. The main assumptions inherent in this isotherm are as follows[9]:

- All adsorption sites have the same activity (homogeneous binding sites).
- Only one molecule may be absorbed on any one site.
- There are no interactions between adsorbed molecules on adjacent sites.
- Dynamic equilibrium exists between adsorbed and free molecules.
- The adsorbed molecules would form only one layer (maximum of monolayer coverage).

$$\frac{1}{\theta} = 1 + \frac{1}{K_L C} \qquad 4\text{-}7$$

where, θ the degree of surface coverage, C is the concentration and K_L is the characteristic parameter.

The second model was the Freundlich isotherm, which is widely applied in heterogeneous systems especially for organic compounds or highly interactive species on rough surface (activated carbon)[10, 11,12]. The Freundlich adsorption isotherm often fails at higher pressure. This model of adsorption can be described by the following equation:

$$ln\theta = \frac{1}{n}\ln C + lnK_F \qquad 4\text{-}8$$

where, all symbols are as mentioned before, K_F is an indicator of the maximum amount that can be adsorbed (adsorption capacity), and 1/n is a measure of intensity of adsorption. Higher the 1/n value more favourable is the adsorption (in general n < 1). This isotherm based on the following assumptions:

- The adsorption process is taking place on a heterogeneous surface
- It denotes the non-ideal and reversible adsorption
- This empirical model can be applied to multilayer adsorption

Thirdly, the Temkin isotherm was proposed with the aim of considering the effects of adsorbate / adsorbate interactions on adsorption isotherms. This model has been used in the following form:

$$\theta = \frac{1}{f}\ln K_T + \frac{1}{f}\ln C \qquad 4\text{-}9$$

where, K_T ($dm^3 \cdot g$) plays the role of an equilibrium constant. What distinguishes this isotherm from the others is the heterogeneity of the surface (sites with different energies). It assumes that the heat of adsorption decreases linearly with coverage[13, 14]. The best example for the Temkin isotherm is the adsorption of hydrogen onto platinum electrodes from acid solution.

Fourthly, the Frumkin isotherm was used. This model is appropriate mostly for non-ionic surfactants. It builds on the Langmuir isotherm by accounting for solute-solute interactions at a non-ideal surface[15]. Its usual stated form is;

$$f\theta = ln[\frac{1-\theta}{C\theta}] + lnK_{Fr} \qquad 4\text{-}10$$

where, K_{Fr} is the Frumkin equilibrium adsorption constant. The Frumkin adsorption isotherm is generally a reasonable model for $0 \leq \theta \leq 1$.

The applicability of these isotherms to be applied with each process:

In general, all these isotherms can be represented in straight line equation ($A = B + CD$) so when a plot of D versus A produces a straight line with slope equal C and intercept equal B, the process follows that isotherm should give a good fitting (more linearity). However, for each metal ion, the data of frequency changes for a range of different concentrations (1-100 ppm) were used to plot all experimental data with the theoretically predicted isotherms. These can be seen in figures 4:14, 4:15 and 4:16; the numerical data can be found in tables I, II and III at the appendix.

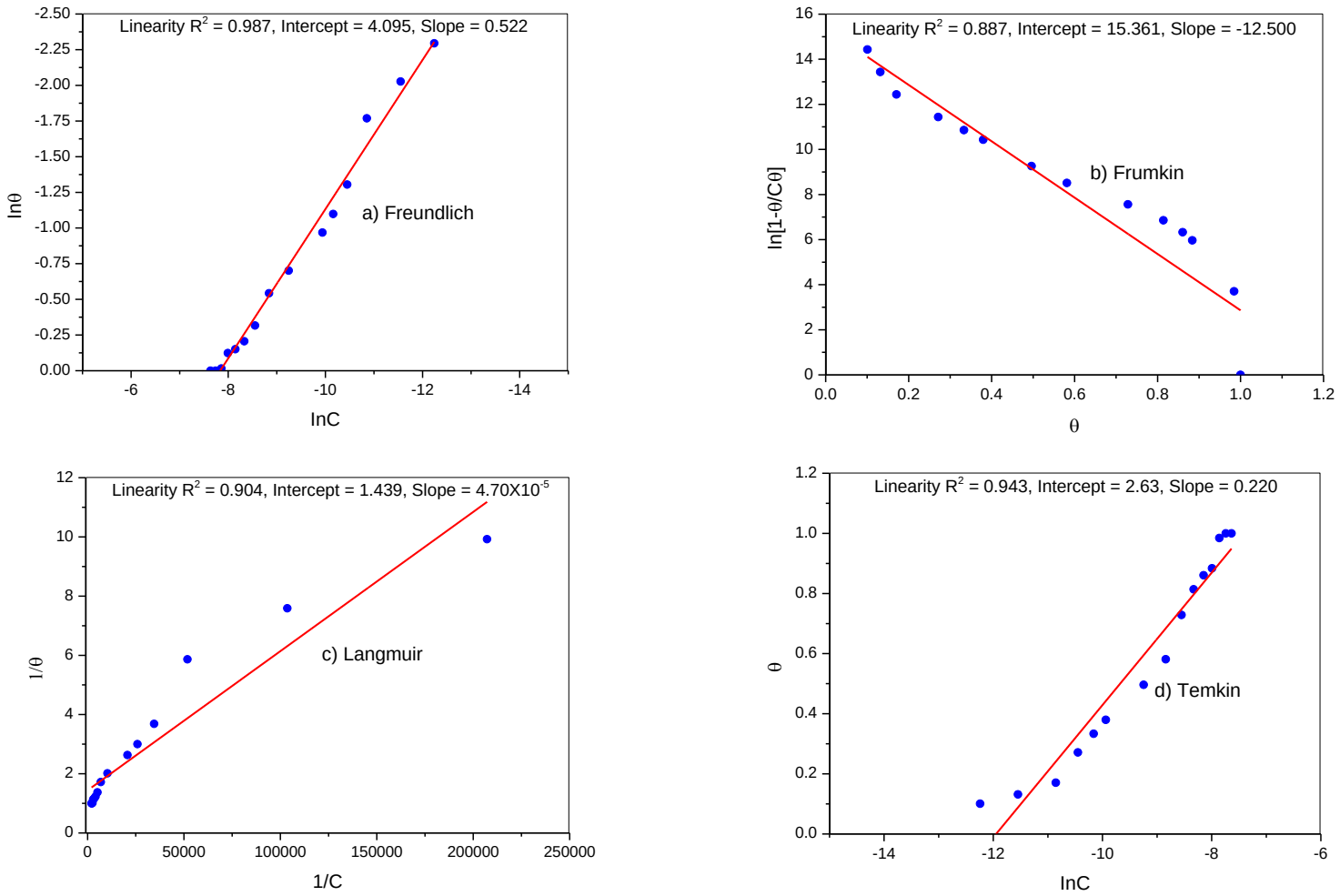

Figure 4-14 fitting the data of the Complexation process of lead with MSA to four different kinds of isotherms; a) Freundlich isotherm, b) Frumkin isotherm, c) Langmuir isotherm, and d) Temkin isotherm.

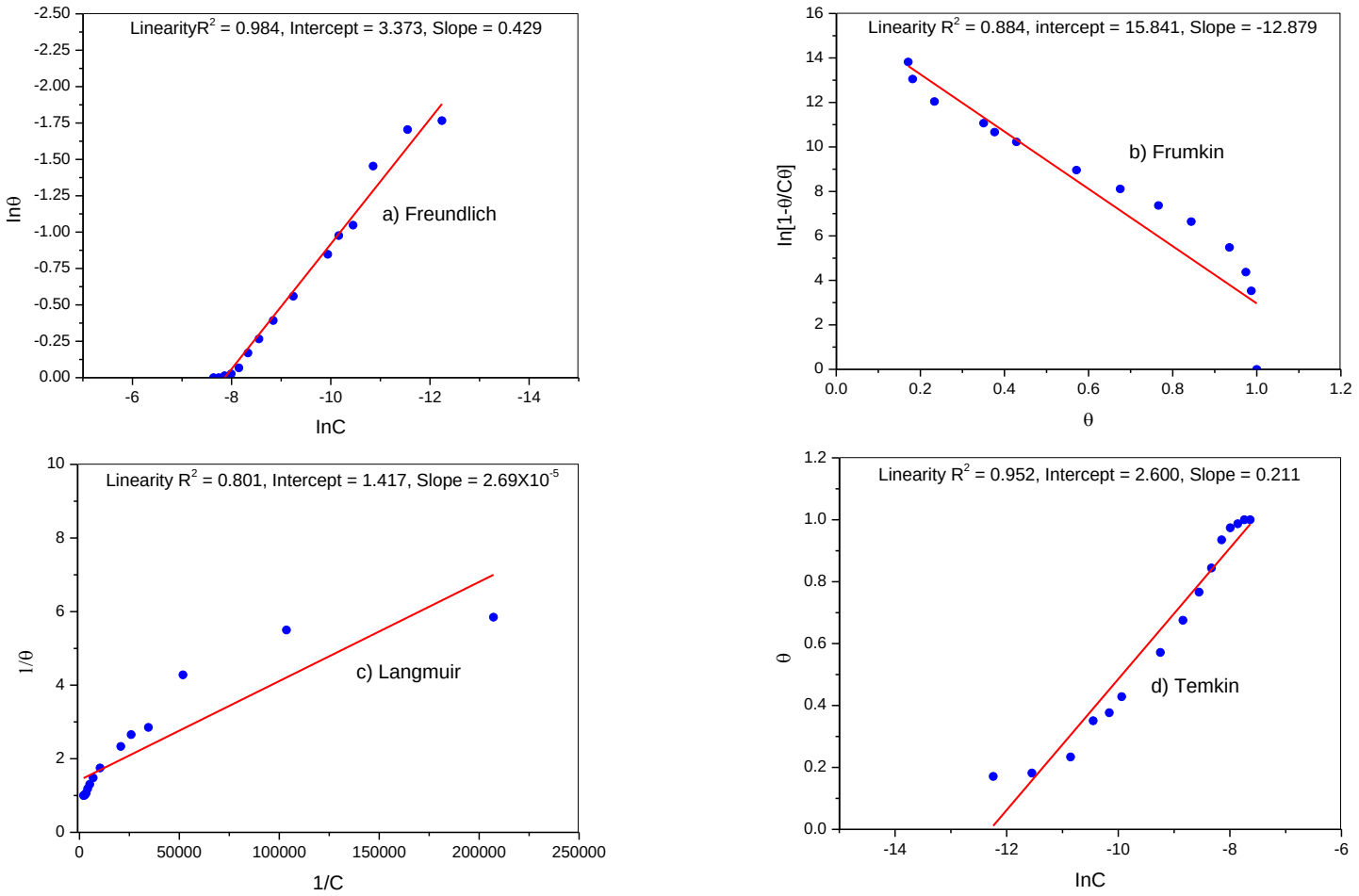

Figure 4-15 fitting the data of the Complexation process of nickel with MSA to four different kinds of isotherms; a) Freundlich isotherm, b) Frumkin isotherm, c) Langmuir isotherm, and d) Temkin isotherm.

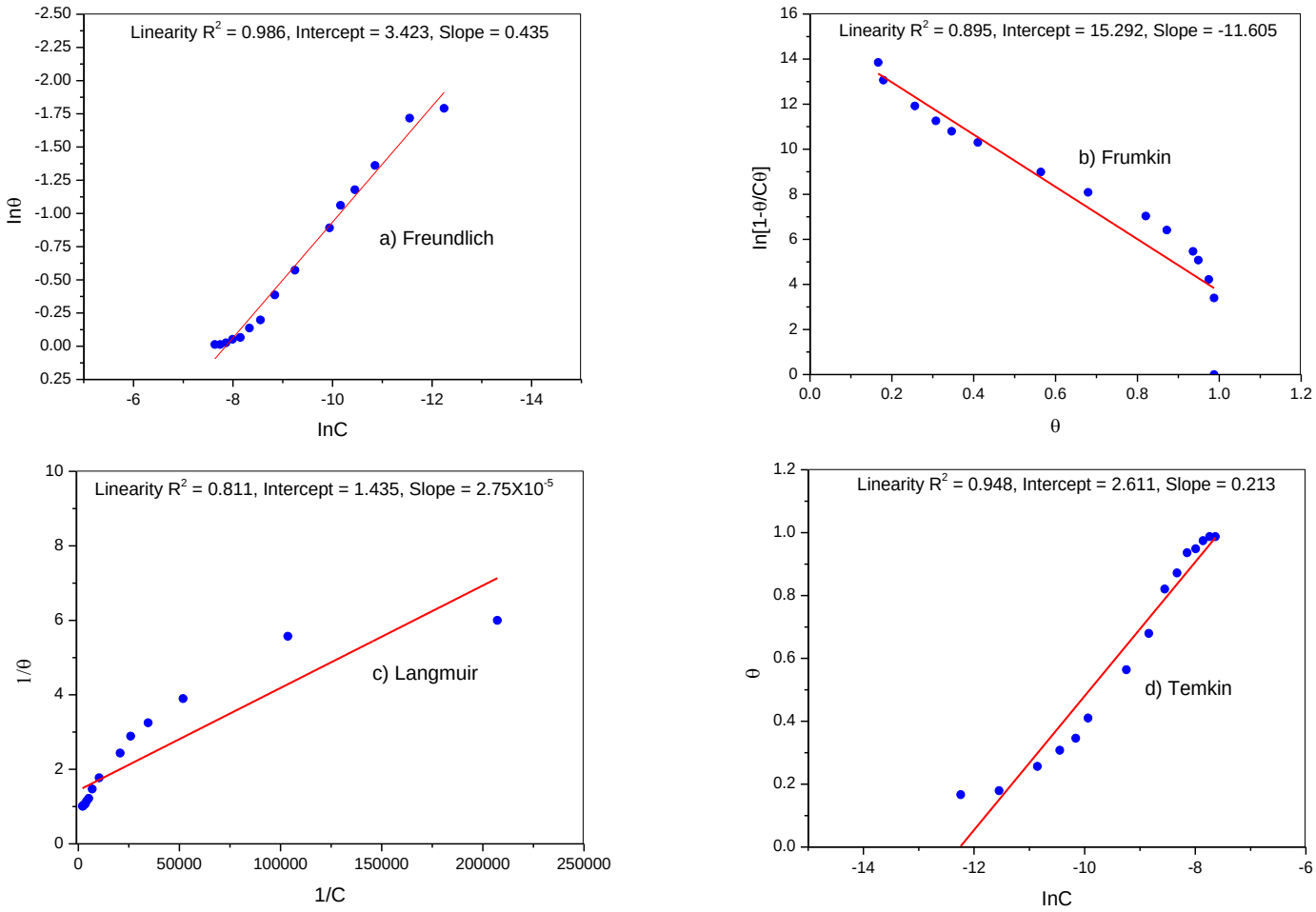

Figure 4-16 fitting the data of the Complexation process of cobalt with MSA to four different kinds of isotherms; a) Freundlich isotherm, b) Frumkin isotherm, c) Langmuir isotherm, and d) Temkin isotherm.

The results extracted from the above figures, show that the Freundlich isotherm provided the best fitting for the adsorption of these metal ions with MS-Au, so depending on the linearity of the curves, one can put above isotherms in the order. However, R^2 values show that Ni & Co follows the next order:

Freundlich > Temkin > Frumkin > Langmuir.

But in the case of lead the order was slightly different, since Langmuir isotherm has taken advantage over Frumkin isotherm, so the priority will be as follows Freundlich > Temkin > Langmuir > Frumkin.

4.2.6 Calculation of Binding constant

Since Frendlich isotherm gave best fitting, characteristic parameters K & $\frac{1}{n}$ can be calculated for each metal ion, where K represents the adsorption capacity and the value of $\frac{1}{n}$ is a measure of the strength of adsorption, as in the next table.

Table 4-8 shows the values of calculated parameters

$ln\theta = \ln K_F + \frac{1}{n} \ln C$					
parameter	Slope ($\frac{1}{n}$)	n	Intercept (lnK)	K	logK
Pb:MA-Au	0.522	1.916	4.095	60.039	1.778
Co:MA-Au	0.435	2.294	3.423	30.685	1.487
Ni:MA-Au	0.429	2.331	3.373	29.165	1.465

The calculated binding constant was also compared with the binding constant values for the interested metal ions complexes with mercaptosuccinic acid in aqueous medium[16], and detailed in table 4:9, where very good agreement has been noticed regarding the stability of the produced complexes (K). However, it should be taken into account that the values of log K calculated from the experimental data were smaller than those from the literature. In our experiment the ligand was restricted on the gold surface, while values from literature relate to the free ligand in aqueous media meaning more freedom for complexation to occur.

Table 4-9 show the comparison between calculated binding constants with literature

	Pb	Co	Ni
Log K from literature	2.8	1.7	1.6
Log K from experiment data	1.78	1.49	1.47

The result suggests that the adsorption isotherm of Pb increased more sharply than Co and Ni, and for that reason Pb should be more attracted to the selected ligand (Au-MSA) compared with Co and Ni, since both of them have a lower binding affinity.

4.2.7 Complexation a mixture of metal ions with selected SAM

Au-MSA was used to analyse different mixtures of metal ions. Three binary mixtures (lead & nickel, lead & cobalt and a mixture of nickel & cobalt); then the same ligand was also used to analyse a mixture of all these metal ions mixed together (lead, nickel and cobalt).

4.2.7.1 Using Au-MSA to analyse a binary mixture of metal ions

The purpose of mixture analysis is to study the effect of interference metal ions (B^{2+}) on the complexation process of the ligand with another metal ion (A^{2+}). The idea of work

is based on fixing the concentration of one metal ion B^{2+} and changing the concentration for the other A^{2+} and observing the change in frequency. After that the process has to be reversed by fixing A^{2+}concentration and changing the concentration of B^{2+} as in the next table.

Table 4-10 shows a general plan to analysis mixture of two metal ions (A^{2+} and B^{2+})

Stage 1	**A^{2+}**		**B^{2+}**		**Added water**	**Conc. in mixture**	
						[A^{2+}]	**[B^{2+}]**
1	**9ml**	**100ppm**	**1ml**	**100ppm**	**-**	**90ppm**	**10ppm**
2	**6ml**	**100ppm**	**1ml**	**100ppm**	**3ml**	**60ppm**	**10ppm**
3	**3ml**	**100ppm**	**1ml**	**100ppm**	**6ml**	**30ppm**	**10ppm**
4	**1ml**	**100ppm**	**1ml**	**100ppm**	**8ml**	**10ppm**	**10ppm**
5	**9ml**	**1ppm**	**1ml**	**100ppm**	**-**	**0.9ppm**	**10ppm**
Stage 2	**A^{2+}**		**B^{2+}**		**Added water**	**Conc. in mixture**	
						[A^{2+}]	**[B^{2+}]**
1	**1ml**	**100ppm**	**9ml**	**100ppm**	**-**	**10ppm**	**90ppm**
2	**1ml**	**100ppm**	**6ml**	**100ppm**	**3ml**	**10ppm**	**60ppm**
3	**1ml**	**100ppm**	**3ml**	**100ppm**	**6ml**	**10ppm**	**30ppm**
4	**1ml**	**100ppm**	**1ml**	**100ppm**	**8ml**	**10ppm**	**10ppm**
5	**1ml**	**100ppm**	**9ml**	**1ppm**	**-**	**10ppm**	**0.9ppm**

- **The competitive process between nickel and lead**

Graph 4:17 shows the competitive reaction result for lead and nickel with Au-MSA. The experiment was divided into two stages. The first step involved the nickel concentration kept fixed and the concentration of lead was varied. In stage two the nickel concentration was changed and lead concentration fixed.

In the case 1 it was found that the change in frequency considerably increased with the increase of lead concentrations. In the case 2, despite the increase of nickel concentration, the change in frequency was fairly consistent (figure 4:17). The obtained results verify that nickel as an interfering ion has negligible influence on complexation process of Pb:MS-Au.

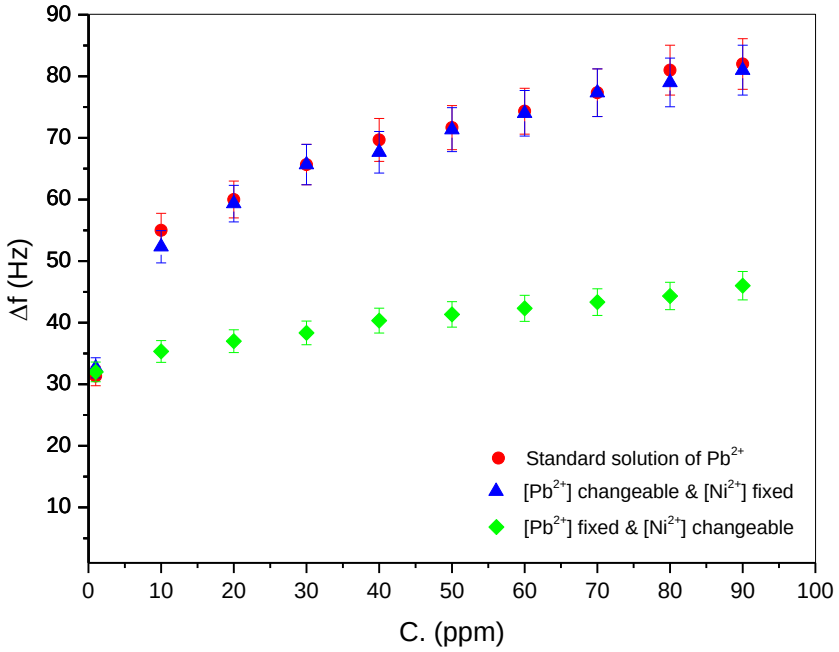

Figure 4-17 Complexation process of different concentration of lead ions with mercaptosuccinic acid in presence of nickel as an interference ion

- **The competitive process between cobalt and lead**

The mixture of lead – cobalt, was treated as the same as lead-nickel mixture, where the frequencies were measured every time by fixing the concentration of cobalt at 10 ppm and changing lead concentration. Additionally the next step involved the concentration of lead being fixed and the cobalt concentration varied as can be seen in figure (4:18). The concentration of cobalt has limited effect on the formation process of Pb:MS-Au.

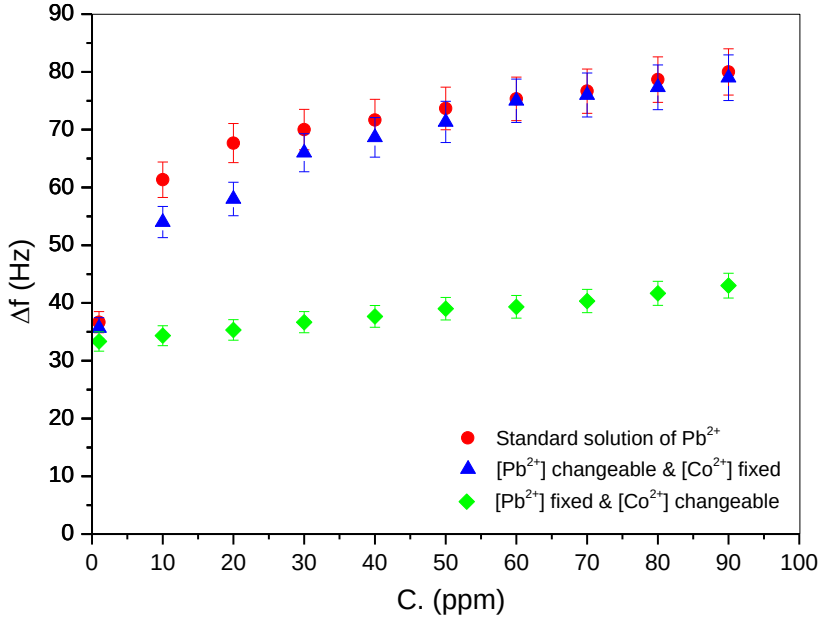

Figure 4-18 Complexation process of different concentration of lead ions with mercaptosuccinic acid in presence of cobalt as an interference ion

- **The competitive process between cobalt and nickel**

The final experiment in the analysis of binary mixtures is for nickel and cobalt mixture, where a different trend was seen compared to the pervious binary solutions. Since the results were approximately the same whatever ion concentration in the mixture was fixed or changed. See figure 4:19, and for more specific numerical details go to the appendix (tables IV, V and VI).

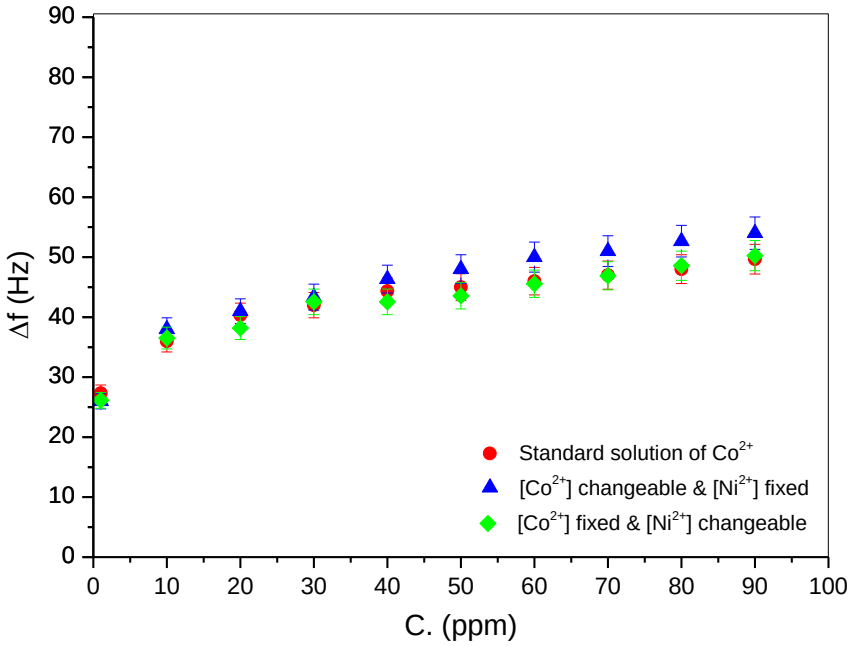

Figure 4-19 Complexation process of different concentration of cobalt ions with mercaptosuccinic acid in presence of nickel as an interference ion

4.2.7.2 Using Au-MSA to analyse a mixture of three metal ions

These experiments are similar to the previous ones except that at this time three interference metal ions (A^{2+}), (B^{2+}) and (C^{2+}) were used instead of a binary mixture to investing all this the concentration of one metal ion was varied and the other two kept constant, see table 4:11. This procedure represents which metal ion has the most influence on the complexation process of Au-MSA with these metal ions.

Table 4-11 shows a general plan to analysis mixture of three metal ions (A^{2+}, B^{2+} and C^{2+}).

Stage1	A^{2+}		B^{2+}		C^{2+}		added water	Conc. in mixture		
								$[A^{2+}]$	$[B^{2+}]$	$[C^{2+}]$
1	8 ml	100ppm	1 ml	100ppm	1 ml	100ppm	-	80 ppm	10 ppm	10 ppm
2	4 ml	100ppm	1 ml	100ppm	1 ml	100ppm	4 ml	40 ppm	10 ppm	10 ppm
3	2 ml	100ppm	1 ml	100ppm	1 ml	100ppm	6 ml	20 ppm	10 ppm	10 ppm
4	1 ml	100ppm	1 ml	100ppm	1 ml	100ppm	7 ml	10 ppm	10 ppm	10 ppm
5	8 ml	1ppm	1 ml	100ppm	1 ml	100ppm	-	0.8 ppm	10 ppm	10 ppm
Stage2	**A^{2+}**		**B^{2+}**		**C^{2+}**		**added water**	**Conc. in mixture**		
								$[A^{2+}]$	**$[B^{2+}]$**	**$[C^{2+}]$**
1	1 ml	100ppm	8 ml	100ppm	1 ml	100ppm	-	10 ppm	80 ppm	10 ppm
2	1 ml	100ppm	4 ml	100ppm	1 ml	100ppm	4 ml	10 ppm	40 ppm	10 ppm
3	1 ml	100ppm	2 ml	100ppm	1 ml	100ppm	6 ml	10 ppm	20 ppm	10 ppm
4	1 ml	100ppm	1 ml	100ppm	1 ml	100ppm	7 ml	10 ppm	10 ppm	10 ppm
5	1 ml	100ppm	8 ml	1ppm	1 ml	100ppm	-	10 ppm	0.8ppm	10 ppm
Stage3	**A^{2+}**		**B^{2+}**		**C^{2+}**		**added water**	**Conc. in mixture**		
								$[A^{2+}]$	**$[B^{2+}]$**	**$[C^{2+}]$**
1	1 ml	100ppm	1 ml	100ppm	8 ml	100ppm	-	10 ppm	10 ppm	80 ppm
2	1 ml	100ppm	1 ml	100ppm	4 ml	100ppm	4 ml	10 ppm	10 ppm	40 ppm
3	1 ml	100ppm	1 ml	100ppm	2 ml	100ppm	6 ml	10 ppm	10 ppm	20 ppm
4	1 ml	100ppm	1 ml	100ppm	1 ml	100ppm	7 ml	10 ppm	10 ppm	10 ppm
5	1 ml	100ppm	1 ml	100ppm	8 ml	1ppm	-	10 ppm	10 ppm	0.8ppm

The analysing process of the three metal ions mixture was even more complicated than the binary mixture. However, the most important result that can be concluded in this case is that the concentration of lead was the only key factor in the analysis of such a mixture as with binary systems. See figure 4:20, and table VII at the appendix where specific numerical details can be found.

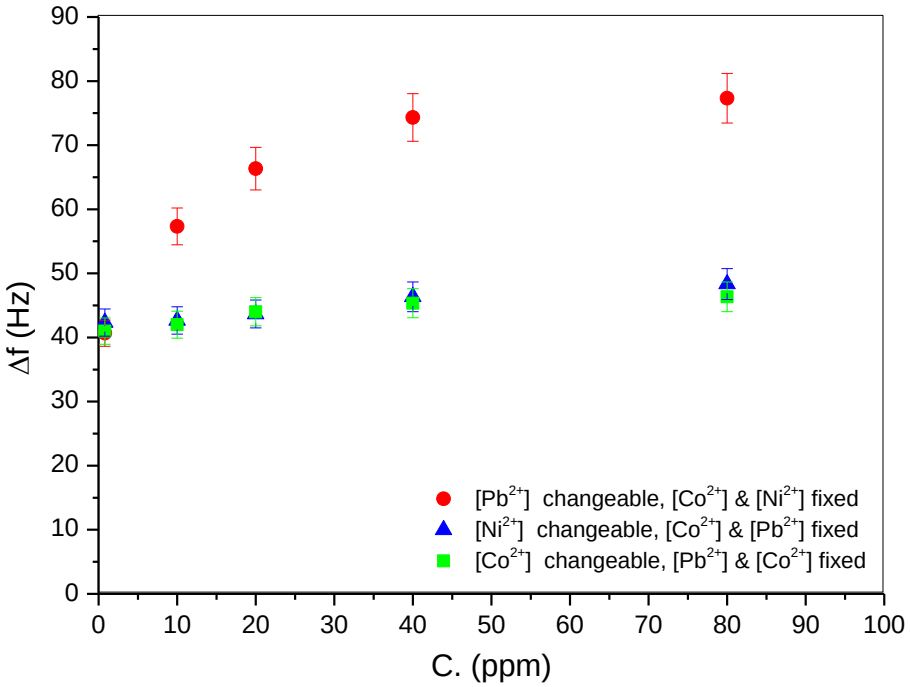

Figure 4-20 Complexation process of different concentration of lead ions with mercaptosuccinic acid in presence of nickel and cobalt as interference ions

It has been also found that modified crystal can be used many times to bind different metal ions from the solution without loss of surface ligand, all you need is to wash the M:MS-Au with 0.1M EDTA solution for three times to restore the initial frequency value, meaning that the adsorption of metal ions was reversible.

4.3 The stability of M:MS-Au complex

In these experiments the accumulation of trace metal ions was conducted under open circuit by immersing Au-MS in a mixture of 0.1 M of potassium nitrate solution containing 1 mM metal ion nitrate for about 15 mints. Removed M: MS-Au, rinsed with Di-water and placed in another potassium nitrate solution free of that metal ion.

4.3.1 Complexation process of Ni^{2+} with Au-MSA

In this experiment we need to investigate the stability of Ni:MS-Au complex by means of electrochemical technique. The cyclic voltammograms were recorded from -0.5 to 0.5V at scan rate 100mVs^{-1}as in figure 4:21, where two small redox peaks appeared at approximately $E_{p,a(ox)}$=0.225 V and $E_{p,c(red)}$=0.1 V, also the formal potential at E^o=0.1512V, these could be attributed from the oxidation and reduction processes for Ni^{2+}/Ni^o.

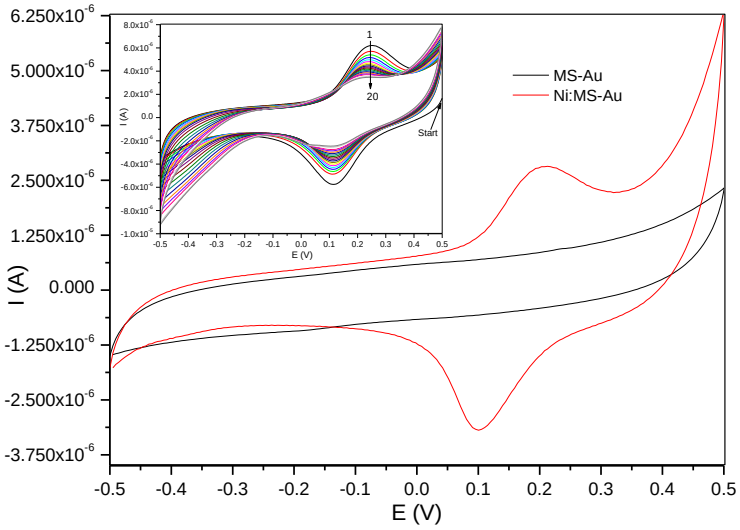

Figure 4-21 cyclic voltammograms of Au-MSA in 0.1 M Ni^{2+}-free KNO_3 solution, (black curve) before exposed modified gold to 1 mM Ni^{2+} solution, (red curve) after being exposed to 1 mM Ni^{2+} solution for 15 minutes. Inset represents the repetitive cycling voltammograms of Ni:MS-Au in Ni^{2+}-free 0.1 M KNO_3 solution, scan rate 100 mVs^{-1}.

The influence of repetitive redox cycles on the nickel ion binding, which demonstrated at the inset, shows the stability of the cyclic voltammograms obtained in this system at 100 mVs^{-1} sweep rate. During the course, cyclic voltammograms undergoes some decreases due to rearrangement of nickel coordination with the ligand that take place in the beginning. However, after cyclic number twelve a stable response was recoded upon repetitively cycling in a nickel-free electrolyte solution. This result suggested that nickel ions and Au-MSA interacted strongly within the potential range of the experiment.

The stability of the cyclic voltammograms was also obtained at different sweep rates, as can be seen in figure 4:22. The peak current increased linearly with increasing the scan rate for both reduction and oxidation processes.

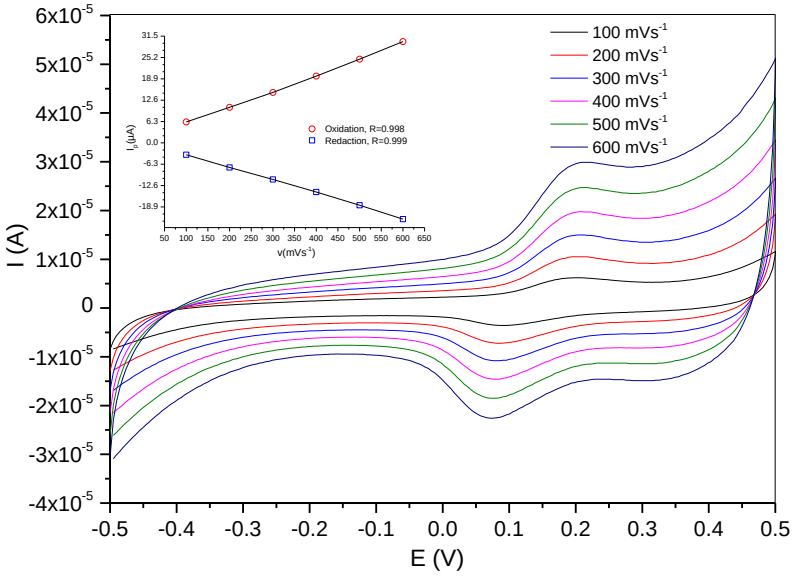

Figure 4-22 the influence of different potential scan rates (100 mVs^{-1}, 200 mVs^{-1}, 300 mVs^{-1}, 400 mVs^{-1}, 500 mVs^{-1}, 600 mVs^{-1}) on the peak current of the voltammogram, taken for 0.1 M of Ni^{2+}-free KNO_3 solution on Ni:MS-Au. Inset shows the variation of anodic and cathodic peak currents versus scan rate.

4.3.2 Complexation process of Co^{2+} with Au-MSA

Compared with nickel, the stability of cobalt complex with Au-MSA is lower as can be seen in the inset repetitive cycling voltammograms (figure 4-23); starting from cyclic number one up to cyclic number seventeen. There is a clear decrease in peak current value and that may be because of more re-arrangement for nickel ions taking place on the electrode surface.

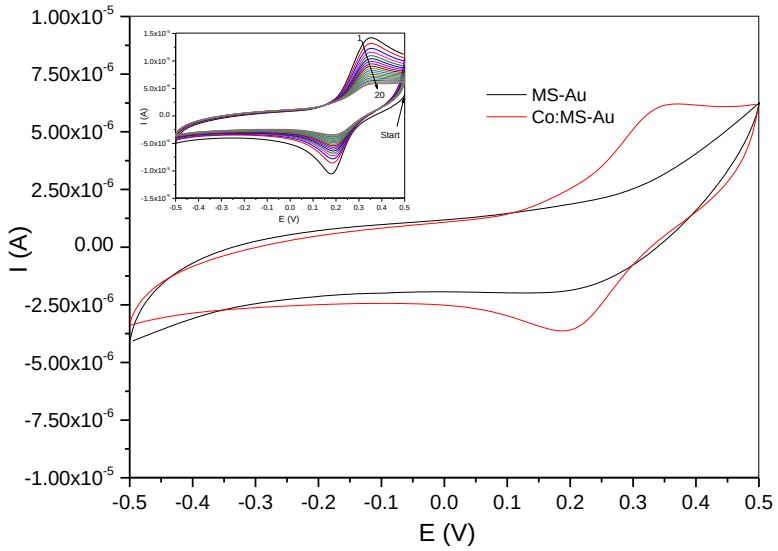

Figure 4-23 cyclic voltammograms of Au-MSA in 0.1 M Co^{2+}-free KNO_3 solution, (black curve) before exposed modified gold to 1 mM Co^{2+} solution, (red curve) after being exposed to 1 mM Co^{2+} solution for 15 minutes. Inset represents the repetitive cycling voltammograms of Co:MS-Au in Co^{2+}-free 0.1 M KNO_3 solution, scan rate 100 mVs^{-1}.

As for nickel the stability at different scan rates for the cyclic voltammogram was also investigated. The result shows a good linearity of increasing peak current by increasing the value of the scan rate for both forward and backward directions; see figure 4-24.

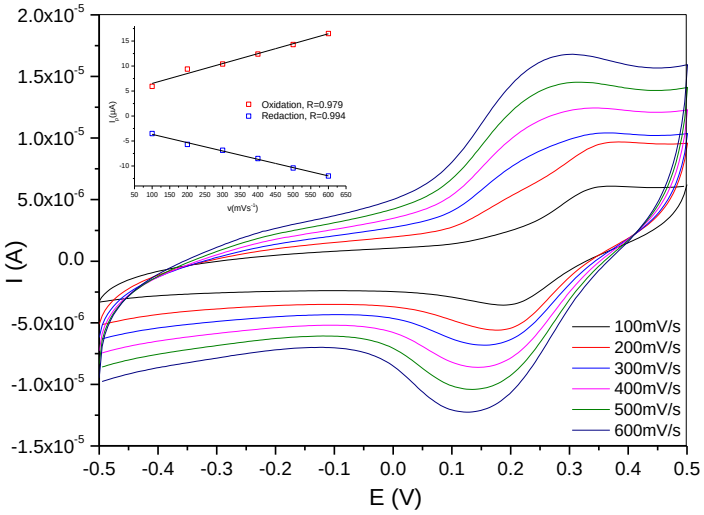

Figure 4-24 the influence of different potential scan rates (100 mVs^{-1}, 200 mVs^{-1}, 300 mVs^{-1}, 400 mVs^{-1}, 500 mVs^{-1}, 600 mVs^{-1}) on the peak current of the voltammogram, taken for 0.1 M of Co^{2+}-free KNO_3 solution on Co:MS-Au. Inset shows the variation of anodic and cathodic peak currents versus scan rate.

4.3.3 Complexation process of Pb^{2+} with Au-MSA

In the case of lead, the electrochemical responses of Pb:MS-Au complex was recorded from +0.5 to -0.5 V, at scan rate 100 mVs^{-1}, before and after the incubation process of lead ions. The electrochemistry due to redox reaction of Pb^{2+}/Pb^{o}, suggests that Pb^{2+} is bound to Au-MSA via carboxylate group, and reaction takes place at Epa=-0.12, Epc=-0.39 V and E^{o}=-0.27. More details about the interaction of lead ions with Au-MSA and the stability of this complex at repeated cyclic scans (20^{th} cycles), 100mVs^{-1} scan rate can be found in figure 4-25.

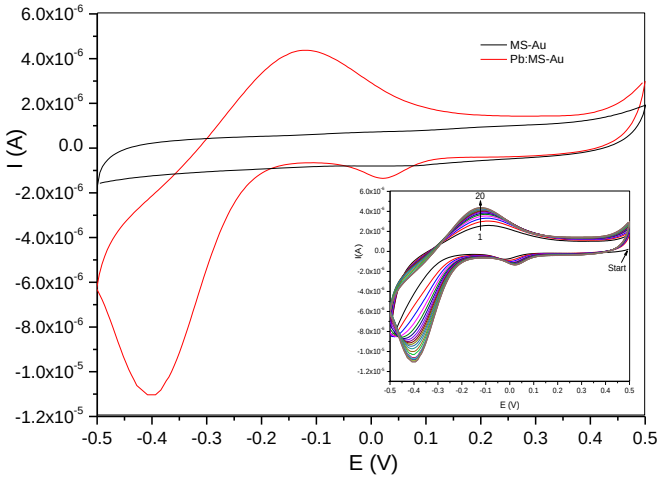

Figure 4-25 cyclic voltammograms of Au-MSA in 0.1 M Pb^{2+}-free KNO_3 solution, (black curve) before exposed modified gold to 1 mM Pb^{2+} solution, (red curve) after being exposed to 1 mM Pb^{2+} solution for 15 minutes. Inset represents the repetitive cycling voltammograms of Pb:MS-Au in Pb^{2+}-free 0.1 M KNO_3 solution, scan rate 100 mVs^{-1}.

The influence of scan rates on the behaviour of the cyclic voltammogram was also studied. Figure 4/26 shows that peak current increases linearly with scan rate.

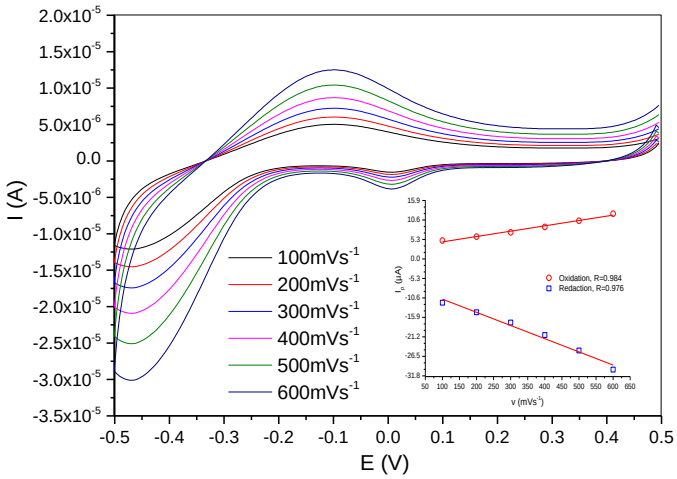

Figure 4-26 the influence of different potential scan rates (100 mVs^{-1}, 200 mVs^{-1}, 300 mVs^{-1}, 400 mVs^{-1}, 500 mVs^{-1}, 600 mVs^{-1}) on the peak current of the voltammogram, taken for 0.1 M of Pb^{2+}-free KNO_3 solution on Pb:MS-Au. Inset shows the variation of anodic and cathodic peak currents versus scan rate.

The amount of each metal ion can also be calculated from the charge (area under the peak) as can be seen in the next figure.

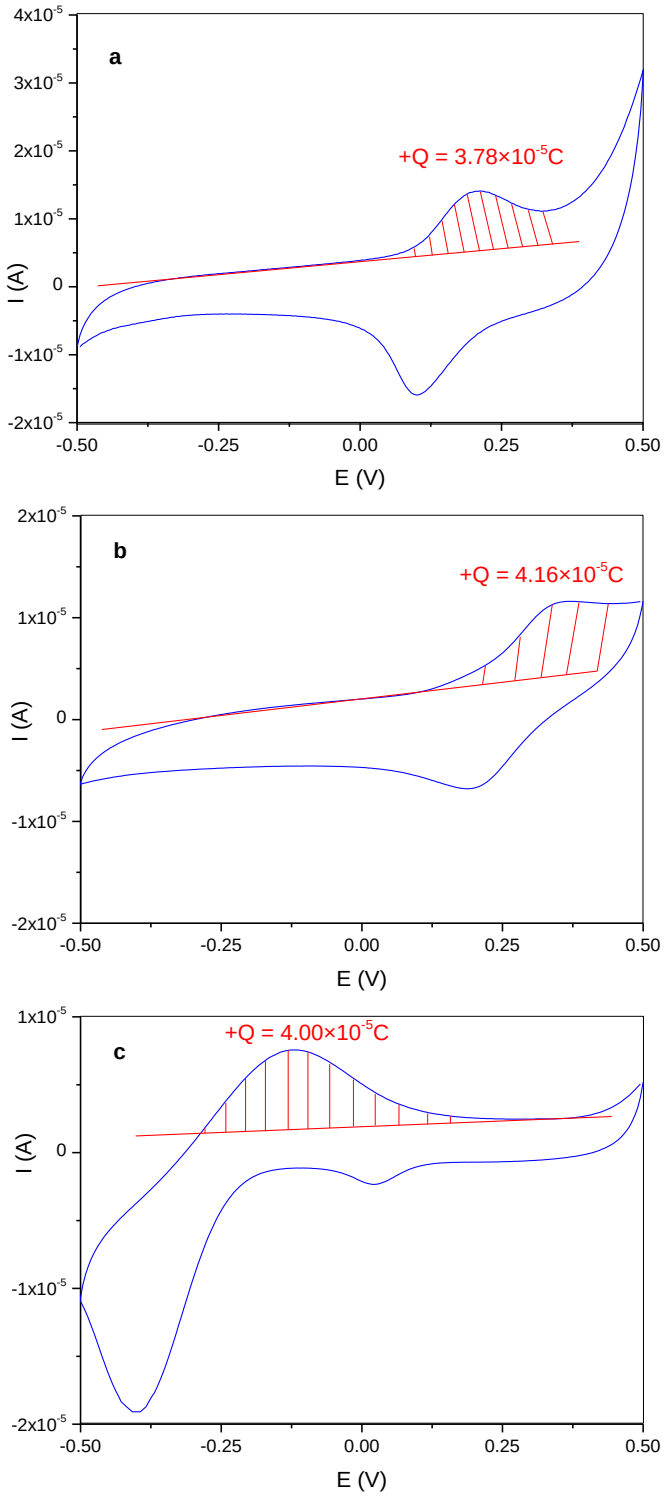

Figure 4-27 shows rough estimate of the charge for each of a) Ni2+ , b) Co2+ & c) Pb2+ , scan rate 100mVs-1, the concentrations of used metal ion solutions 100ppm.

Estimated charge in figure 4-27 can be used to find out the number of mole = $\frac{\mathbf{Q}}{\mathbf{nF}}$, where n is the number of electrons involved in the reaction (in these cases n = 2), and F is the Faraday constant (96485 C mol^{-1}).

Table *4-12*, summarises the amount of nickel, cobalt and lead complexed with Au-MSA individually from 100 ppm metal ion nitrate at open circuit in presence of 0.1M of KNO_3 solution. The result shows a kind of similarity as compared with the calculated number of moles by using QCM in section 4.2.4.

Table 4-12 represent the charge calculated from the above cyclic voltammograms and the number of mole for each metal ion, compared with number of moles gained before by using QCM in section 4.2.4.

	Metal ion	Ni^{2+}	Co^{2+}	Pb^{2+}
QCM	Atomic weight ($gmol^{-1}$)	58.69	58.93	207.2
	Mass calculated by QCM (ng)	13.5	14.3	50.6
	Mass calculated by QCM (g)	13.5×10^{-9}	14.3×10^{-9}	50.6×10^{-9}
	No. of mole based on QCM	2.30×10^{-10}	2.42×10^{-10}	2.44×10^{-10}
CV	+Q (coulomb)	3.78×10^{-5}	4.16×10^{-5}	4.00×10^{-5}
	No. of mole based on CV	1.96×10^{-10}	2.15×10^{-10}	2.07×10^{-10}

4.4 References

1. R. S. Nicholson, *Analytical Chemistry*, 1965, **37**, 1351-1355.
2. I. Lavagnini, R. Antiochia and F. Magno, *Electroanalysis*, 2004, **16**, 505-506.
3. J. C. Love, L. A. Estroff, J. K. Kriebel, R. G. Nuzzo and G. M. Whitesides, *Chemical Reviews*, 2005, **105**, 1103-1170.
4. T. Matsuura and Y. Shimoyama, *Eur. Phys. J. E*, 2002, **7**, 233-240.
5. Z. Hao and K. Eun Sok, *Journal of Microelectromechanical Systems*, 2005, **14**, 699-706.
6. T. Nomura and M. Ando, *Analytica Chimica Acta*, 1985, **172**, 353-357.
7. T. Nomura and T. Kanazawa, *Analytica Chimica Acta*, 1991, **245**, 71-76.
8. T. Nomura and M. Maruyama, *Analytica Chimica Acta*, 1983, **147**, 365-369.
9. N. Yui, *Supramolecular Design for Biological Applications*, Taylor & Francis, 2002.
10. K. Y. Foo and B. H. Hameed, *Chemical Engineering Journal*, 2010, **156**, 2-10.
11. Y.-P. Chin, C. S. Peven and W. J. Weber Jr, *Water Research*, 1988, **22**, 873-881.
12. R. T. Loto, C. A. Loto and T. Fedotova, *Research on Chemical Intermediates*, 2013, **40**, 1501-1516.
13. A. Khaled, A. El Nemr, A. El-Sikaily and O. Abdelwahab, *Desalination*, 2009, **238**, 210-232.
14. M. G. Bridelli and P. R. Crippa, *Adsorption*, 2007, **14**, 101-109.
15. J. O. M. Bockris, A. K. N. Reddy, M. Gamboa-Aldeco and M. E. Gamboa-Aldeco, *Modern Electrochemistry*, Springer, 2000.
16. A. E. Martell and R. M. Smith, *Critical stability constants: Other organic ligands*, Plenum Press, 1977.

Contents

5 Spectroscopic characterisation of solid surfaces

Introduction

The result in chapter four suggested that all of MSA, 4-MBA and 4-MPAA successfully deposited on gold surface, and the interaction of some metal ions with Au-MSA were also observed. To prove the existence of 2-mercaptosuccinic acid (MSA) on gold surface and the complexation process between this ligand and metal ions of interest there are two techniques which were identified to study MSA adsorbed on gold surfaces, which seems to be the best ligand among the others. The first of these techniques is Raman and the second is XPS spectra.

In order to prove that MSA has the largest overall surface coverage, Raman scattering experiments for all SAMs on gold surface were conducted. This technique measures the vibrational spectra of several organic thiols adsorbed on gold surfaces, namely aliphatic and aromatic compounds such as 2-mercaptosuccinic acid, 2, 2'-thiodisuccinic acid, 4-mercaptobinzoic acid and 4-mercaptophenylacetic acid. In general it's known that, any thiol adsorbed on the gold surface via sulphur atom, after losing thiol proton[1].

The study is interesting because a mercaptosuccinic acid are poly-functional compounds (-SH & 2(-COOH)) and are able to interact with the metal surface spontaneously, through -SH, and react with any analyte metal ion through any of -COOH groups or through both of them.

Raman spectroscopy was used to determine which functional groups were involved in the adsorption on the gold surface and which ionic species were responsible for the observed spectra. This was previously identified by monitoring any changes in the

Raman spectrum of thiol deposited on gold surface compared with the Raman spectrum of thiol powder, particularly (-SH) group and carbonyl group (C=O).

XPS was used to provide us with full insight of surface combination (each element on the surface, basically S, O, C, Pb, Co, Ni) and the molar ratio between each metal ion and ligand, also to find out the percentage of the contribution for each metal ion in the complexation process which, carried out from the mixture. Peak position detected by XPS represent specific element in the sample, and the quantity of this metal can be calculated from the area under the peak.

5.1 Raman analysis

5.1.1 Introduction

Raman samples were prepared on microscope glass slices coated with very thin gold layer (30nm) by using a gold coater according to the procedure mentioned in chapter three. This gold layer was modified with thiol to form a SAM simply by immersed coated glass slide in ethanolic solution of the thiol (Mercaptosuccinic acid, 2, 2'-thiodisuccinic acid, 4-mercaptobenzaoic and 4-mercaptophenyalacetic acid) for 24h. This modified gold surface was then exposed to a 100 ppm solution of a heavy metal ion (lead, nickel or cobalt). Afterwards, the slide was dried carefully with nitrogen gas and then introduced to Raman instrument.

5.1.2 Results and discussion

Raman spectrum of MSA powder (blue spectrum) for all expected groups (-SH, -CH_2, -CH, -OH and -C=O) has been taken, and also for mercaptosuccinate attached on gold surface, as can be seen in figure 5:1. The very sharp peaks corresponding to each group

clearly appeared in blue colour spectrum. However, after depositing MSA on gold surface from ethanolic solution the spectrum underwent some slight changes with a bit of noise (red spectrum). By comparing red & blue spectra, the strongest peak in the blue spectrum, which corresponding to –SH at (2548-2564 cm^{-1} region) completely disappeared in red ones. This can be explained by the S-H bond after being adsorbed on gold substrate is no longer sulphur- hydrogen bond, but sulphur-metal bond S-Au. This was confirmed with each of 4-mercaptobenzoic acid and 4-mercaptophenyalacetic acid as can be seen in figures 5:3 and 5:4. However, in case of 2, 2'-thiodisuccinic acid there is no interaction with gold surface and that is because this thiol has no sulphur-hydrogen bond, see figure 5:2.

Green spectrum in figure 5:1 is related to the complexation process of lead with Au-MSA, and that will be discussed in more detail later on.

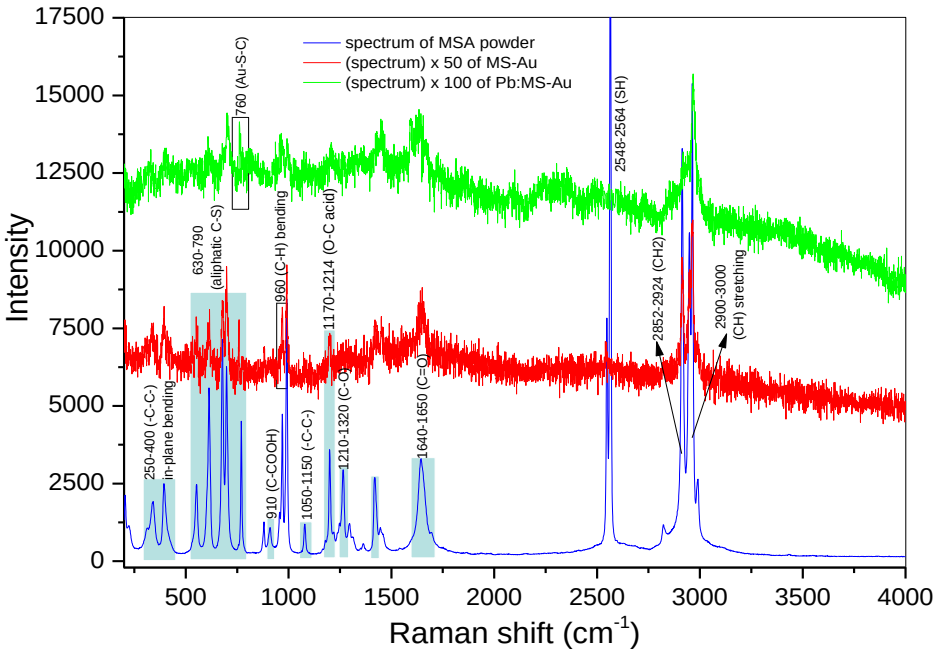

Figure 5-1 shows different types of Raman spectra for mercaptosuccinic acid as a powder (blue), as a ligand attached on gold surface (red) and as a ligand after complexed with lead ions (green).

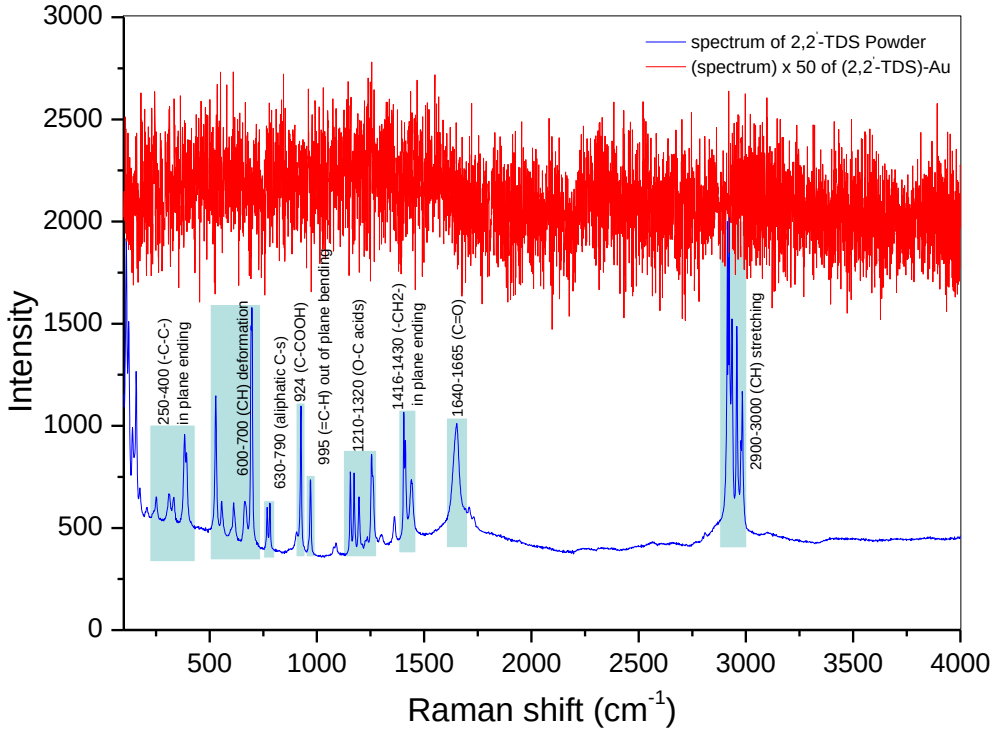

Figure 5-2 shows different types of Raman spectra for 2, 2'-thiodisuccinic acid as a powder (blue) and as a ligand attached on gold surface (red).

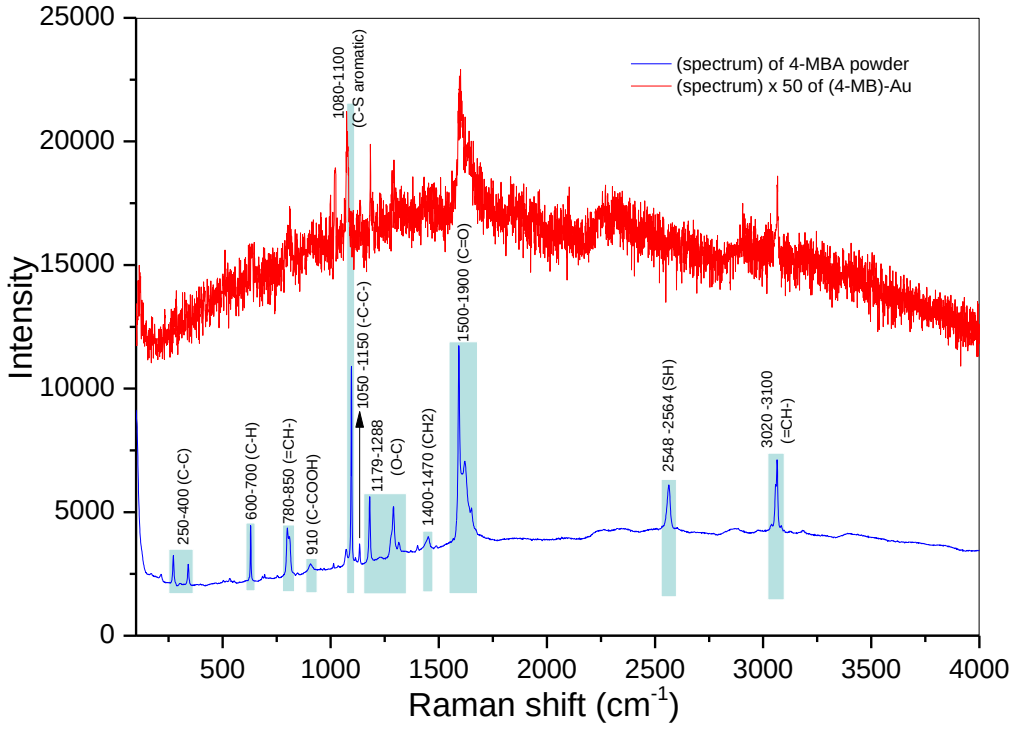

Figure 5-3 shows different types of Raman spectra for 4-mercaptobenzoic acid as a powder (blue), and as a ligand attached on gold surface (red).

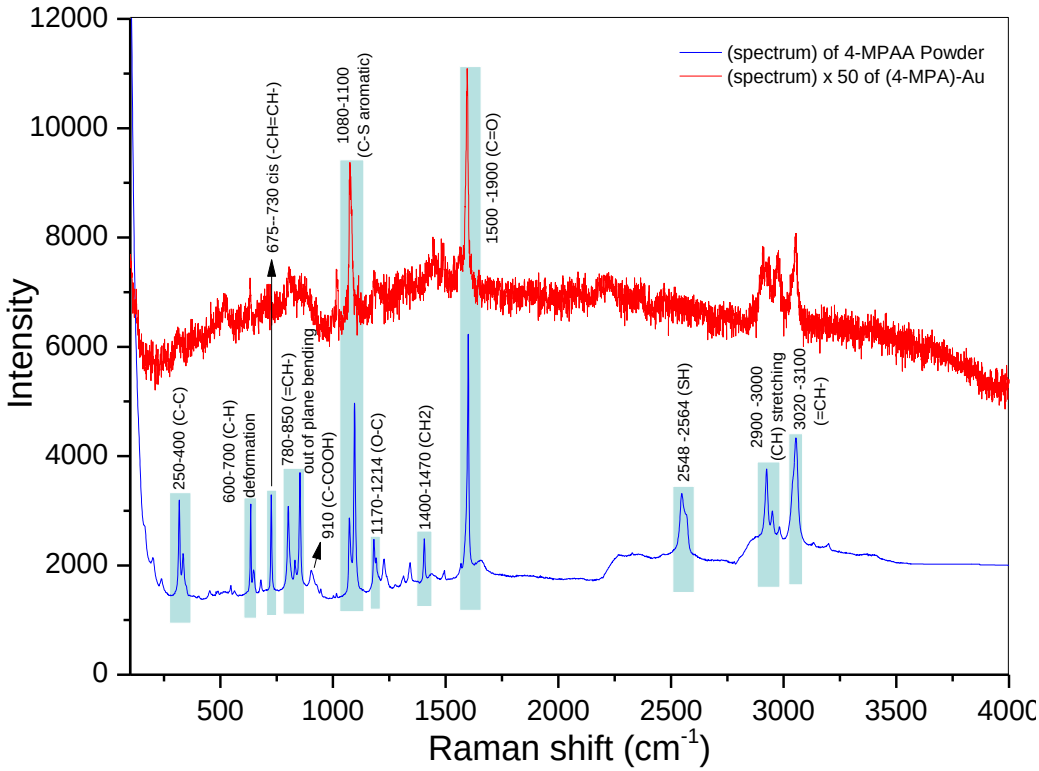

Figure 5-4 shows different types of Raman spectra for 4-mercaptophenyalacetic acid as a powder (blue), and as a ligand attached on gold surface (red).

Raman spectra at small expansion window

The strong band recorded at 1644 cm^{-1} in the spectra of mercaptosuccinic acid powder is assigned to (C=O) group, and any shift in this band is significant in respect of analyte metal ion binding. For the purposes of certainty and clarity, the Raman scan was repeated at a small range of Raman shift (1000-2000 cm^{-1}) as in figure 5:6 (a, b and c). In this spectrum, the shift for the peak belongs to (C=O) from 1644 cm^{-1} blue and red spectrum to 1630 cm^{-1} in green spectra, meaning that the group attached with C=O is no longer –H but probably another group which is a metal ion. Figure 5:5 shows the hypothesised product of this reaction.

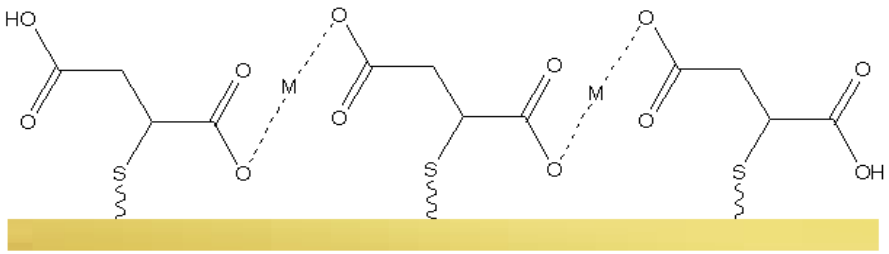

Figure 5-5 Virtual image of complexation process taking place between metal ions and MSA ligand.

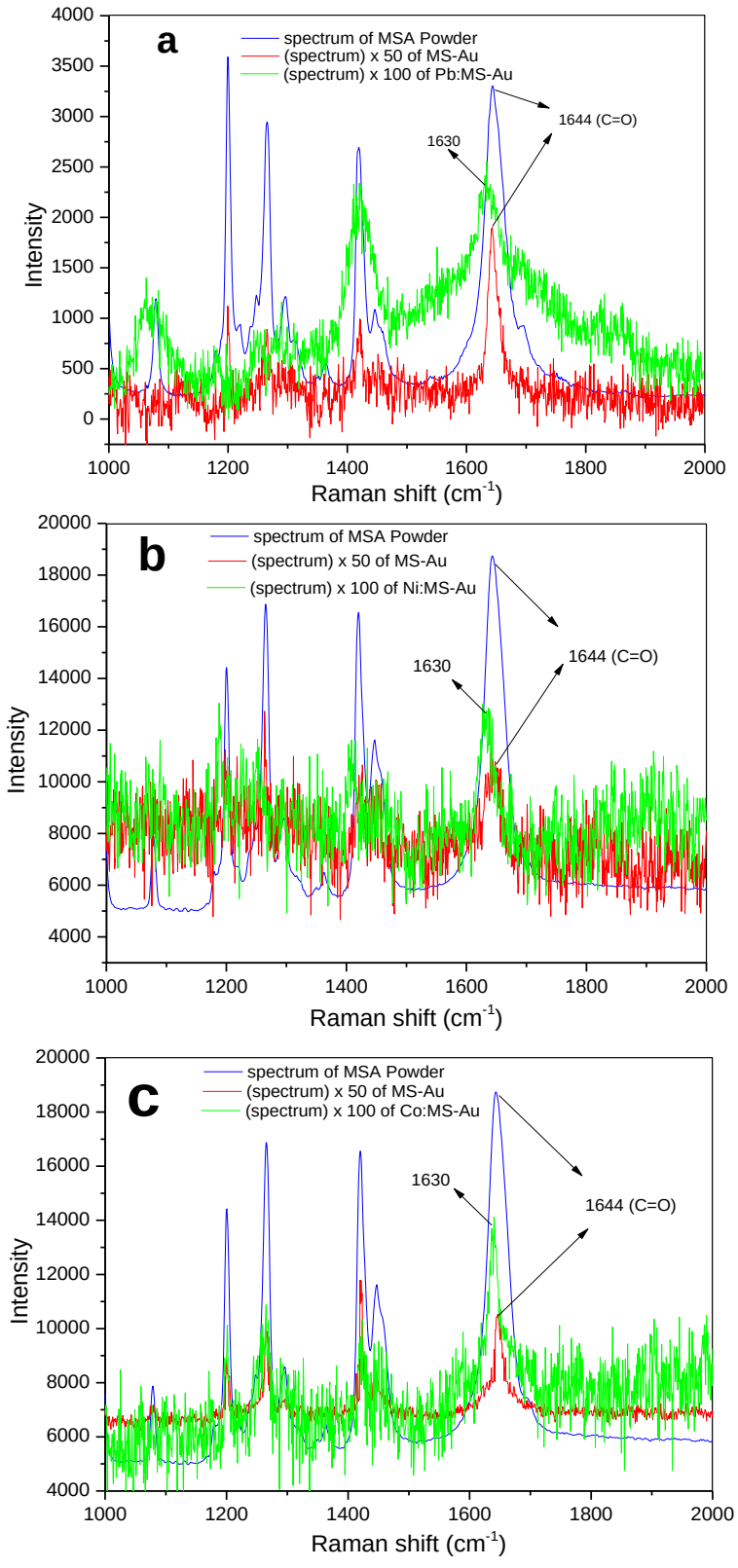

Figure 5-6 Narrow window for Raman spectra showing carbonyl group shift of MSA powder (blue), MSA ligand attached on gold surface (red), and MSA ligand on gold surface after complexed with; a) lead, b) nickel and c) cobalt ions (green).

From Raman spectrum of MSA (powder), Au-MSA and M:MS-Au, it is also possible to highlight some other important peaks, such as the one appeared at 250-400 cm^{-1} which is assigned to C-C, also the other band recorded at 1416-1430 cm^{-1},which is corresponding to $CH_{2,}$ while the band for CH stretching most likely to be at 2900-3000 cm^{-1}.

In conclusion, Raman spectroscopy was effectively used to prove the immobilization process of thiol SAM on the substrate by comparing Raman spectrum for both of thiol powder and thiolate mounted on the substrate, also to monitor the composition of modified gold surface, before and after the interaction with the metal ions.

5.2 XPS analysis

5.2.1 Introduction

It is not easy to investigate the electrode surface structure (Au-MSA & metal ions) after the equilibrium step by electrical techniques. However, XPS can be used to determine surface composition for the immobilization of the MSA attached with gold layer on glass microscope slide, and also to probe the nature of the adsorbed metal ion, oxidation state and mole ratio between metal ion and Au-MSA. There are also many details about the local environment and degree of packing and covering can be gained from peak positions.

High resolution x-ray photoelectron spectroscopy has often been used to identify the interaction of a metal ion with the surface chemical groups, because the creation of a chemical bond between a metal ion and an atom on the adsorbent surface, changes the distribution of the electrons around the corresponding atoms. In general, electron donating ligands can lower the binding energy (BE) of the core level electrons, while electron-withdrawing ligands can increase the BE value[2, 3, 4].

With the aim of investigating the gold film, immobilized mercaptosuccinate layer and the adsorption of metal ions; the following samples were scanned with XPS.

1) Au slide, 2) Au-MSA, 3) Pb:MS-Au, 4) Ni:MS-Au, 5) Co:MS-Au and 6) M:MS-Au.

Samples three, four, five and six were introduced into the spectrometer after preconcentration step in 0.01M metal ion solution (in case of sample six, a mixture of metal ions) and washing with deionised water, then an initial survey was performed followed by high resolution scans 160 of the Au 4f, O 1s, C 1s, S 2s, S 2p, Pb 4f, Ni 2p and Co 2p regions.

Samples analysis

Analysis of the mercaptosuccinate ligand attached to the gold substrate on the glass microscope slide, which was prepared as mentioned in chapter three, and the analysis was carried on the model considered to be:

1. Three chemical environments for C: -COO (carboxyl, 2x per MSA molecule), CHS (1x per MSA molecule), CH_2 (1x per MSA molecule)

2. Two chemical environments for O: O=C (2x per MSA molecule) and O-C (2x per MSA molecule)

3. One chemical environment for S: S-CH (1x per MSA molecule)

The model has been used to find the components for C, O and S and adding a minimum number of additional components to fit the narrow scans for each element. Additional components then will be assumed not to represent MSA. As a part of the initial guesses it has been assumed that the C 1s peak for the COO group is expected to have a value around 288-289 eV, and C 1s peak for -CH_2- group is expected to be about 285 eV, while the carbonyl oxygen (O=C- in COO) O 1s peak is expected to be at roughly 531.5 eV, the carboxyl oxygen (O-C in COO) at around 533.5 eV in BE, and S 2p peak should be around 162 eV.

The scale in BE is calibrated in all cases with respect to the Au 4f 5/2 peak = 84 eV. Once the spectra were fitted, the quantitative analysis was done as a consistency check.

The metals in different chemical states of each sample, was labelled with numbers, for instance; Pb (1), Pb (2) and Pb (3) are the possible chemical states for lead. The ratio of each oxidation states of the metal with the amount of MSA was calculated as M:CHS,

where it is possible in this case to use CHS or CH_2 to find the molar ratio M:MSA. The reason is that the contribution of the MSA molecule to the C 1s spectrum is calculated by fitting a model of three peaks, namely -COO, -CH_2- and CHS. Inside the MSA molecule there is 2x COO carbons and only 1x CH_2 and 1x CHS carbons, therefore the COO C1s peak has double the area of each CHS and CH_2 peaks, thus it is equivalent to calculate the molar ratio M:MSA from CH_2 and CHS peaks since the fitting model assumes they have the same area.

XPS analysis software was used to analyse XPS spectra (fitting peaks, quantification components…etc). However, important information such as the relative sensitivity factors, full width at half maximum (FWHM), area under the peak and elemental binding energy can also be taken from the CasaXPS Kratos library.

5.2.2 Results and discussions

The initial survey for each sample provides important information about the chemical contents of that sample. Nevertheless, XPS core level analysis based on C and O are not good reference signals due to the existence of these elements often in the surface material as a contaminants from aerobic adsorption, which could be misleading as can be seen in the XPS survey for sample one, which supposedly consists of a thin gold layer on glass slide. In this case the spectra should give a signal for gold only, but in figure 5:7, shows that there are some unexpected materials such as the peak at 100 eV for silicone (probably from the glass) and the peak at 1071 eV corresponding to sodium atom as well as carbon atoms C-C have a peak at 284 eV. Nevertheless, this result indicated that the gold evaporated on glass slide in order to prepare a thin gold layer was of acceptable purity and no significant amounts of unexpected elements were detected.

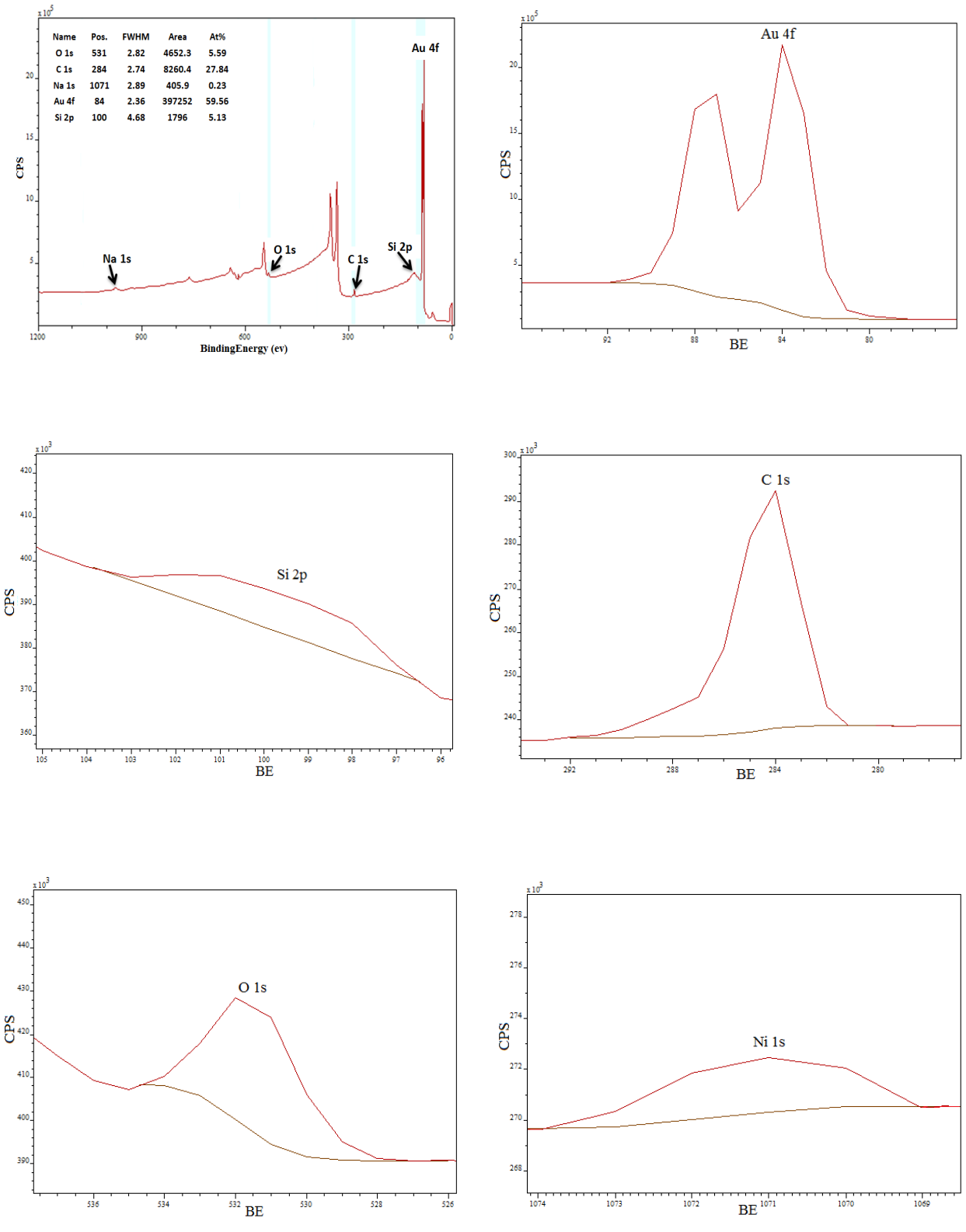

Figure 5-7 XPS survey spectrum of sample one (Au on glass slide) showing five peaks attributed to the main components presented on the surface.

In sample two the XPS analysis of the thiol SAM used in our experiments, the signal related to sulphur is very important as compared with the rest of the components because it is presents the degree of immobilized SAM gold surface (Au-S). Sample two, confirms this, where a clear single (peak) for sulphur atom at BE of 163 eV appeared as in figure 5:8.

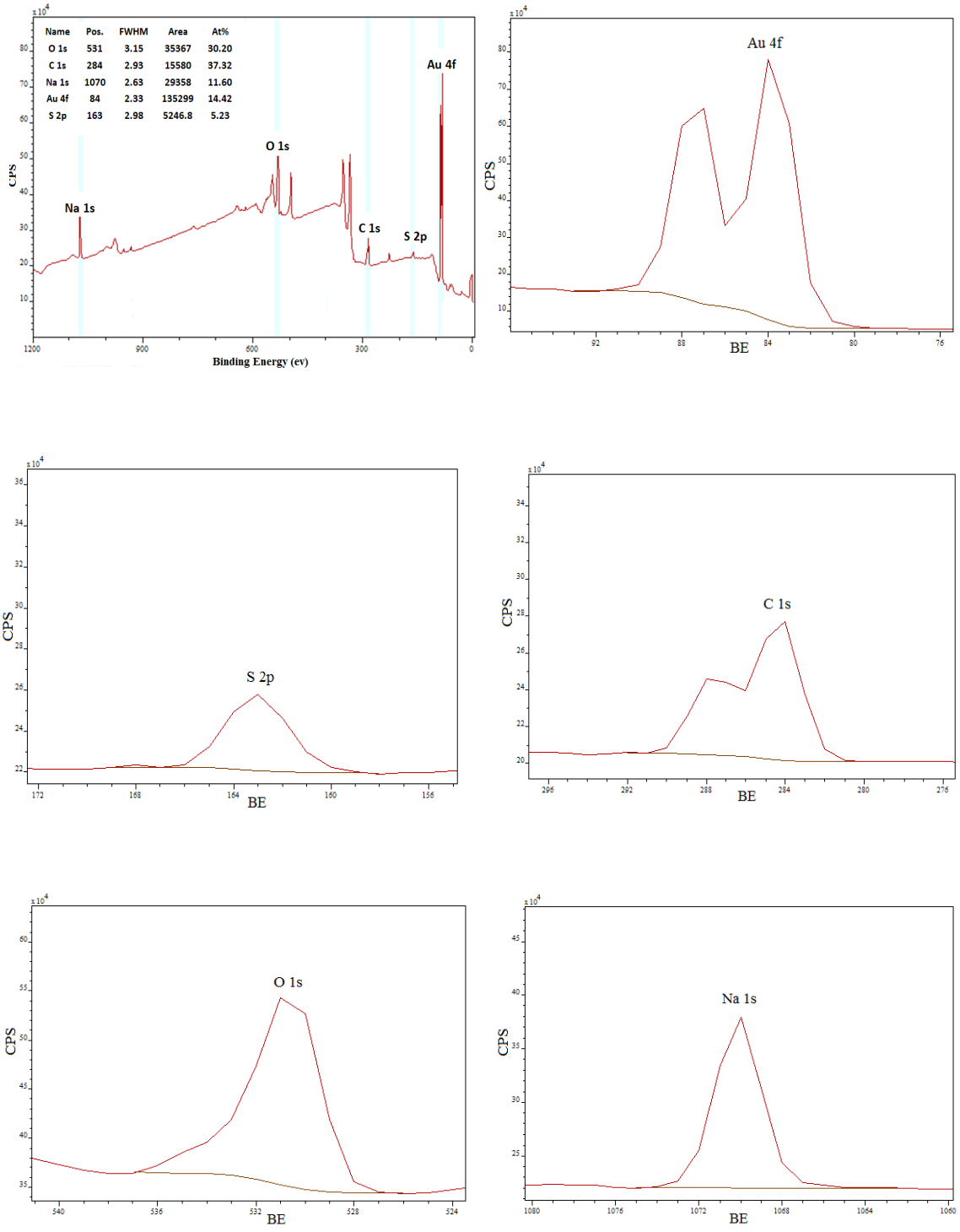

Figure 5-8 shows XPS survey spectrum of sample two (Au-MS), where the results illustrate that SAM of mercaptosuccinic acid has a strong S2p signal, and the same other main components as well.

Peaks fitting:

The information about chemical environment provided by XPS was used to distinguish the kind of bonding for the elements on the surface (binding energy)[5].

XPS analysis of mercaptosuccinate on gold substrate after the adsorption of metal ions (sample 3, 4, 5 and 6) were carried out in order to identify the native of Pb, Ni and Co atoms interaction with the ligand on the gold surface.

The comparison between the XPS spectrum for sample three (Pb: MSA-Au) and XPS spectrum for sample two (Au-MSA) provides a clear picture of any peak position shift for the main peaks produced by a) mercaptosuccinate adsorbed on gold substrate or b) the same ligand adsorbed on gold surface and interacted with a metal ion. For instance in figure 5:9, C 1s peak for –COOH has a value of binding energy about 288.6 eV for mercaptosuccinate on gold substrate and then shifted to 288.43 eV after interacted with Pb ions. However, C1s core level peak for -CH_2- group has a 284.5 eV binding energy (before lead added, spectrum a) and 284.55 eV after lead added (b), so this group has not been much effected by the reaction, and this result is fully compatible with our expectations which were mentioned earlier. Likewise one can generalize this discussion for the rest of metal ions (Ni & Co) in samples four and five respectively.

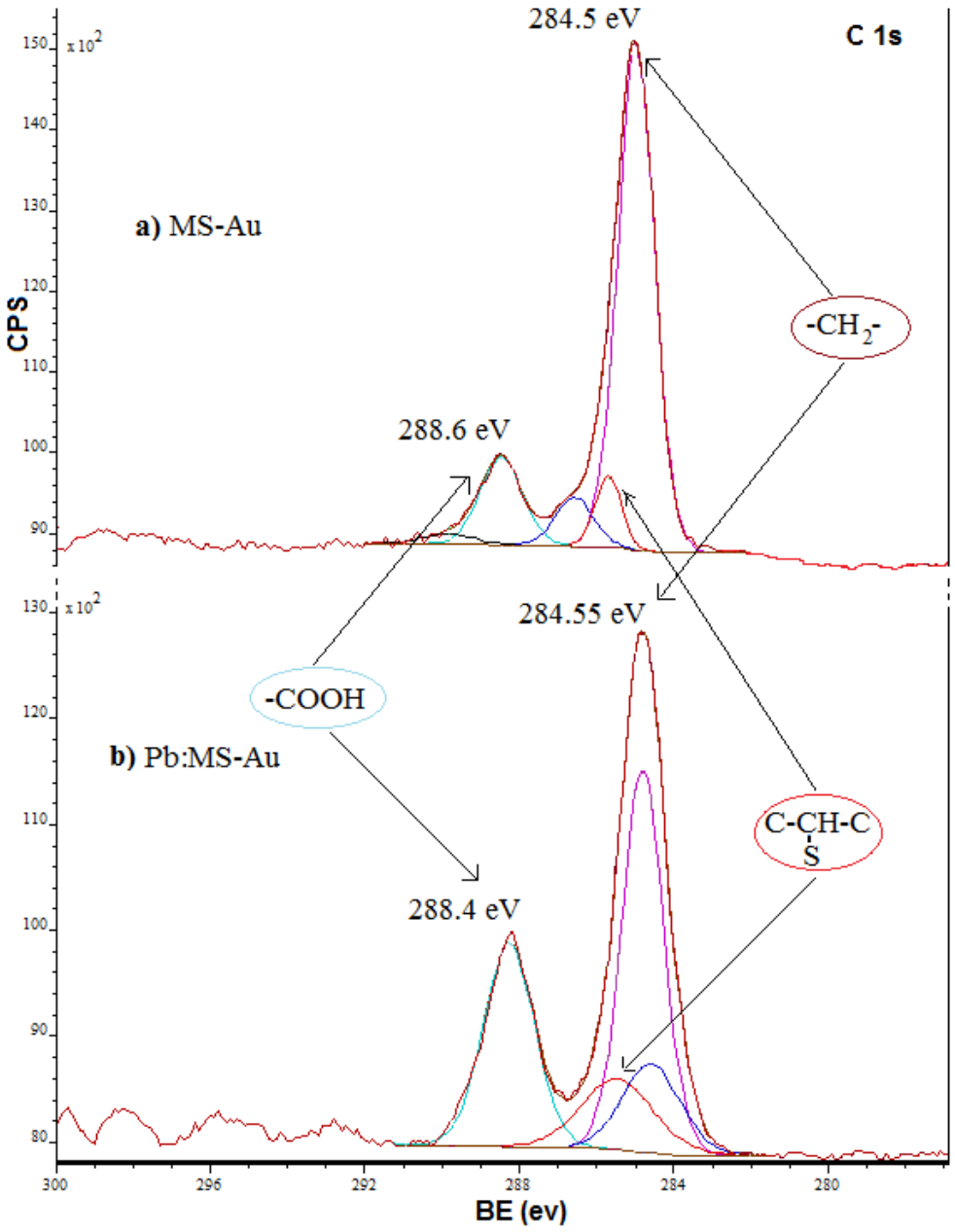

Figure 5-9 XPS C 1s spectra for mercaptosuccinate ligand adsorbed on gold substrate a) before and b) after interacted with lead ions.

While figure 5:10 shows the signal assigned to carbonyl oxygen C=O in carboxylic groups, where O 1s peak appeared at 531.25 eV corresponding to the free end of mercaptosuccinate on gold before interacted with lead (a), but in the case of spectrum (b) this value undergoes a slight shift towards 531.95 eV caused by the formation of a complex between lead ions and this ligand, as well as carbonyl oxygen C-O in

carboxylic groups, the O 1s peak appeared at 532.25 eV for (a) and after the complexation process, it was shifted to 533.08 eV in (b). However, these values can also be assigned to the oxygen in hydroxide group[6, 7].

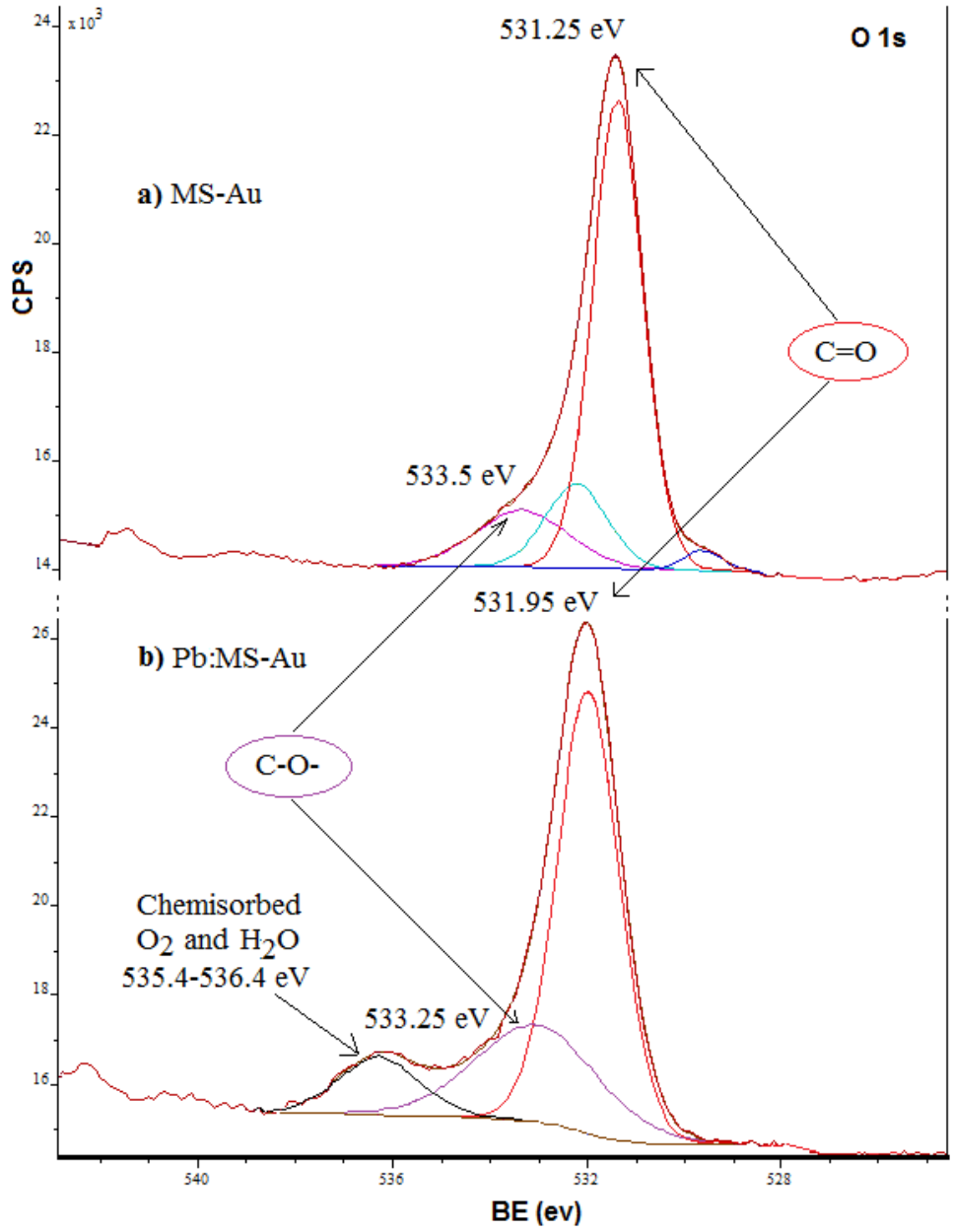

Figure 5-10 XPS O 1s spectra for mercaptosuccinate ligand adsorbed on gold substrate a) before and b) after interacted with lead ions.

The result comes in a good agreement with our expectations, except the peak at 535.4-536.4 in spectrum (b). This unique signal could be assigned to the chemisorption of oxygen on metal surface, or to water species when they are at equilibrium with the surrounding gases in the vacuum chamber, meaning the vacuum has high residual water content, which is not desirable. There is also the possibility for water to be interact with Au-MSA through hydrogen bonding as presented in figure 5:11. If this is the case, immersion of the glass slide in (10 mM) metal ions solution, may cause the structure change due to the interaction of the metal ion with carboxyl groups as previously presented in figure 5:5. Each of possibilities likely give peak points within a limited region (535.4-535.8 eV)[6,8] but the last two reasons are most likely, since gold surface is inert, so there is no chance for oxygen to be chemisorbed on it (O-Au bond not possible).

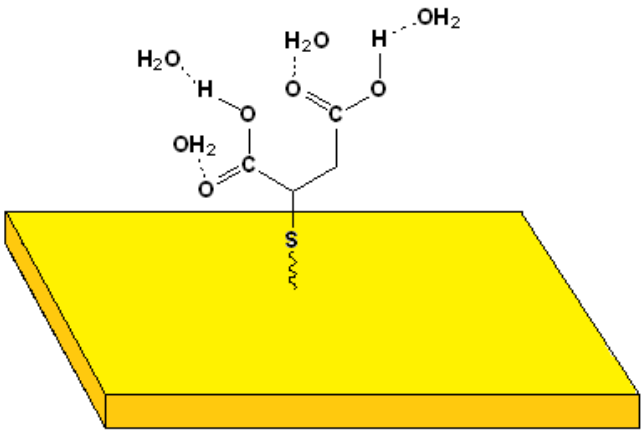

Figure 5-11 Virtual image of mercaptosuccinate ligand forming cluster structure with water adsorbed on gold substrate before interacted with lead ions.

Quantification of metal ions

The study of high resolution XPS spectra for each metal ion revealed the existence of expected metal ions. The narrow scans of sample three, for instance, shows a clear signal at BE region of 138.3 eV and this peak attributed to the bond of Pb-O, as shown in figure 5:12. No lead signal is observed at 139.2 eV (Pb^{2+} in $Pb(NO_3)_2$) meaning there is no free lead ions are present on the sample.[9, 10] Table 5-1 represents all details for analysis of sample 3.

Table 5-1 shows XPS results for the analysis of sample 3

Pb:MS-Au							
Name	Position	FWHM	RSF	Area	% Conc.	Mole ratio	
O-C 1s	533.08	2.219	0.780	3706.25	5.83		
O=C 1s	531.95	1.490	0.780	3704.56	5.82		
O(1) 1s	531.10	1.216	0.780	16884.39	26.55		
O(2) 1s	529.37	0.923	2.930	556.27	0.23		
C 1s	284.91	1.309	0.278	7380.33	32.56		
CH_2 1s	284.55	0.907	0.278	767.06	3.38		
COO 1s	288.43	1.676	0.278	1533.41	6.76		
CHS 1s	286.48	1.229	0.278	766.88	3.38		
C 1s	288.08	0.893	1.000	2097.58	2.57		
S(1) 2p	161.90	0.902	0.668	1515.48	2.78		
S(2) 2p	161.07	0.994	0.668	463.90	0.85		
S(3) 2p	163.49	0.895	0.668	760.13	1.4		
Pb(1) 4f	138.45	1.196	8.329	49060.71	7.22	2.14	2.3
Pb(2) 4f	137.03	1.505	8.329	1761.51	0.26	0.08	
Pb(3) 4f	138.37	5.602	8.329	2710.40	0.4	0.12	

From table 5-1, to some extent there is a kind of similarity between this mole ratio and the mole ratio calculated in chapter four by taking advantages of QCM technique. The quantification of Pb:-CHS- mole ratio, was used for each chemical states of lead with the amount of MSA, and the overall mole ratio (Pb:MS-Au) was about 2.3, as in previous table.

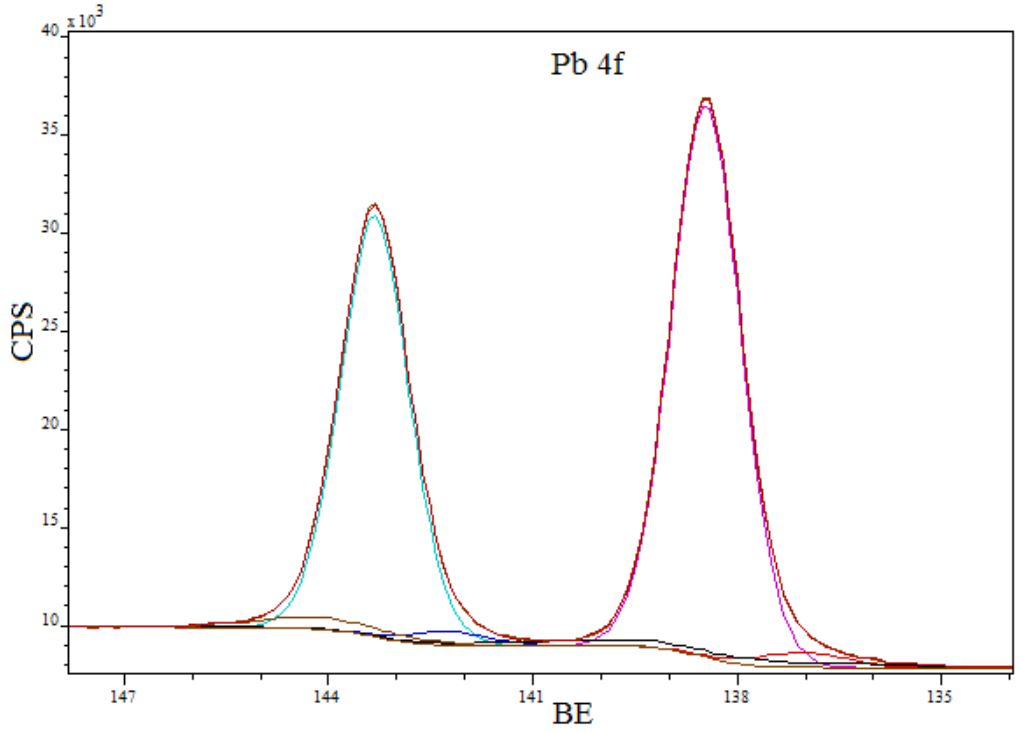

Figure 5-12 XPS 4f spectra from sample 3, shows the interaction of lead ions with mercaptosuccinate ligand on gold substrate (Pb-O).

Sample four was also scanned by XPS where detectable signal has been observed at 856-860eV, as in Figure 5-13. However, mole ratio Ni:MS-Au was detected for the two possible chemical states, and the overall was about 0.7, and this small value gives the impression that water molecules may also be involved in the complexation process between Ni and Au-MSA. More details are in the next table.

Table 5-2 shows XPS results for the analysis of sample 4

Ni:MS-Au							
Name	Position	FWHM	RSF	Area	% Conc.	Mole ratio	
O=C 1s	531.9	2.192	0.780	5196.15	13.78		
O-C 1s	532.42	1.895	0.780	5197.45	13.78		
O 1s	531.03	1.064	0.780	1308.69	3.47		
C 1s	284.81	1.404	0.278	5372.08	39.98		
CH_2 1s	284.58	0.881	0.278	846.77	6.30		
COO 1s	288.15	2.046	0.278	1692.82	12.60		
CHS 1s	286.36	1.064	0.278	846.59	6.30		
S(1) 2p	161.97	1.104	0.668	676.03	2.09		
S(2) 2p	160.94	0.497	0.668	92.05	0.29		
Ni(1) 2p	855.76	1.794	4.044	1262.51	3.65	0.58	0.7
Ni(2) 2p	860.16	5.000	4.044	1490.69	0.76	0.12	

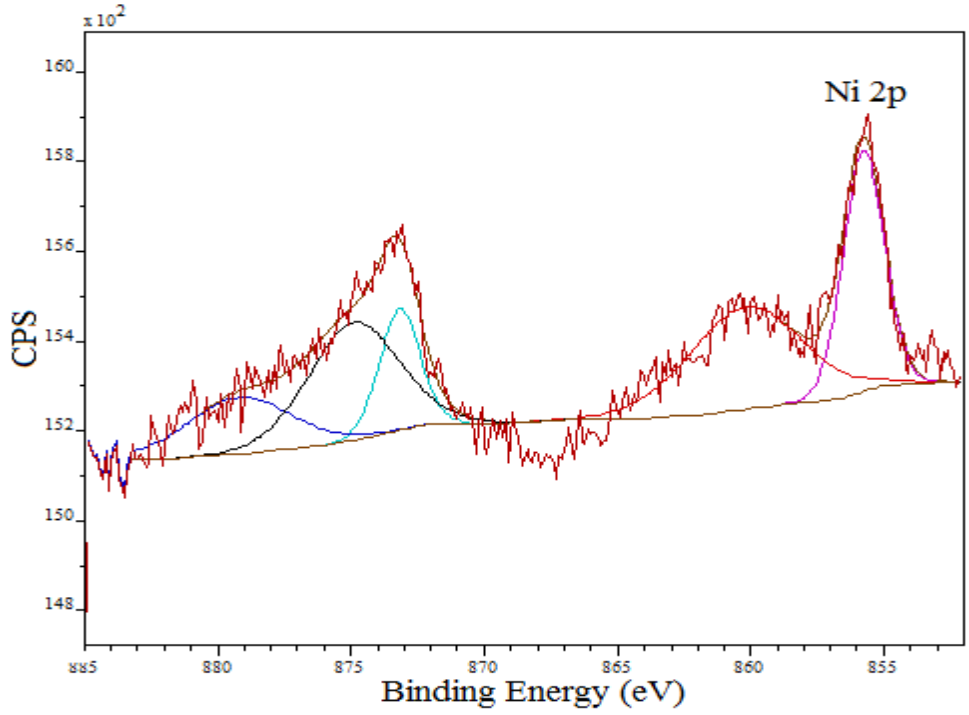

Figure 5-13 XPS 4f spectra from sample 4, shows the interaction of nickel ions with mercaptosuccinate ligand on gold substrate (Ni-O).

Similarly in sample five, the analysis of cobalt gave spectrum presented in Figure 5-14, where the peak at 781-787 eV indicates the presence of cobalt.

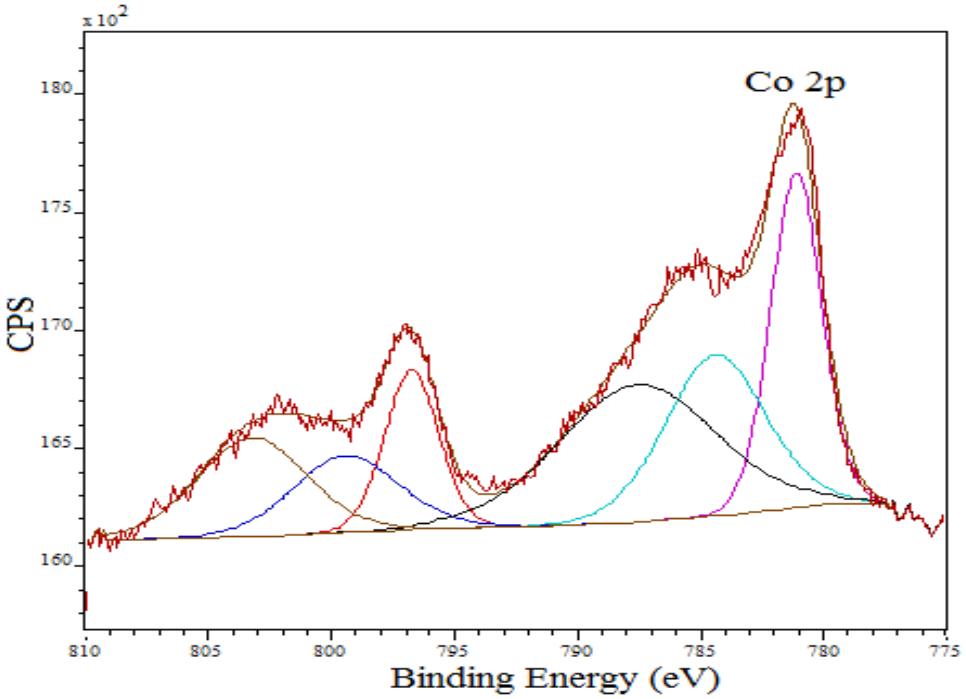

Figure 5-14 *XPS 4f spectra from sample 5, shows the interaction of cobalt ions with mercaptosuccinate ligand on gold substrate (Co-O).*

The mole ratio Co:MS-Au in table 5-3 uggested that both hydroxyl groups at Au-MSA were contributed in the binding of cobalt ion.

Table 5-3 shows XPS results for the analysis of sample 5

Co:MS-Au							
Name	Position	FWHM	RSF	Area	% Conc.	Mole ratio	
O-C 1s	532.57	2.051	0.78	6803.50	14.47		
O=C 1s	531.48	1.434	0.78	6800.40	14.46		
O 1s	529.58	1.407	0.78	204.85	0.44		
C 1s	284.93	1.380	0.278	6439.33	38.43		
CH_2 1s	284.67	0.871	0.278	987.19	5.89		
COO 1s	288.25	1.677	0.278	1973.53	11.78		
CHS 1s	286.44	1.107	0.278	986.97	5.89		
S(1) 2p	162.21	1.154	0.668	668.83	1.66		
S(2) 2p	161.26	0.597	0.668	94.75	0.24		
Co(1) 2p	781.11	2.449	3.59	4566.50	2.11	0.36	1.15
Co(2) 2p	784.39	4.797	3.59	4296.07	1.99	0.34	
Co(3) 2p	787.57	7.551	3.59	5752.15	2.66	0.45	

XPS was successfully used to confirm that lead, nickel and cobalt ions were adsorbed in the carboxylic groups of the Au-MSA, and the mole ratios were variance according to each metal ion. However, comparing these results with the values gained from QCM technique (section 4.2.4) shows good similarity although the differences in techniques used, see table 5-4.

Table 5-4 shows comparison all molar ratios, which calculated by QCM and XPS between each metal ion and Au-MSA.

	mole ratio	
	XPS	QCM
Pb:MS-Au	2.33	1.7
Ni:MS-Au	0.7	1.2
Co:MS-Au	1.15	1.4

XPS was also used to analysis a mixture of all these metal ions (sample six) complexed with gold mercaptosuccante (M:MS-Au) and the outcome are in the *Table 5-6*.

Same as samples three, four and five there are a similar spectra for lead, nickel and cobalt ions were detected for sample six, which was immersed in diluted mixture of these metal ions. The result suggested that lead ions are interacting with mercaptosuccinate ligand even under competitive process with the interfering ions (Ni & Co).

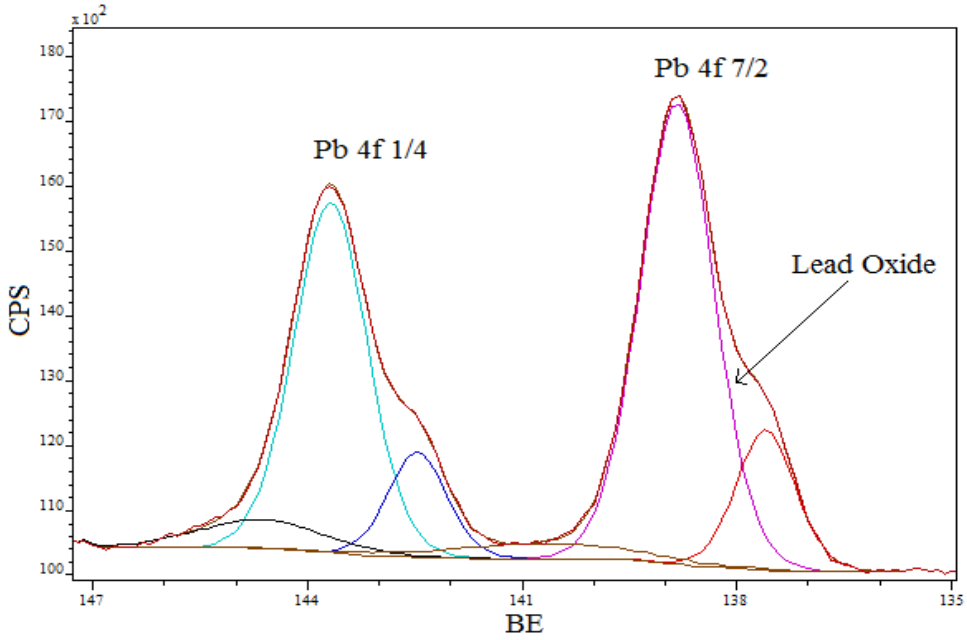

Figure 5-15 XPS 4f spectra from sample 6, shows the interaction of lead ions with mercaptosuccinate ligand on gold substrate (Pb-O).

What mentioned for lead is also true for nickel and cobalt, where very similar results were gained for these metal ions by scanning sample six, as can be seen in the next spectra.

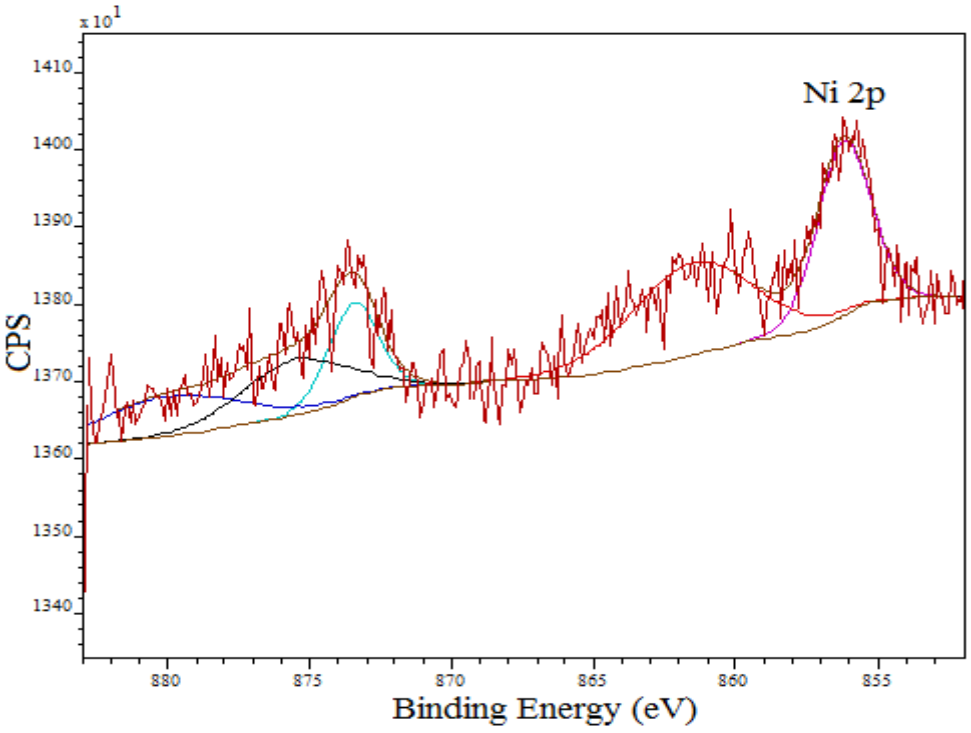

Figure 5-16 *XPS 4f spectra from sample 6, shows the interaction of nickel ions with mercaptosuccinate ligand on gold substrate (Ni-O).*

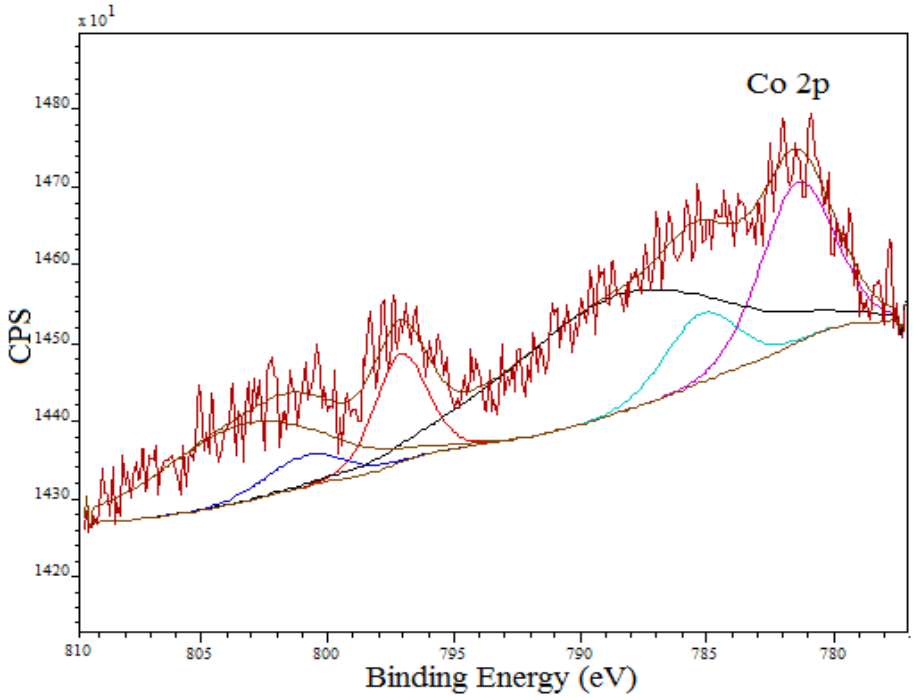

Figure 5-17 *XPS 4f spectra from sample 6, shows the interaction of cobalt ions with mercaptosuccinate ligand on gold substrate (Co-O).*

Table 5-5 shows XPS results for the analysis of sample 6

M:MS-Au, where M is (Pb, Ni or Co)							
Name	Position	FWHM	RSF	Area	% Conc.	Mole ratio	
O=C 1s	531.23	1.177	0.78	5140.82	9.83		
O-C 1s	532.22	1.367	0.78	5142.95	9.84		
O(1) 1s	532.74	1.901	0.78	3920.75	7.5		
O(2) 1s	529.59	0.965	0.78	143.56	0.27		
C 1s	284.88	1.121	0.278	8567.69	45.97		
CH_2 1s	285.62	0.815	0.278	860.02	4.61		
COO 1s	288.41	1.499	0.278	1719.47	9.23		
CHS 1s	286.39	1.143	0.278	859.95	4.61		
S 2s	226.71	2.979	0.391	929.37	3.55		
Pb(1) 4f	138.75	1.271	8.329	10680.78	1.91	0.41	0.58
Pb(2) 4f	137.47	0.971	8.329	3244.04	0.58	0.13	
Pb(3) 4f	140.33	3.288	8.329	1080.77	0.19	0.04	
Ni(1) 2p	856.19	2.201	4.044	652.07	0.24	0.05	0.11
Ni(2) 2p	861.53	5	4.044	782.72	0.29	0.06	
Co(1) 2p	781.43	3.354	3.59	905.35	0.38	0.08	0.30
Co(2) 2p	785.23	3.297	3.59	382.57	0.16	0.03	
Co(3) 2p	788.52	10.068	3.59	1997.33	0.83	0.18	

XPS result indicated that total mole ratio calculated from each metal ion contribution and mercaptosuccante (M:MS-Au) comes to be 99%. Table 5-6 represent the percentage contribution of each metal ion.

Table 5-6 shows percentage contribution of each metal ion in the complex produced M:MS-Au.

Element		Relative atomic composition of dopant metals (%)	M:MS-Au
M	Ni	11	99 %
	Co	30	
	Pb	58	

All mentioned results about binding energy values and mole ratios are summarized at the appendix in table VIII.

5.3 Conclusions

In general, results show that both Raman and XPS techniques have been used successfully to study the formation of SAMs on gold surface, also the interaction between mercaptosuccinate ligand and the interested metal ions have been investigated by these techniques. The interaction between MSA ligand and gold occurs via de-protonation of -SH group. The basic spectrum band which belongs to C=O group has negatively shifted after the complexation process with any of interested metal ions. These results were also confirmed by using XPS technique. The values of mole ratio calculated by QCM and XPS were to some extent close.

5.4 References

1. C. D. Bain, E. B. Troughton, Y. T. Tao, J. Evall, G. M. Whitesides and R. G. Nuzzo, *Journal of the American Chemical Society*, 1989, **111**, 321-335.
2. S. Deng, Bai and J. P. Chen, *Langmuir*, 2003, **19**, 5058-5064.
3. M. Sánchez-Polo and J. Rivera-Utrilla, *Environmental Science & Technology*, 2002, **36**, 3850-3854.
4. A.-S. Duwez, *Journal of Electron Spectroscopy and Related Phenomena*, 2004, **134**, 97-138.
5. D. Briggs and J. T. Grant, *Surface Analysis by Auger and X-Ray Photoelectron Spectroscopy*, SurfaceSpectra2003.
6. S. D. Gardner, C. S. K. Singamsetty, G. L. Booth, G.-R. He and C. U. Pittman, *Carbon*, 1995, **33**, 587-595.
7. M. Pakuła, S. Biniak and A. Świątkowski, *Langmuir*, 1998, **14**, 3082-3089.
8. S. W. Knipe, J. R. Mycroft, A. R. Pratt, H. W. Nesbitt and G. M. Bancroff, *Geochimica et Cosmochimica Acta*, 1995, **59**, 1079-1090.
9. R. Szargan, A. Schaufuß and P. Roßbach, *Journal of Electron Spectroscopy and Related Phenomena*, 1999, **100**, 357-377.
10. I. G. Casella, *Journal of Applied Electrochemistry*, 2001, **31**, 481-488.

Contents

6 Extraction of metal ions by using ionic liquid

6.1 Introduction

The use of ionic liquids is a reliable and promising method for extracting contaminants metal ions from water[1, 2]. These ionic liquids, as mentioned before in section 1.3, can be more environmentally friendly solvents. Depending on composition they may either be miscible or immiscible with water. 1-butyl-3-methylimidazolium hexafluorophosphate ([BMIM][PF_6])[3, 4] and betaine bis[(trifluoromethyl) sulfonyl] imide ([Hbet][Tf_2N])[5, 6] as can be seen in figure 6:1 are examples of liquids that are immiscible with water. The fact being that these two ILs are immiscible with water makes them easy to separate.

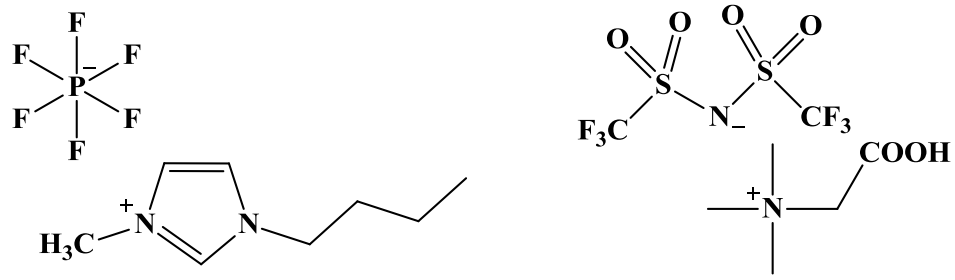

a **b**

Figure 6:1 shows the structure of (a) [BMIM][PF_6], (b) ([Hbet][Tf_2N])

This chapter focuses on two objectives, which are the following. Firstly, to investigate the ability of ([Hbet][Tf_2N]) to remove the metal ions of interest from their aqueous solutions by taking advantage of the possibility of measuring mass change using in situ QCM. Secondly, dimethylglyoxime (DMG) and rhodizonic acid indicators will be used in order to give good insight for the extraction process based upon [Hbet][Tf_2N] and [BMIM][PF_6] ionic liquids. These ionic liquids have been chosen for many reasons, where the materials required to prepare them are available and safe, also the procedures to prepare them considered to be easy.

6.2 Cell design

In order to use QCM to follow the extraction process of metal ions by ionic liquid, a cell with two crystals has been designed for simultaneous mass measurement in both phases, see figure 6:2.

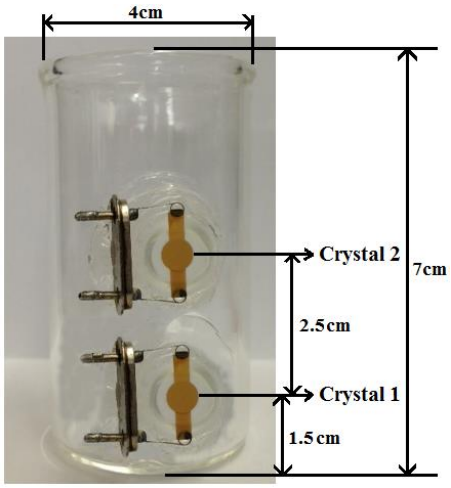

Figure 6:2 the characteristics of designed cell, which is used in this experiment

The QCM technique is successfully used to track the process of extraction by measuring the change in frequency for the two modified piezoelectric devices mounted on a glass cell, which is a glass cylinder 8cm length and 3cm diameter as represented above. There are two holes on a side of this cell to install the crystals, first one is located at 1.5 cm from the cell bottom and the second is located 2 cm above the first one. Both crystals were mounted on a vertical line along the Y axis for cell by using silicone rubber adhesive (3145 RTV-CLEAR MIL-A-45146), and then left for 24 hours at room temperature to dry.

The two crystals were then connected in parallel as in the next schematic diagram, where red wires will finish with one end and the black ones represented the other end as in the figure 6:3.

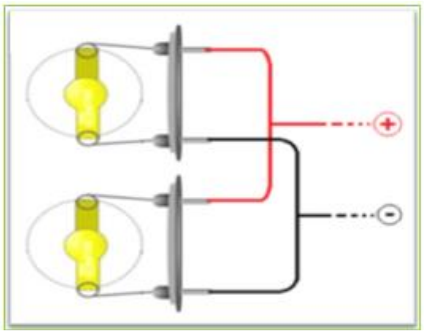

Figure 6:3 schematic diagram shows how to connect crystal 1 and crystal 2, in parallel

6.3 Procedure

By adding the binary liquid mixture of metal ions to the cell (at room temperature), the two immiscible liquids separated; upper layer, which is the aqueous phase (covered crystal 2) and lower layer, which is the ionic liquid phase (covered crystal 1) as in the next figure.

An important point must be taken into account is that to measure mass change of each crystal separately, the response of the frequency should give two separated peaks, and because we are using the same type of the crystal (unpolished 10MHz At-cut), the two frequency peaks were identical to each other. However, the mass of one of crystals can be increased by electroplating it with gold (crystal 1) in order to obtain separation between the two peaks.

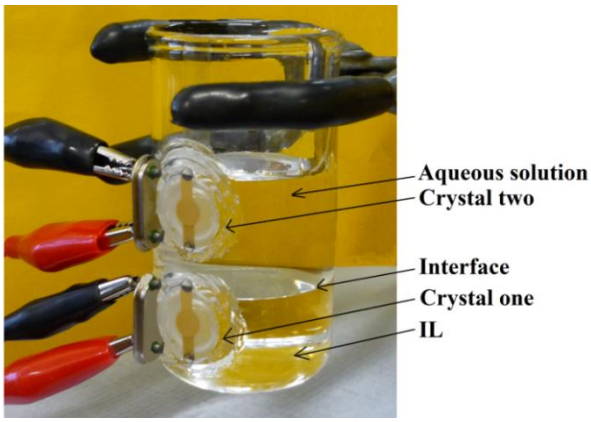

Figure 6:4 shows the cell filled with a binary mixture used to extract metal ions

6.4 Tracking of the extraction process via QCM technique

In this experiment betainium is used to remove lead, nickel and cobalt ions from their solutions and the steps of this procedure are as follows:

- Measure the frequency in air for both modified crystals with mercaptosuccinic acid SAM.
- A mixture of 20 ml of betainium and 20 ml of diluted metal ions in aqueous solution (200ppm) was stirring gently and extreme care was taken to avoid any contact between the magnetic stirrer and crystal number one, which is close to the bottom of the cell.
- The mixture was allowed to settle for 10 minutes and then the frequency was measured again for both of the wet crystals.
- The cell was emptied by withdrawing each layer individually; using a pipette and every effort was made to prevent ionic liquid from touching crystal number two. The crystals were washed with De-ionized water, dried with nitrogen, and the change in frequency for dry crystals in air was re-measured again.
- The last step, mass transfer between ionic liquid phase and water phase was calculated from frequency shifts

6.5 Results and discussion

Figure 6:5 shows the QCM response (shift peaks) due to mass change on the crystals as a result of nickel extraction from diluted standard nickel water solution 200 ppm by betainium at room temperature.

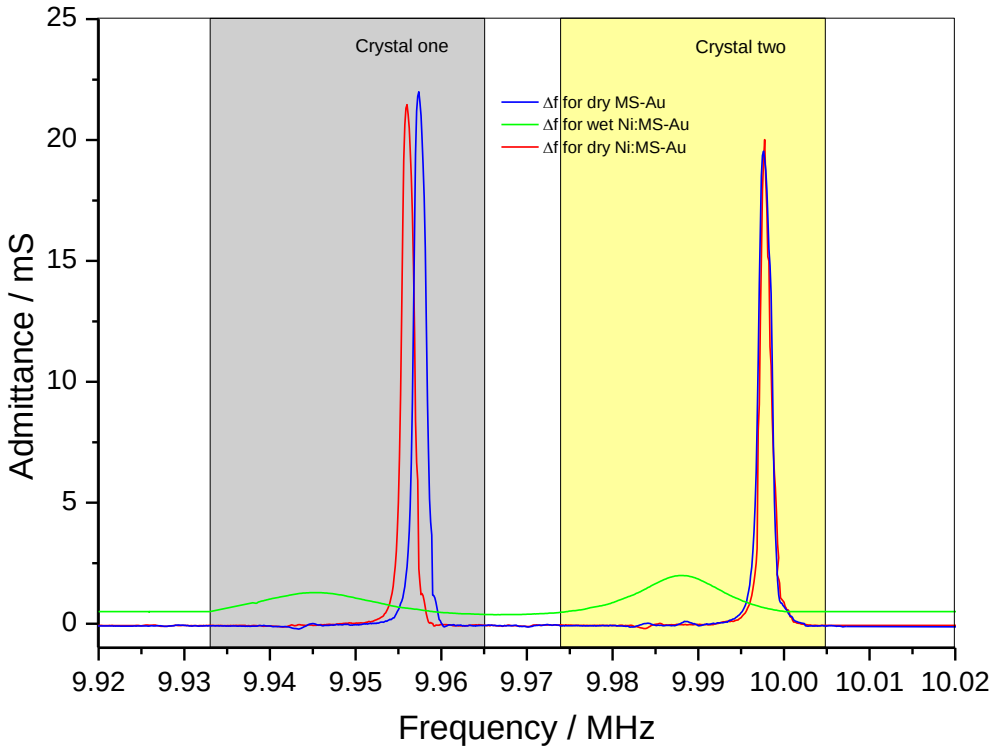

Figure 6:5 the admittance spectra for crystals modified with mercaptosuccinic acid and immersed in binary mixture, crystal one was immersed in betaine and crystal two was immersed in 200 ppm of aqueous nickel solution.

From this spectrum the shift peaks in grey box used to monitor the increasing mass (intracted nickel) on crystal one, which was immersed in betaine, so any change in its mass reflects the amount of nickel extracted from the upper layer to lower layer, while any change in mass on crystal two is related to the amount of un-extracted nickel ions, which can be calculated from shift peaks in the yellow box.

The above admittance spectra can be summarized as in the following table, in order to calculate the change in mass on each crystal due to nickel ions movement from phase to phase.

Table 6-1 shows frequency responses for distributed Ni ions between two phases, betaine and water.

Nickel					
Crystal one			Crystal two		
frequency	Hz	Δm /ng	frequency	Hz	Δm/ng
d(Au-MSA)	9957380		d(Au-MSA)	9997750	
d(Ni:MS-Au)	9956000		d(Ni:MS-Au)	9997720	
Δf	-1380	1518	Δf	-30	33

The result presented in this table gives clear evidence that nickel was extracted by betaine and the amount removed can be calculated using Sauerbrey equation described in section 2.1.2.2, and going back to the original amount of nickel in the solution, which was 200 ppm. There is no direct comparison possible here, because not all of the extracted nickel will have interacted with the ligand on gold quartz crystal. However, as we will see later on by using coloured indicators in section 6.7, the nickel ions undergo almost complete extraction.

The extraction process of cobalt ions by betaine was also followed by using QCM and the result shows not much difference compared with nickel and the calculating amount of cobalt interacted with the ligand is in the table 6-2. Again this is not the whole amount of extracted cobalt, but we still think that cobalt ions was completely removed by this type of ionic liquid from its solution and that also was confirmed by the coloured indicators, as we will see later on in the next section.

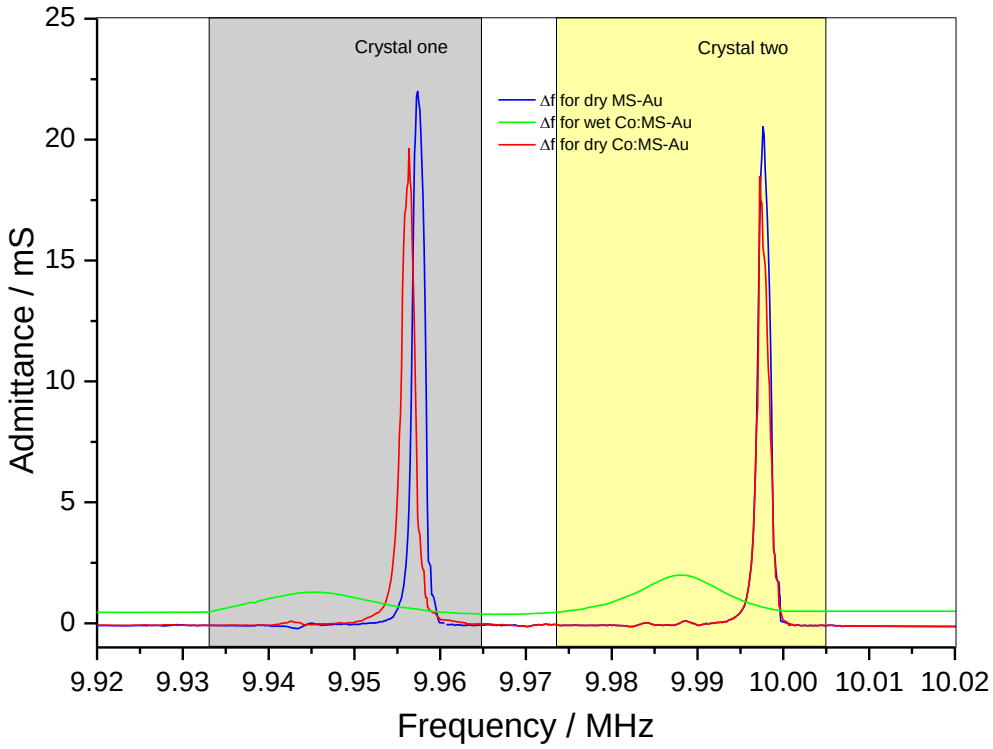

Figure 6:6 the admittance spectra for crystals modified with mercaptosuccinic acid and immersed in binary mixture, crystal one was immersed in betaine and crystal two was immersed in 200 ppm of aqueous cobalt solution.

Table 6-2 shows frequency responses for distributed Co ions between two phases, betaine and water.

Cobalt					
Crystal one			Crystal two		
frequency	Hz	Δm /ng	frequency	Hz	Δm/ng
d(Au-MSA)	9957380		d(Au-MSA)	9997620	
d(Co:MS-Au)	9956370		d(Co:MS-Au)	9997370	
Δf	-1010	1110	Δf	-250	275

As regarding to lead, a big difference has been noticed, since both of the crystals undergo almost the same distance shift, and that means lead ions are likely distributed between aqueous phase and ionic liquid phase evenly. See the next spectrum and table.

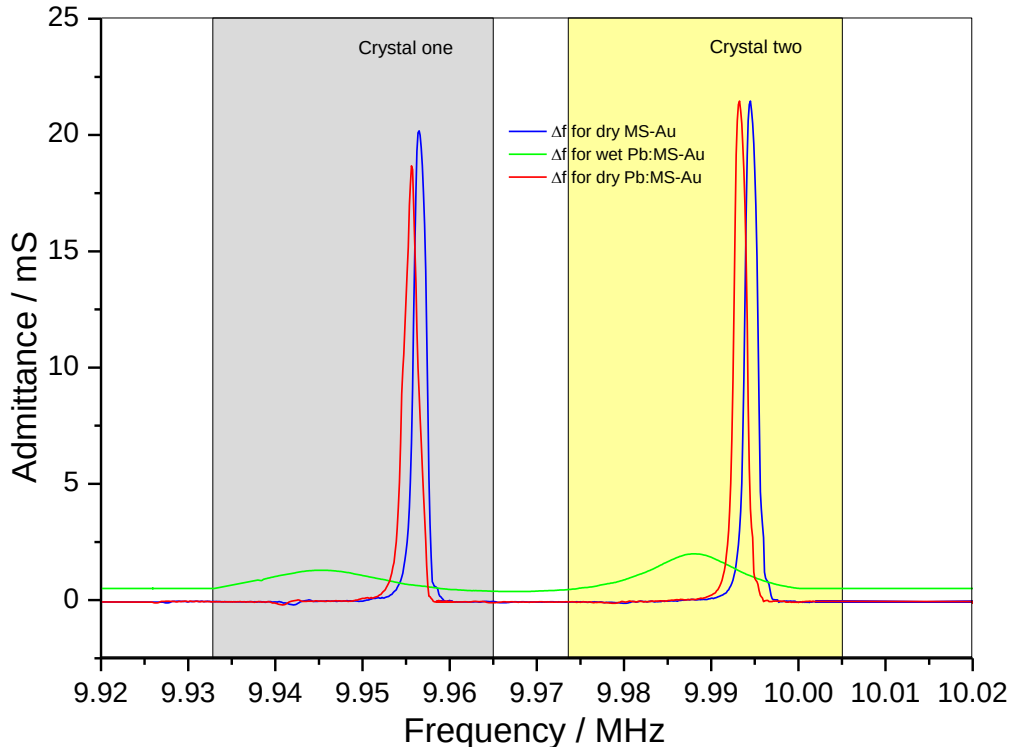

Figure 6:7 the admittance spectra for crystals modified with mercaptosuccinic acid and immersed in binary mixture, crystal one was immersed in betaine and crystal two was immersed in 200 ppm of lead solution.

Table 6-3 shows frequency responses for distributed Pb ions between two phases, betaine and water.

lead					
Crystal one			Crystal two		
frequency	Hz	Δm /ng	frequency	Hz	Δm/ng
d(Au-MSA)	9956540		d(Au-MSA)	9994478	
d(Pb:MS-Au)	9955550		d(Pb:MS-Au)	9993252	
Δf	-990	1089	Δf	-1230	1349

6.6 Tracking of extraction processes using colored reagents

As a confirmation for the extraction of the interested metal ions a number of colorimetric indicators were used. These reagents have the ability to interact individually with these metal ions producing a very clear coloured complex, for example dimethylglyoxime (DMG), which has a significant tendency to interact with nickel forming pink coloured complex according to this reaction:

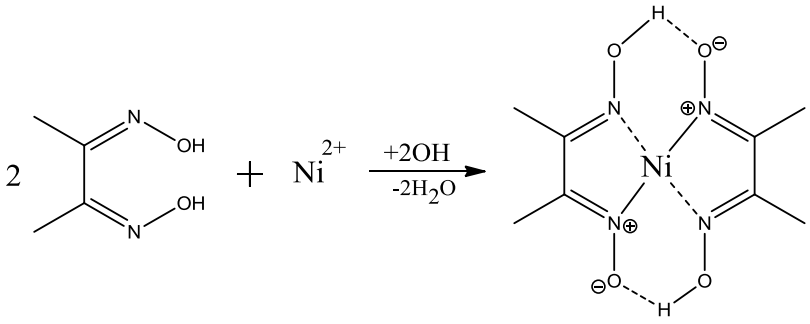

Reaction 6-1 represents the complexation process of DMG with nickel ions to give pink complex.

DMG can also be used for cobalt analysis in the presence of pyridine to produce a yellow brown complex (DMG:Co) as in the following reaction:

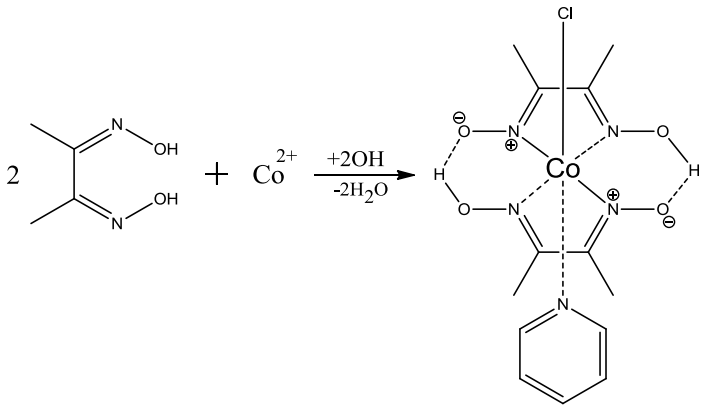

Reaction 6-2 represents the complexation process of DMG with cobalt ions to give yellow complex.

A different indicator called sodium rhodizonate dibasic was used to investigate the movement of lead ions from phase to phase. Disodium rhodizonate easily dissolves in water producing rhodizonic acid, which reacts with lead ions to form a ruby red coloured complex easily observed as shown below:

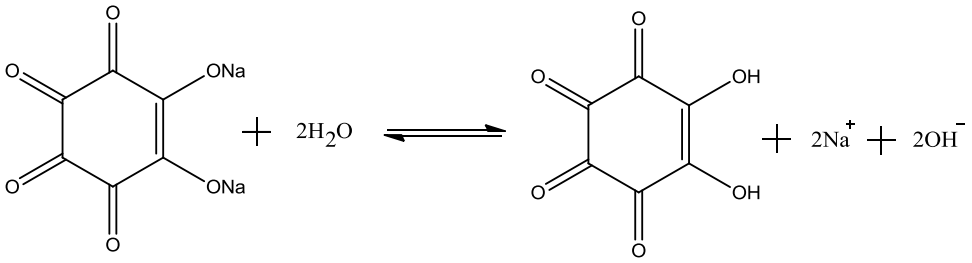

Rhodizonic acid disodium

5,6-dihydroxycyclohex-5-ene-1,2,3,4-tetraone

Reaction 6-3 represents the hydrolysis process of rhodizonic acid disodium.

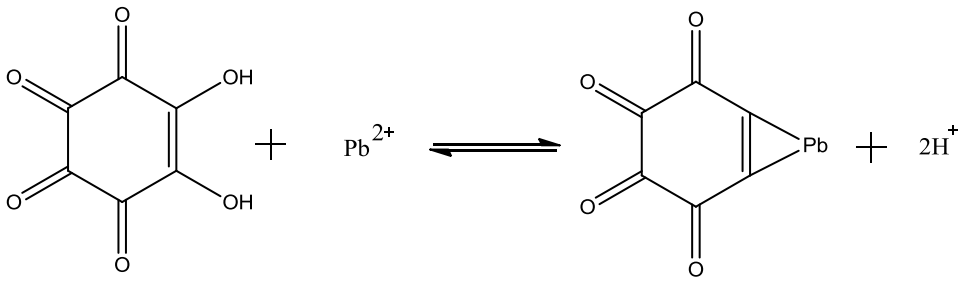

Rhodizonic acid

Rhodizonate-Pb (Brown colour)

Reaction 6-4 represents the complexation process of rhodizonic acid with lead ions to give brown complex.

These indicators were used in following the movement process of each metal ion from phase to phase (from aqueous layer to ionic liquid layer). Two kinds of ionic liquid solutions were used as immiscible systems to extract lead, nickel and cobalt from their solutions. The first one is, betaine bis[(trifluoromethyl) sulfonyl] imide ([Hbet][Tf_2N]),

and the second one 1-butyl-3-methylimadazolium hexafluorophosphate ([BMIM][PF_6]), which are prepared as described in section 3.1.4.

Dimethylglyoxime was used with nickel to make it visual by forming a pink coloured complex, in order to follow the movement process of this ion from water to betaine as mentioned before.

6.7 Results and discussion

In this experiment ionic liquid was added to the metal ion solution (200ppm) by tilting the tube and adding it on the wall of the tube gently without any shaking. In the case of nickel, the presence of DMG indicator leads to formation of two separated phases, which can clearly distinguish. The upper coloured layer (pink) represent the aqueous phase of (DMG:Ni) solution, and the lower layer is betaine ionic liquid (colourless). But after shaking this binary mixture for a few seconds, the complex of DMG:Ni, which is responsible for the pink colour transferred from the aqueous solution to the ionic liquid. The upper layer became colourless, while the lower layer changed to a pink colour, as can be seen in figure 6:8 (a & b). Interestingly the intensity of this pink colour start to become lighter and lighter and soon disappeared completely within few minutes see (C), and the real reason behind this change, could be related to a formation of a new complex between nickel and betaine which is more stable than that one between nickel and DMG.

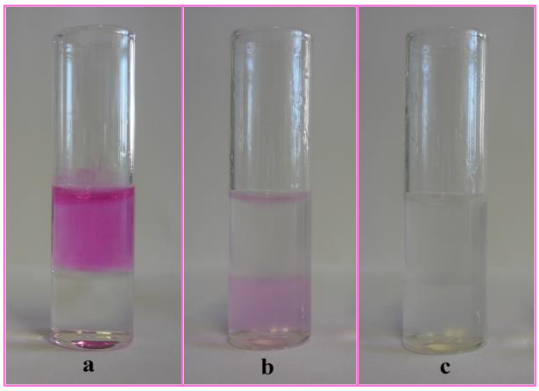

Figure 6:8 shows the extraction of nickel ions by using betaine, a) before shaking, b) after shaking and c) a few seconds after settling down.

The procedure for monitoring nickel extraction was also followed for cobalt in addition to adding a drop of pyridine, and the switching of yellow brown colour now from upper layer to the lower layer was also noticed, figure 6:9 a & b shows a very clear picture for this result.

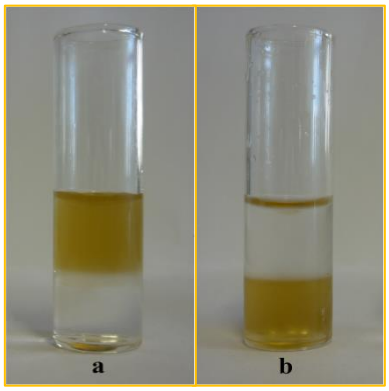

Figure 6:9 shows the extracted of cobalt ions by using betaine, a) before shaking and b) after shaking.

A similar result has been noticed for lead with sodium rhodizonate dibasic indicator, where the coloured complex moved from aqueous layer to ionic liquid layer by gently shaking the binary mixture, then put it aside to settle down, figure 6:10.

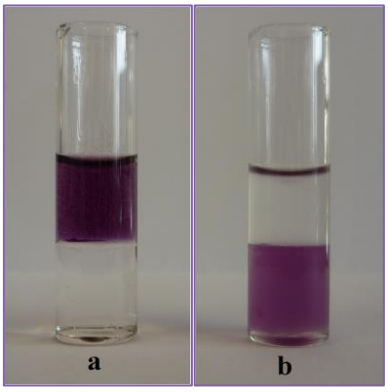

Figure 6:10 shows the extracted of lead ions by using betaine, a) before shaking and b) after shaking.

In this case the extraction process for lead by betaine is an incomplete process, since adding one drop of the reagent to the extracted aqueous layer will gave the same colour,

but with less intensity as can be seen in figure 6:11, which means some of lead ions are still remain un-extracted. In general, one can conclude that lead was partially extracted, but nickel and cobalt were completely removed by betaine.

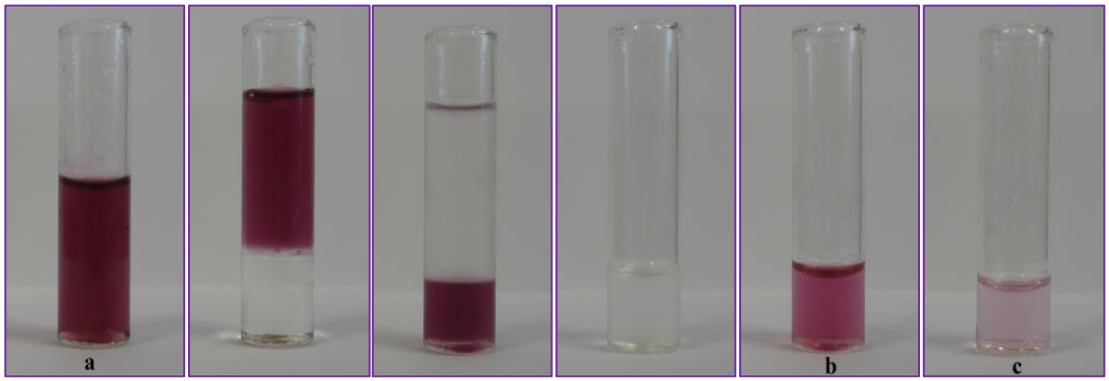

Figure 6:11 shows a positive result of lead ions, in the extracted aqueous layer by using same indicator, a) the test runs for 200ppm of lead solution, b) after one extraction step and c) after repeating the extraction process in two steps.

UV/visible spectroscopy was also used to study these coloured samples (10 ml of each sample) for both cobalt and lead. The nickel system could not be studied due to the instability of the Ni:DMG colour in betainum ionic liquid.

In this experiment similar volumes of metal ion solution and ionic liquid were added in test tube in presence of the indicator and UV/visible spectra were taken for 2ml from each phase (H_2O & IL) individually twice before and after shaking the mixture in the test tube.

By using the Beer–Lambert law ($A=\varepsilon CL$), where A is the absorbance, ε is the molar absorptivity and L is the path length, it was possible to calculate the concentration of the species, C. Assuming that ε is the same in water and betainum ionic liquid is the same, using the same cell (L constant), the ratio of absorbances yields the ratio of concentrations. Thus, one can calculate the extent of extraction process, starting from the initial concentration of 200 ppm. The extracted amount of lead can be calculating from figure 6-12 (a) and as follows:

	Conc.	Ads.
Before extraction	200ppm	0.273
After extraction	?	0.145

The end result is that the concentration of lead in the aqueous phase after the extraction process is 106ppm, i.e. almost half of the lead was extracted by betainum. This is similar to the result obtained from the QCM data in section 6.5. For cobalt we believe that almost all of cobalt ions were extracted by this ionic liquid since no cobalt appeared after the extraction process; see the black dashed line in figure 6-12 (b).

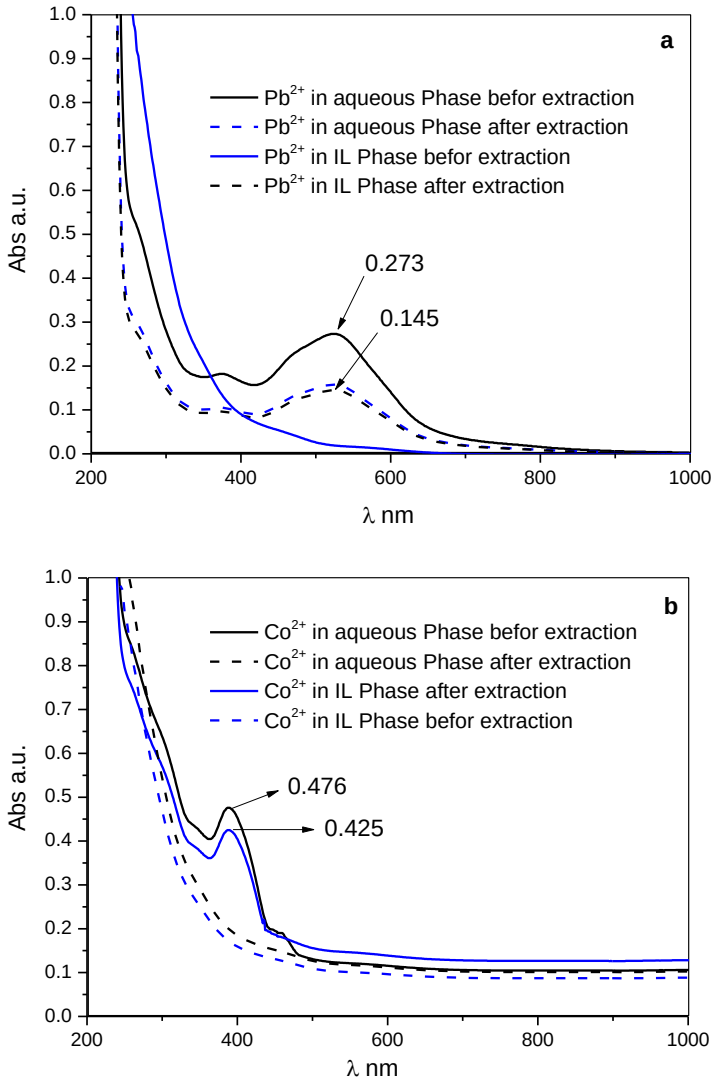

Figure 6-12 *shows UV spectra for a) 200ppm lead ions distributed between aqueous and betainum solutions, b) 200ppm cobalt ions distributed between aqueous and betainum solutions.*

Since these two indicators were working well with nickel, cobalt and lead, so another type of ionic liquid was tested for removing these metal ions, and that is [BMIM][PF_6]. However, this ionic liquid was also succeeded in removing of nickel ions but in this case the coloured complex was stable even after a long time as in the figure 6:12.

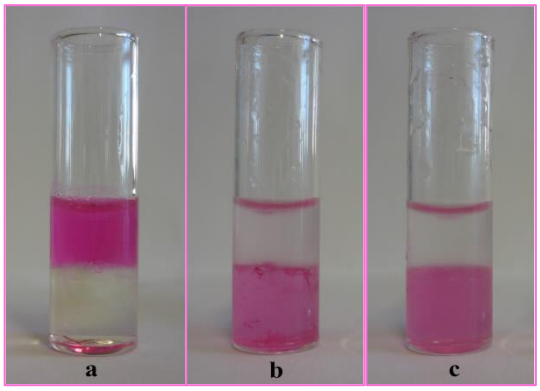

Figure 6-13 shows the extraction of nickel ions by using [BMIM][PF_6], a) before shaking and b) a few seconds after shaking and c) a few minutes after settling down.

A positive result was also gained in extracting cobalt by [BMIM][PF_6] from its aqueous solution, where a yellow oily complex (DMG:Co) transferred from upper layer to the tower layer as can be seen in the next picture.

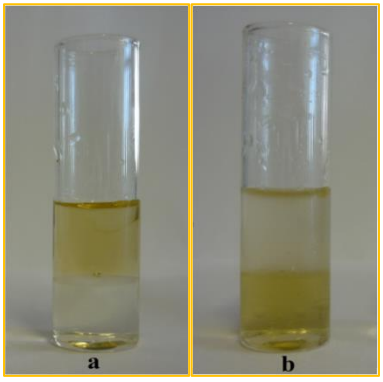

Figure 6-14 shows the extracted of cobalt ions by using [BMIM][PF_6], a) before shaking and b) after shaking.

Nevertheless, 1-butyl-3-methylimadazolium hexafluorophosphate failed to extract lead ions as indicated in the next figure. The extraction behaviour of these metal ions was studied at the room temperature and under the same conditions.

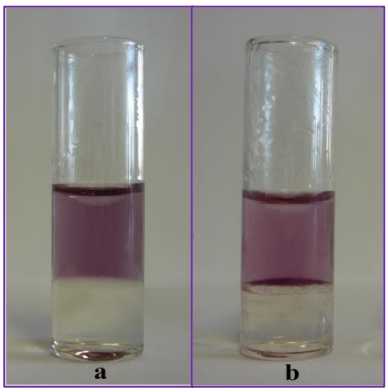

Figure 6-15 shows the extracted of lead ions by using betaine, a) before shaking and b) after shaking.

From the experimental results mentioned above we concluded that the ionic liquid of betaine was successfully extracted nickel and cobalt ions from their solutions, but it extracted lead ions partially. Whilst [BMIM][PF_6] succeeded in removing some of nickel and cobalt ions from water, nevertheless it failed with the lead ions.

6.8 References

1. A. P. de los Ríos, F. J. Hernández-Fernández, L. J. Lozano, S. Sánchez, J. I. Moreno and C. Godínez, *Journal of Chemical & Engineering Data*, 2010, **55**, 605-608.
2. A. E. Visser, R. P. Swatloski, S. T. Griffin, D. H. Hartman and R. D. Rogers, *Separation Science and Technology*, 2001, **36**, 785-804.
3. A. Dungca, WORCESTER POLYTECHNIC INSTITUTE.
4. S. Carda–Broch, A. Berthod and D. Armstrong, *Analytical and bioanalytical chemistry*, 2003, **375**, 191-199.
5. P. Nockemann, B. Thijs, S. Pittois, J. Thoen, C. Glorieux, K. Van Hecke, L. Van Meervelt, B. Kirchner and K. Binnemans, *The journal of physical chemistry. B*, 2006, **110**, 20978-20992.
6. C. Jagadeeswara Rao, R. Venkata Krishnan, K. A. Venkatesan, K. Nagarajan and T. G. Srinivasan, *Journal of Thermal Analysis and Calorimetry*, 2009, **97**, 937-943.

Contents

7 General conclusion and future work

7.1 General conclusion

The development of the preparation and characterization of SAMs has been improved rapidly in the last few years. This work is demonstrating the success of the immobilisation of MSA, 4-MBA and 4-MPAA on gold surface by using cyclic voltammetry and QCM measurements. Cyclic voltammetry experiments were carried out for $K_3Fe(CN)_6$ as a typical redox couple at clean and modified gold electrodes, where the oxidation-reduction reactions were clearly influenced by formed MSA, 4-MBA and 4-MPAA, SAMs on the electrode surface, while 2,2'-TDS shows slight effect meaning little covrage. This technique gives scope for a good future use to investigate the quality of these SAMs especially in terms of pinhole defects.

The successful immobilisation for these thiols on the gold surfaces of QCM has been monitored by QCM measurments. The shift in frequency was conducted for clean and modified, dry and wet crystals in order to calculate the added mass in each case using Sauerbrey equation. Morover, Raman spectroscopy was also used to confirm the results gained from CV and QCM. All these techniques indicated that MSA formed the most cohesive SAM which could be used to investigate metal absorption onto these surfaces. The absorption of common pollutants such as lead, nickel and cobalt were investigated as a preliminary step for the purpose of finding an easy and simple mechanism to track the concentration of such serious pollutants in order to generalize it over all the rest of toxic metal ions.

The binding of these metal ions to Au-MSA has also been studied by using all of the QCM, Raman and XPS, where in QCM experiments the frequency shift was observed

for the binding of a single, binary mixtures and ternary mixture of these metal ions to Au-MSA. In each case a range of different concentrations were bound to the ligand and Saurebrey equation again used to find out the amount of added metal ions. The results show that the mole ratio between Au-MSA and Pb, Ni and Co are 1.7, 1.2 and 1.4 respectively.The fitting of exprimental data to Freundlich, Frumkin, Languir and Temkin adsorption isotherms revealed that Freundlich isotherm gave better fitting and from this the binding constants with Au-MSA were determined at the natural pH value for each metal ion solution, and the results were 1.83 for Pb, 1.45 for Ni and 1.52 for Co. Depending on this, Pb will preferentially bind over Ni & Co, since both of them have a weaker binding constants than lead.

Again Raman spectrum gave another evidence in the form that these ions were complexed to Au-MSA by using the shift of C=O group from the original position before the complexation process had taken place.

Further confirmation was conducted by XPS technique, where the existence of these metal ions and the mole ratios between each one and Au-MSA were measured. However, the mole ratio for Pb:MS-Au was 2.33, for Ni:MS-Au 0.7 and for Co:MS-Au 1.15, one can see a kind of similarity between these values and the previous one regarding the mole ratio, where the order in both cases was Pb > Co > Ni.

In the last part of this study two types of immsible ionic liquid were used successifully to remove Pb, Ni and Co from aqueous solutions. For the first time QCM was used to follow this process, Which showed a promising way to keep track of extraction procedure.

The coloured indicators dimethylglyoxime and rhodizonic acid were used to give a concrete picture about the fact that the extraction of each type of ions successfully conducted.

7.2 Future Expectations

These studies have demonstrated that MSA is a promising molecule to be used as a chemical receptor for detecting some metal ions presented in aqueous solutions. However, for this typical alkane thiol SAM the basic properties, especially the chemical state of the adsorbed molecules are not well understood at the moment. Furthermore, the relationship between the molecular structure and local functions (electrical-conduction, etc.) is not completely clear yet. The study has been carried out in the natural values of the pH for the interested metal ion solutions at room temperature, because the sensor should be applicable to be used in analysing the trace of metal ions in the natural water at the environment. The repetition of all the experiments at different temperatures may also reveal some interesting results. In future the aim is to use other metal ions in different oxidation states such Cr (III) and Cr (VI), or Sn (II) and Sn (IV) with MSA, and with other SAMs containing different free terminal functional groups on gold substrate. In this work, we have focused on mercaptosuccinate ligand on Au surface, but it would be useful to try different thiol molecules on other suitable substrates, and to test the capability of these sensors. Furthermore, the future stability and reliability of these devices would have to be considered.

The other suggestion for the future work is to improve the designed cell in section (6.2) to be used as an electrochemical cell (see figure 7-1). In this developed cell each phase should be treated individually as if it was a separated cell consisting of working electrode, reference electrode and counter electrode immersed in an aqueous or ionic liquid solution.

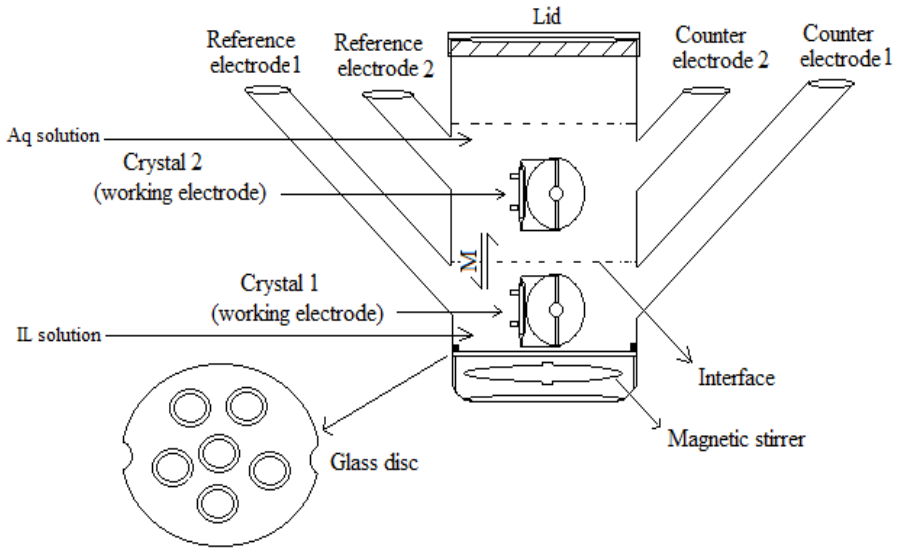

Figure 7-1 schematic diagram shows the designation of new cell, which is proposed to be used in EQCM experiments.

This cell is provided with four entrances for the electrodes, and magnetic stirrer in separated compartment to prevent any contact with the crystals (special crystal 1) during the stirring as well as lid for covering. The suggested procedure is as follows:

1- Fill the cell in figure 7-1 with the binary immiscible mixture.

2- Insert the reference and counter electrodes in the lower layer and then run EQCM.

3- Remove these electrodes and then insert another reference and counter electrodes this time in the upper layer (aqueous solution of diluted metal ion such as lead, nickel or cobalt); again run EQCM.

4- Remove electrodes and stir the binary mixture for a few minutes then leave it to settle down.

5- Repeat step 2 and 3, and compare them before and after the mixing of the binary solutions.

Appendix

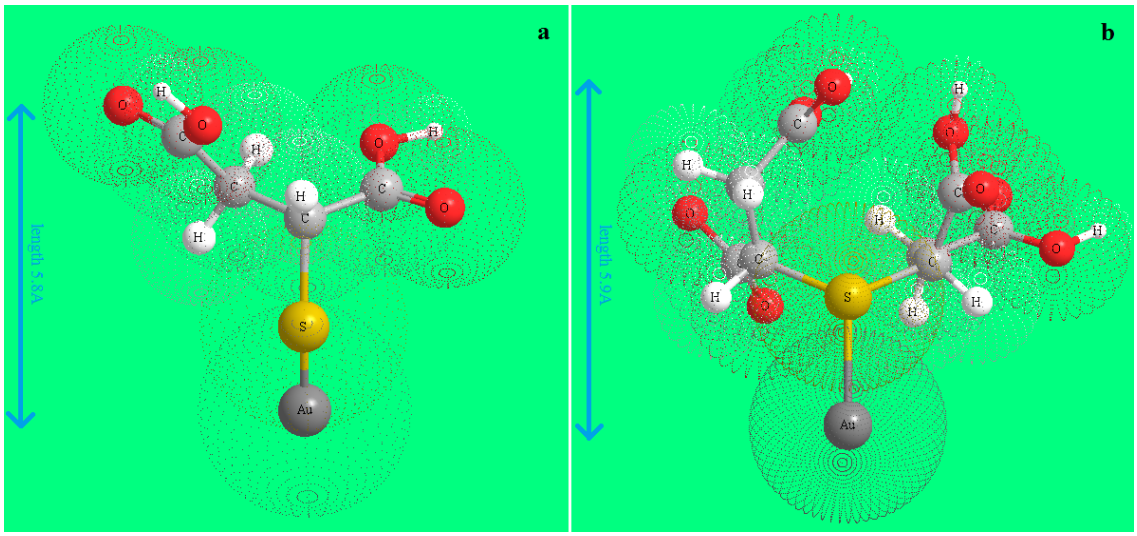

Figure 7-2 the structures of a) Au-MSA& b) 2.2'-TDS-Au. The high distance for each molecular was calculated by Chem3D pro.

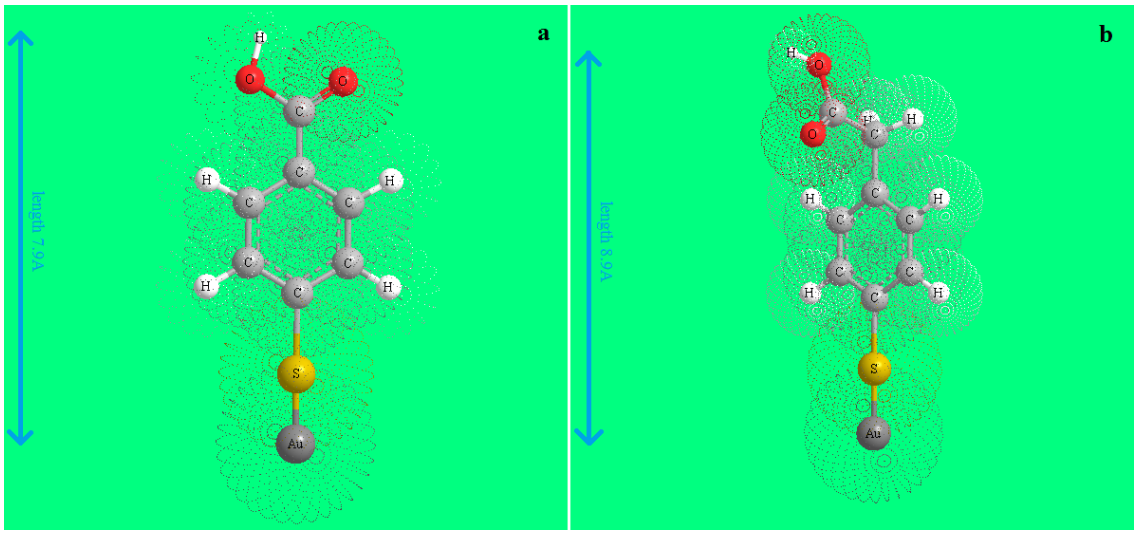

Figure 7-3 the structures of a) 4-MBA-Au & b) 4-MPAA-Au. The high distance for each molecular was calculated by Chem3D pro.

Table I shows frequency response to the complexation process of 1ppm-100ppm lead ions with MA-Au.

$C(ppm)$	$C(M)$	$\frac{1}{C}$	lnC	Δf	$\frac{\Delta f}{\Delta f_\infty}$	$\frac{1}{\theta}$	$ln\theta$	$1-\theta$	$C\theta$	$\frac{1-\theta}{C\theta}$	$\ln[\frac{1-\theta}{C\theta}]$
1	4.83×10^{-6}	207200	-12.241	13	0.101	9.923	-2.294	0.899	4.86×10^{-7}	1848862	14.430
2	9.65×10^{-6}	103600	-11.548	17	0.132	7.588	-2.026	0.868	1.27×10^{-6}	682541.2	13.433
4	1.93×10^{-5}	51800	-10.855	22	0.170	5.863	-1.768	0.829	3.29×10^{-6}	251936.4	12.437
6	2.90×10^{-5}	34533	-10.449	35	0.271	3.685	-1.304	0.728	7.86×10^{-6}	92746.67	11.437
8	3.86×10^{-5}	25900	-10.162	43	0.333	3.000	-1.098	0.666	1.29×10^{-5}	51800	10.855
10	4.83×10^{-5}	20720	-9.938	49	0.379	2.632	-0.967	0.620	1.83×10^{-5}	33828.57	10.429
20	9.65×10^{-5}	10360	-9.245	64	0.496	2.015	-0.701	0.504	4.79×10^{-5}	10521.88	9.261
30	1.45×10^{-4}	6906	-8.840	75	0.581	1.720	-0.542	0.418	8.42×10^{-5}	4972.8	8.512
40	1.93×10^{-4}	5180	-8.552	94	0.728	1.372	-0.316	0.271	1.41×10^{-4}	1928.72	7.564
50	2.41×10^{-4}	4144	-8.329	105	0.814	1.228	-0.206	0.186	1.96×10^{-4}	947.2	6.853
60	2.9×10^{-4}	3453	-8.147	111	0.860	1.162	-0.150	0.139	2.49×10^{-4}	560	6.328
70	3.38×10^{-4}	2960	-7.993	114	0.884	1.131	-0.123	0.116	2.99×10^{-4}	389.47	5.965
80	3.8610^{-4}	2590	-7.859	127	0.984	1.015	-0.015	0.015	3.80×10^{-4}	40.79	3.708
90	4.34×10^{-4}	2302	-7.741	129	1	1	0	0	4.34×10^{-4}	0	0
100	4.83×10^{-4}	2072	-7.636	129	1	1	0	0	4.83×10^{-4}	0	0

Table II shows frequency response to the complexation process of 1ppm-100ppm nickel ions with MA-Au.

$C(ppm)$	$C(M)$	$\frac{1}{C}$	lnC	Δf	$\frac{\Delta f}{\Delta f_\infty}$	$\frac{1}{\theta}$	$ln\theta$	$1-\theta$	$C\theta$	$\frac{1-\theta}{C\theta}$	$\ln[\frac{1-\theta}{C\theta}]$
1	4.83×10^{-6}	207200	-12.24	13	0.171	5.85	-1.766	0.829	8.26×10^{-7}	1004123	13.820
2	9.65×10^{-6}	103600	-11.55	14	0.182	5.50	-1.705	0.818	1.76×10^{-6}	466200	13.052
4	1.93×10^{-5}	51800	-10.86	18	0.234	4.28	-1.453	0.766	4.51×10^{-6}	169789	12.042
6	2.90×10^{-5}	34533.33	-10.45	27	0.351	2.85	-1.048	0.649	1.02×10^{-5}	63950.62	11.066
8	3.86×10^{-5}	25900	-10.16	29	0.377	2.66	-0.977	0.623	1.45×10^{-5}	42868.97	10.666
10	4.83×10^{-5}	20720	-9.94	33	0.429	2.33	-0.847	0.571	2.07×10^{-5}	27626.67	10.227
20	9.65×10^{-5}	10360	-9.25	44	0.571	1.75	-0.560	0.429	5.52×10^{-5}	7770.00	8.958
30	1.45×10^{-4}	6906.67	-8.84	52	0.675	1.48	-0.393	0.325	9.78×10^{-5}	3320.51	8.108
40	1.93×10^{-4}	5180	-8.55	59	0.766	1.31	-0.266	0.234	1.48×10^{-4}	1580.34	7.365
50	2.41×10^{-4}	4144	-8.33	65	0.844	1.18	-0.169	0.156	2.04×10^{-4}	765.05	6.640
60	2.90×10^{-4}	3453.33	-8.15	72	0.935	1.07	-0.067	0.065	2.71×10^{-4}	239.81	5.480
70	3.38×10^{-4}	2960	-7.99	75	0.974	1.03	-0.026	0.026	3.29×10^{-4}	78.93	4.369
80	3.86×10^{-4}	2590	-7.86	76	0.987	1.01	-0.013	0.013	3.81×10^{-4}	34.08	3.529
90	4.34×10^{-4}	2302.22	-7.74	77	1	1	0	0	4.34×10^{-4}	0	0
100	4.83×10^{-4}	2072	-7.64	77	1	1	0	0	4.83×10^{-4}	0	0

Table IV shows frequency response to the complexation process of 1ppm-100ppm cobalt ions with MA-Au.

$C(ppm)$	$C(M)$	$\frac{1}{C}$	lnC	Δf	$\frac{\Delta f}{\Delta f_\infty}$	$\frac{1}{\theta}$	$ln\theta$	$1-\theta$	$C\theta$	$\frac{1-\theta}{C\theta}$	$\ln[\frac{1-\theta}{C\theta}]$
1	4.83×10^{-6}	207200	-12.24	13	0.167	6.00	-1.792	0.833	8.04×10^{-7}	1036000	13.851
2	9.65×10^{-6}	103600	-11.55	14	0.180	5.57	-1.718	0.821	1.73×10^{-6}	473600	13.068
4	1.93×10^{-5}	51800	-10.86	20	0.256	3.90	-1.361	0.744	4.95×10^{-6}	150220	11.919
6	2.90×10^{-5}	34533.33	-10.45	24	0.308	3.25	-1.179	0.692	8.91×10^{-6}	77700	11.260
8	3.86×10^{-5}	25900	-10.16	27	0.346	2.89	-1.061	0.654	1.34×10^{-6}	48922	10.798
10	4.83×10^{-5}	20720	-9.94	32	0.410	2.44	-0.891	0.590	1.98×10^{-5}	29785	10.302
20	9.65×10^{-5}	10360	-9.25	44	0.564	1.77	-0.573	0.436	5.45×10^{-5}	8005.46	8.988
30	1.45×10^{-4}	6906.67	-8.84	53	0.679	1.47	-0.386	0.321	9.84×10^{-5}	3257.87	8.089
40	1.93×10^{-4}	5180	-8.55	64	0.821	1.22	-0.198	0.179	1.58×10^{-4}	1133.13	7.033
50	2.41×10^{-4}	4144	-8.33	68	0.872	1.15	-0.137	0.128	2.10×10^{-4}	609.41	6.412
60	2.90×10^{-4}	3453.33	-8.15	73	0.936	1.07	-0.066	0.064	2.71×10^{-4}	236.53	5.466
70	3.38×10^{-4}	2960	-7.99	74	0.949	1.05	-0.053	0.051	3.21×10^{-4}	160.00	5.075
80	3.86×10^{-4}	2590	-7.86	76	0.974	1.03	-0.026	0.026	3.76×10^{-4}	68.16	4.222
90	4.34×10^{-4}	2302.22	-7.74	77	0.987	1.01	-0.013	0.013	4.29×10^{-4}	29.89	3.398
100	4.83×10^{-4}	2072	-7.64	77	0.987	1.01	-0.013	0.013	4.76×10^{-4}	26.91	0

Table IV represents data collected from analysis of binary mixture of lead and nickel ions.

	Standard solution of Pb^{2+}					$[Ni^{2+}]$ 10ppm & $[Pb^{2+}]$ changeable					$[Pb^{2+}]$ 10ppm & $[Ni^{2+}]$ changeable				
Conc.	f_1	f_2	f_3	Ave. f	St. E	f_1	f_2	f_3	Ave. f	St. E	f_1	f_2	f_3	Ave. f	St. E
90	81	83	82	82.00	4.1	82	81	80	81.00	4.05	47	46	45	46.00	2.30
80	80	82	81	81.00	4.05	80	78	79	79.00	3.95	46	43	44	44.33	2.23
70	79	77	76	77.33	3.87	79	77	76	77.33	3.87	45	42	43	43.33	2.17
60	76	73	74	74.33	3.72	75	73	74	74.00	3.70	44	41	42	42.33	2.12
50	73	72	70	71.67	3.58	73	70	71	71.33	3.57	44	40	40	41.33	2.07
40	70	70	69	69.67	3.48	67	68	68	67.67	3.38	43	39	39	40.33	2.02
30	68	65	64	65.67	3.28	66	66	65	65.67	3.28	42	36	37	38.33	1.92
20	62	60	58	60.00	3.00	58	61	59	59.33	2.97	41	35	35	37.00	1.85
10	56	55	54	55.00	2.75	50	54	53	52.33	2.62	39	34	33	35.33	1.77
1	33	31	30	31.33	1.57	34	33	31	32.67	1.63	31	32	33	32.00	1.60

Table V represents data collected from analysis of binary mixture of lead and cobalt ions.

	Standard solution of Pb^{2+}					$[Co^{2+}]$ 10ppm & $[Pb^{2+}]$ changeable					$[Pb^{2+}]$ 10ppm & $[Co^{2+}]$ changeable				
Conc.	f_1	f_2	f_3	Ave. f	St. E	~~f1~~	f_2	f_3	Ave. f	St. E	f_1	f_2	f_3	Ave. f	St. E
90	82	78	80	80.00	4.00	80	79	78	79.00	3.95	42	44	43	43.00	2.15
80	82	77	77	78.67	3.93	77	78	77	77.33	3.87	40	43	42	41.67	2.08
70	81	75	74	76.67	3.83	76	77	75	76.00	3.80	39	42	40	40.33	2.02
60	80	74	72	75.33	3.77	75	76	74	75.00	3.75	38	41	39	39.33	1.97
50	79	72	70	73.67	3.68	73	70	71	71.33	3.57	38	40	39	39.00	1.95
40	77	70	68	71.67	3.58	69	69	68	68.67	3.43	37	39	37	37.67	1.88
30	75	69	66	70.00	3.50	65	66	67	66.00	3.30	36	38	36	36.67	1.83
20	70	68	65	67.67	3.38	58	56	60	58.00	2.90	35	36	35	35.33	1.77
10	61	62	61	61.33	3.07	53	54	55	54.00	2.70	34	35	34	34.33	1.72
1	35	38	37	36.67	1.83	35	36	36	35.67	1.78	34	32	34	33.33	1.67

Table VI represents data collected from analysis of binary mixture of cobalt and nickel ions.

	Standard solution of Co^{2+}					$[Ni^{2+}]$ 10ppm & $[Co^{2+}]$ changeable					$[Co^{2+}]$ 10ppm & $[Ni^{2+}]$ changeable				
Conc.	f_1	f_2	f_3	Ave. f	St. E	f_1	f_2	f_3	Ave. f	St. E	f_1	f_2	f_3	Ave. f	St. E
90	50	49	50	49.67	2.48	54	53	55	54	2.7	50	49	51	50	2.5
80	49	47	48	48	2.40	53	52	53	52.67	2.63	48	49	48	48.33	2.42
70	48	46	47	47	2.35	50	51	52	51	2.55	46	47	47	46.67	2.33
60	47	45	46	46	2.30	49	50	51	50	2.5	45	45	46	45.33	2.27
50	46	44	45	45	2.25	48	49	47	48	2.4	43	44	43	43.33	2.17
40	45	44	44	44.33	2.22	46	47	46	46.33	2.32	42	43	42	42.33	2.12
30	42	43	41	42	2.10	44	43	43	43.33	2.17	42	43	42	42.33	2.12
20	40	41	40	40.33	2.02	41	42	40	41	2.05	37	39	38	38	1.9
10	35	37	36	36	1.80	39	38	37	38	1.9	36	37	36	36.33	1.82
1	27	28	27	27.33	1.37	26	25	27	26	1.3	25	26	27	26	1.3

Table VII represents data collected from analysis of ternary mixture of lead, nickel and cobalt ions.

	$[Pb^{2+}]$ 10ppm & $[Ni^{2+}]$ & $[Co^{2+}]$ changeable					$[Ni^{2+}]$ 10ppm & $[Pb^{2+}]$ & $[Co^{2+}]$ changeable					$[Co^{2+}]$ 10ppm & $[Pb^{2+}]$ & $[Ni^{2+}]$ changeable				
Conc.	f_1	f_2	f_3	Ave. f	St. E	f_1	f_2	f_3	Ave. f	St. E	f_1	f_2	f_3	Ave. f	St. E
80	77	79	76	77.33	3.87	48	50	47	48.33	2.42	46	48	45	46.33	2.32
40	76	74	73	74.33	3.72	46	47	46	46.33	2.32	45	47	44	45.33	2.27
20	68	66	65	66.33	3.32	45	44	42	43.67	2.18	45	44	43	44.00	2.20
10	59	58	55	57.33	2.87	44	43	41	42.67	2.13	44	42	40	42.00	2.10
0.8	44	38	40	40.67	2.03	44	43	40	42.34	2.12	43	41	39	41.00	2.05

Table VI shows binding energy values for all samples.

Sample	2	3	4	5	6
	Au-MSA	Pb:MS-Au	Ni:MS-Au	Co:MS-Au	M:MS-Au
O-C 1s	532.25	533.08	532.42	532.57	532.22
O=C 1s	531.25	531.95	531.9	531.48	531.23
O 1s	531.15	531.1	531.03		532.74
O 1s	535.4	529.37		529.58	529.59
C 1s	284.8	284.91	284.81	284.93	284.88
-CH_2- 1s	284.5	284.55	284.58	284.67	285.62
COOH 1s	288.6	288.43	288.15	288.25	288.41
-CHS- 1s		286.48	286.36	286.44	286.39
C 1s	288.16	288.08			
S 2s	227.6				226.71
S(1) 2p		161.9	161.97	162.21	
S(2) 2p		161.07	160.94	161.26	
S(3) 2p	163.3	163.49			
Pb(1) 4f	-	138.45	-	-	138.75
Pb(2) 4f	-	137.03	-	-	137.47
Pb(3) 4f	-	138.37	-	-	140.33
Ni(1) 2p	-	-	855.76	-	856.19
Ni(2) 2p	-	-	860.16	-	861.53
Co(1) 2p	-	-	-	781.11	781.43
Co(2) 2p	-	-	-	784.39	785.23
Co(3) 2p	-	-	-	787.57	788.52

Activities

Oral presentations

I. Oral presentation in Post graduate research day June 26th 2012 at the University of Leicester.

II. Oral presentation in Midlands Electrochemistry Group Meeting at the University of Birmingham on June 27th 2012.

Poster presentations

I. electrochemical behaviour of nickel hydroxide films (Midlands Electrochemistry Group, University of Leicester, 19th Apr 2010)

II. Study of nickel ion complexation process with thiomalic acid on gold electrode (Chemistry department research symposium, University of Leicester, 6th June 2011)

III. Study of lead ion complexation with mercaptosuccinic acid on a piezoelectric device (Electrochemistry conference, University of Bath, 4-6 Sep. 2011).